Fluorogenic and Affinity Derivatization Methods to Enable Proteomic Study of 3-Nitrotyrosine and 3,4-Dihydroxyphenylalanine as Markers of Oxidative Stress

By

Maria B. Feeney

Submitted to the graduate degree program in Pharmaceutical Chemistry and the Graduate Faculty of the University of Kansas in partial fulfillment of the requirements for the degree of Doctor of Philosophy.

_____

Chairperson Christian Schöneich

_____

John F. Stobaugh

_____

Teruna J. Siahaan

_____

Susan M. Lunte

_____

Rick T. Dobrowsky

Date Defended: May 20, 2013

The Dissertation Committee for Maria B. Feeney

certifies that this is the approved version of the following dissertation:

Fluorogenic and Affinity Derivatization Methods to Enable Proteomic Study of 3-Nitrotyrosine and 3,4-Dihydroxyphenylalanine as Markers of Oxidative Stress

_____

Chairperson Christian Schöneich

Date approved: May 20, 2013

Abstract

Purpose: Oxidative post-translational modification of protein-bound tyrosine residues can have a significant impact on protein structure and function and thus may be important to physiological and pathological processes. Oxidative stress has been correlated with biological aging and many disease states, including diabetes, atherosclerosis, and neurodegeneration. Proteomic methods targeted to these modifications are important tools for determining which specific modifications may be significant in these conditions. Toward this end, a method designed to fluorogenically label the protein oxidation products 3-nitrotyrosine (3NY) and 3,4-dihydroxyphenylalanine (DOPA) using benzylamine-dependent chemistry is applied to model peptides and proteins, as well as cardiac tissue samples from a rat model for aging.

Methods: Peptides or proteins are reacted with excess benzylamine (or a derivative thereof), in the presence of potassium ferricyanide, to fluorescently label DOPA residues by forming 2-phenylbenzoxazole derivatives. To label 3NY residues, the peptides or proteins are first reduced with sodium dithionite to give 3-aminotyrosine, which can undergo a similar reaction with benzylamine and oxidant to give the same products. Products are characterized by fluorescence spectroscopy, high-performance liquid chromatography (HPLC) with UV and fluorescence detection, mass spectrometry, and amino acid analysis. For enrichment by boronate-affinity HPLC, the benzylamine derivative (3R, 4S)-1-(4-(aminomethyl)phenylsulfonyl) pyrrolidine-3,4-diol (APPD) is used as the tagging reagent.

Results: Cardiac proteins have been fluorescently labeled and separated, and some putative identifications have been made. A model protein, glycogen phosphorylase *b* (Ph-b), has been nitrated *in vitro* and labeled within a matrix of cardiac homogenate, and the products exhibit concentration-dependent fluorescence. The loss of 3NY from nitrated Ph-b upon mixing with

cardiac homogenate has been observed and examined. Five model peptides have been labeled with APPD to determine the effect of primary structure on labeling efficiency, fluorescence quantum yield, and molar absorptivity.

Conclusions: This method has great potential to aid identification of the protein oxidation products DOPA and 3NY in proteomic studies of tissue samples and can also be adapted for affinity enrichment and relative quantification of these low-abundance species.

To my husband, Matt, and our children, Hugh and Hannah.

Acknowledgements

I would like to thank my adviser, Christian Schöneich, for his mentorship and guidance throughout my graduate career. Not only have I learned a great deal about proteomics, oxidative stress, biochemistry, and physical chemistry but, even more importantly, my mind has been trained for rigorous scientific analysis and creative problem-solving. I am also grateful for the opportunity to attend and present at multiple national and international meetings.

I also wish to extend my gratitude to the other members of my dissertation committee for their advice at review meetings and their service at my defense: John Stobaugh, Teruna Siahaan, Susan Lunte, and Rick Dobrowsky. I am especially grateful for your patience and understanding during the last month before my defense, which allowed me to finish on a tight schedule that was not entirely under my control. Thank you to John Stobaugh and Teruna Siahaan for also serving as readers for my dissertation. Thanks also to Elias Michaelis for his insightful contributions at multiple committee review meetings, although scheduling conflicts prevented his attendance at my final defense. I would also like to thank Rick Dobrowsky for stepping in as a substitute in his absence.

To all current and former members of the Schöneich lab, it has been an honor to have you as colleagues, and I am deeply grateful for your scientific insights, practical assistance in the lab, and your friendship. I would like to thank especially Elena Dremina and Victor Sharov, who have worked extensively on the nitrotyrosine labeling project and thus have been able to share results and theories that have been very helpful during the course of my project. Likewise, special thanks go to Xiabao Li, who synthesized the labeling reagents and boronate-affinity material, and Sung Jung Hong, who also worked on labeling nitrotyrosine. Olivier Mozziconacci has always been eager to help, especially when I was facing a difficult obstacle in my research.

Gary Gerstenecker taught me almost everything I know about troubleshooting HPLC problems, or at least pointed me in the right direction as I learned by experience – and plenty of mistakes. He also set up and ran several nanflow mass spectrometry experiments with me. Giri Gokulrangan helped to run some of the early mass spectrometry experiments and trained me on the instruments and data analysis. Asha Hewarathna has been a constant friend and great support. Thanks also to Jessica Haywood, Daniel Steinmann, Shuxia Zhou, Vikram Sadineni, and Rupesh Bommana.

The highly collaborative environment in the Department of Pharmaceutical Chemistry and the university as a whole has provided many opportunities to enhance my research. This project would not have been possible without work of Justin Pennington and Jacque Killmer in the Stobaugh lab to develop the benzylamine labeling method and apply it to model compounds. Their expertise in and equipment for packing nanoflow chromatography columns was also crucial to my work. The Forrest lab graciously allowed me to use their spectroscopy instruments. Todd Williams and Nadya Galeva provided valuable service in the Mass Spectrometry Laboratory, both in running our samples and in allowing us to use instruments and re-configure them for our specific applications. Finally, through collaboration with the group of James Jorgenson at the University of North Carolina, we have begun to test ultra-high-performance liquid chromatography with mass spectrometry to improve column capacity and resolution. This approach is an important future direction for this project, as it may be crucial for detection and identification of low-abundance nitrotyrosine- and DOPA-modified proteins. Many thanks to Jordan Stobaugh for running some of our samples on their instrument, and good luck to Josh Woods as he implements this technique here at KU.

I am deeply grateful to the Department of Pharmaceutical Chemistry for academic and financial support. Nancy Helm always has the answer to every question and the ability to solve any administrative problem. The department has also provided me with the opportunities to serve on the planning committee for the international meeting of the Globalization of Pharmaceutics Education Network and on a search committee for a new faculty hire, as well as in various positions on the executive board of the KU student chapter for the American Association of Pharmaceutical Scientists. Through all of the medical and personal challenges I have faced during my graduate career, the entire department has been extremely supportive and has enabled me to complete my degree despite difficult circumstances.

I would like to thank the Madison and Lila Self Graduate Fellowship for financial support and especially for a unique and powerful opportunity for leadership development. To Al Self, who passed away earlier this year, thank you for your example, your vision, and your tenacity in bringing it to fruition. Thank you to the entire staff who served during my time on the fellowship: Patty Dannenberg, Cathy Dwigans, Sharon Graham, Howard Mossberg, and Jimmy Morrison. As a Self Graduate Fellow, I have also greatly valued the opportunity to interact with students and faculty across a variety of disciplines. I am also grateful to the fellowship for extending my financial support during my recovery from a motor vehicle accident in 2008.

I am also grateful for financial support from a scholarship funded by Amgen and from grants from the National Institutes of Health.

I would like to thank Genentech, and specifically Aditya Wakankar and Y. John Wang, for the opportunity of an internship in the summer of 2008 and the subsequent publication of the work I did there.

For their friendship and their collaboration as study partners, I am deeply grateful to Courtney Kuhnline Sloan, Natalie Ciaccio, Brooke Barrett Milner, Diana Sperger Davey, and Taryn Bagby. I have also been very fortunate to have as friends Michelle Strauss, Mary Krause, Kelly and Jason Desino, Bob Berendt, Sarah Pyszczynski, Elodie Dempah, Joe Lubach, and Dewey Barich. Thanks especially to Dewey for coordinating the department's co-ed softball team, which, though not very successful in the win column, was great fun.

I am in the unique position of having many people to thank for literally saving my life. Following a head-on collision on the highway on October 23, 2008, the quick action and skilled care of first responders and many other medical practitioners, most of whom I do not remember, ultimately brought me to stable condition at The University of Kansas Hospital. I also want to thank the multitude of friends and strangers around the world who were praying for me in those precarious minutes, hours, and days after the accident, and throughout my recovery. In a very special way, I would like to thank Archie Headings, an extremely talented orthopedic surgeon who patched my bones back together and provided excellent care for the next three years. He has a great passion for making his patients whole, which goes beyond simply reconstructing their bodies. I also cannot thank enough Diane Bell, who helped me through every stage of my recovery as my primary physical therapist. Thanks also to the rest of the staff at Lawrence Therapy Services, where I was a familiar face for two years, with daily sessions for much of that time.

For spiritual support and friendship, I am deeply grateful to the St. Lawrence Catholic Campus Center; its director, Fr. Steve Beseau; my spiritual director, Sr. Clara Remartini, AVI; and my dear friend, Jeanne Meier. Thanks be to God for all of the good things He has given me during my eight years in Lawrence.

To my family, my first and greatest support network, I can never thank you enough. Thank you to all of the Thorsons: my mother, Amy; father, John; siblings and siblings-in-law Andrew, Heather, Louis, Jessica, Paul, Mary, John, Molly, Beatrice, and Alex; and nieces and nephew Abigail, Lydia, Eliot, and one more still *in utero*. I would like to especially thank my mother for moving to Kansas for five months when I could not walk or take care of myself, my father for taking care of everything at home in her absence, and my siblings for chipping in during this time. Thank you also to my parents-in-law, Debby and Tom Feeney, for your constant support and encouragement.

Finally, words cannot express my gratitude to my husband, Matt, who has made more sacrifices than anyone else so that I can finish this degree – too many to list them all here. Thank you for your constant encouragement, for the occasional push you gave me to work my hardest, and for your patience. Thank you for our beautiful children, Hugh and Hannah, and for always keeping our family focused on the things that are truly most important. To Hugh and Hannah, thank you each for accompanying me for nine months in the lab and for your patience and understanding while I worked long hours to finish all of my experiments and writing. Thanks especially to Hannah for waiting to be born until my defense was finished.

Chapter 4: Effect of Amino Acid Sequence on Fluorescence Quantum Yield, Molar Absorptivity, and Reaction Yield for a Series of Model Synthetic Nitropeptides Labeled with (3R,4S)-1-(4-(aminomethyl)phenylsulfonyl)pyrrolidine-3,4-diol (APPD)

Chapter 5: Conclusions and Future Directions

List of Abbreviations

$^{\bullet}NO_2$	nitrogen dioxide
2D-PAGE	two-dimensional polyacrylamide gel electrophoresis
3AY	3-aminotyrosine
3ClY	3-chlorotyrosine
3NY	3-nitrotyrosine
3NY-Ph-b	nitrated glycogen phosphorylase *b*
AAA	amino acid analysis
ABCA1	ATP-binding cassette transporter A1
ABS	4-(aminomethyl)benzenesulfonic acid
Ac_2O	acetic anhydride
ACN	acetonitrile
AD	Alzheimer's disease
ALS	amyotrophic lateral sclerosis
Ang II	angiotensin II
apoAI	apolipoprotein A-I
APPD	(3*R*,4*S*)-1-(4-(aminomethyl)phenylsulfonyl)pyrrolidine-3,4-diol
BA	benzylamine
BA-HPLC	boronate-affinity high-performance liquid chromatography
BSA	bovine serum albumin
BSA	bovine serum albumin
capLC	capillary liquid chromatography
CHAPS	3-[(3-cholamidopropyl)dimethylamonio]-1-propanesulfonate
COFRADIC	combined fractional diagonal chromatography
cPILOT	combined precursor isotopic labeling and isobaric tagging

DiClY	3,5-dichlorotyrosine
DiY	3,3’-dityrosine
DMSO	dimethyl sulfoxide
DOPA	3,4-dihydroxyphenylalanine
DQ	dopaquinone
DTT	dithiothreitol
EDTA	ethylenediaminetetraacetic acid
EPO	eosinophil peroxidase
ESI	electrospray ionization
EtOH	ethanol
FeSOD	iron superoxide dismutase
FL	fluorescence detection
FSPE	fluorinated solid-phase extraction
FTICR	Fourier transform ion cyclotron resonance
GAPDH	glyceraldehyde-3-phosphate dehydrogenase
GnHCl	guanidinium hydrochloride
GSH-TG1	glutathione-ThioGlo®1
HDL	high-density lipoprotein
HOBr	hypobromous acid
HOCl	hypochlorous acid
HPLC	high-performance liquid chromatography
HPLC-MS/MS	high-performance liquid chromatography-tandem mass spectrometry
IMAC	immobilized metal affinity chromatography
IT	ion trap
iTRAQ	isobaric tag for relative and absolute quantitation

LOD	limit of detection
LTQ	linear trap quadrupole (linear ion trap)
MALDI	matrix-assisted laser desorption/ionization
MnSOD	manganese superoxide dismutase
MPO	myeloperoxidase
MS	mass spectrometry
MS/MS	tandem mass spectrometry
m-Tyr	*meta*-tyrosine, 3-hydroxyphenylalanine
NHS	N-hydroxysuccinimide
NHS-acetate	acetic acid N-hydroxysuccinimide ester
NHS-biotin	biotinyl N-hydroxysuccinimide ester
NO	nitric oxide
NTA	nitrilotriacetic acid
Nva	norvaline
$ONOO^-$	peroxynitrite
OPA	O-phthalaldehyde
o-Tyr	*ortho*-tyrosine, 2-hydroxyphenylalanine
PD	Parkinson's disease
PDA	photodiode array
PF	potassium ferricyanide
Ph-b	glycogen phosphorylase *b*
PTM	post-translational modification
PVDF	polyvinylidene fluoride
ROS	reactive oxygen species
RP	reverse-phase

RP-HPLC	reverse-phase high-performance liquid chromatography
RT	room temperature
SCX	strong cation exchange
SDS	sodium dodecyl sulfate
SDS-PAGE	sodium dodecyl sulfate polyacrylamide gel electrophoresis
SDT	sodium dithionite
SE-HPLC	size-exclusion high-performance liquid chromatography
SPAER	solid-phase active ester reagent
SPE	solid-phase extraction
TCA	trichloroacetic acid
TEAB	tetraethylammonium bicarbonate
TFA	trifluoracetic acid
THF	tetrahydrofuran
TMT	tandem mass tags
TNM	tetranitromethane
TOF	time-of-flight
TOF/TOF	tandem time-of-flight
TPO	thyroid peroxidase
UV	ultraviolet absorbance detection

Chapter 1: Introduction to Oxidative Post-Translational Modifications of Protein-Bound Tyrosine Residues

1.1 Tyrosine Modifications in Aging

This section has previously been published as a review article (22).

1.1.1 Introduction

Various oxidative post-translational modifications (PTMs) of proteins accumulate in cells during aging and disease, particularly age-related diseases such as atherosclerosis, cataracts, type 2 diabetes, and neurodegenerative diseases. Such modifications can alter protein structure and function by inducing conformational changes, partial or complete unfolding, cross-linking, and/or aggregation, or by modifying enzyme active sites, phosphorylation sites, or binding sites. These modifications can lead to either gain or loss of function and may serve physiological/regulatory purposes or contribute to (or at least accompany) pathogenesis [see (52,67,81) and references cited therein].

Modifications of Tyrosine

Protein Tyr residues are susceptible to an array of oxidative and nitrative modifications (Fig. 1), including the formation of 3-nitrotyrosine (3NY), which may be reduced to 3-aminotyrosine (2,78); 3,4-dihydroxyphenylalanine (DOPA); 3,3'-dityrosine (DiY); 3-chlorotyrosine (3ClY); 3,5-dichlorotyrosine (DiClY); as well as brominated and iodinated forms (11,67,81). Further oxidation can convert DOPA to dopaquinone (DQ) or 3-aminotyrosine to the quinone imine, representing acceptors for conjugate additions. Subsequently, protein-bound DQ and quinone imine may propagate oxidative damage to DNA and lipids, as well as other proteins (54). Additionally, *ortho*-tyrosine (2-hydroxyphenylalanine, *o*-Tyr) and *meta*-tyrosine (3-hydroxyphenylalanine, *m*-Tyr) are products of reaction between hydroxyl radicals (or their metal-bound equivalents) and Phe [(52,67,81) and references cited therein]. While mostly non-

enzymatic, all of these modifications can preferentially accumulate on specific proteins, as well as specific residues within those proteins (2,52,67).

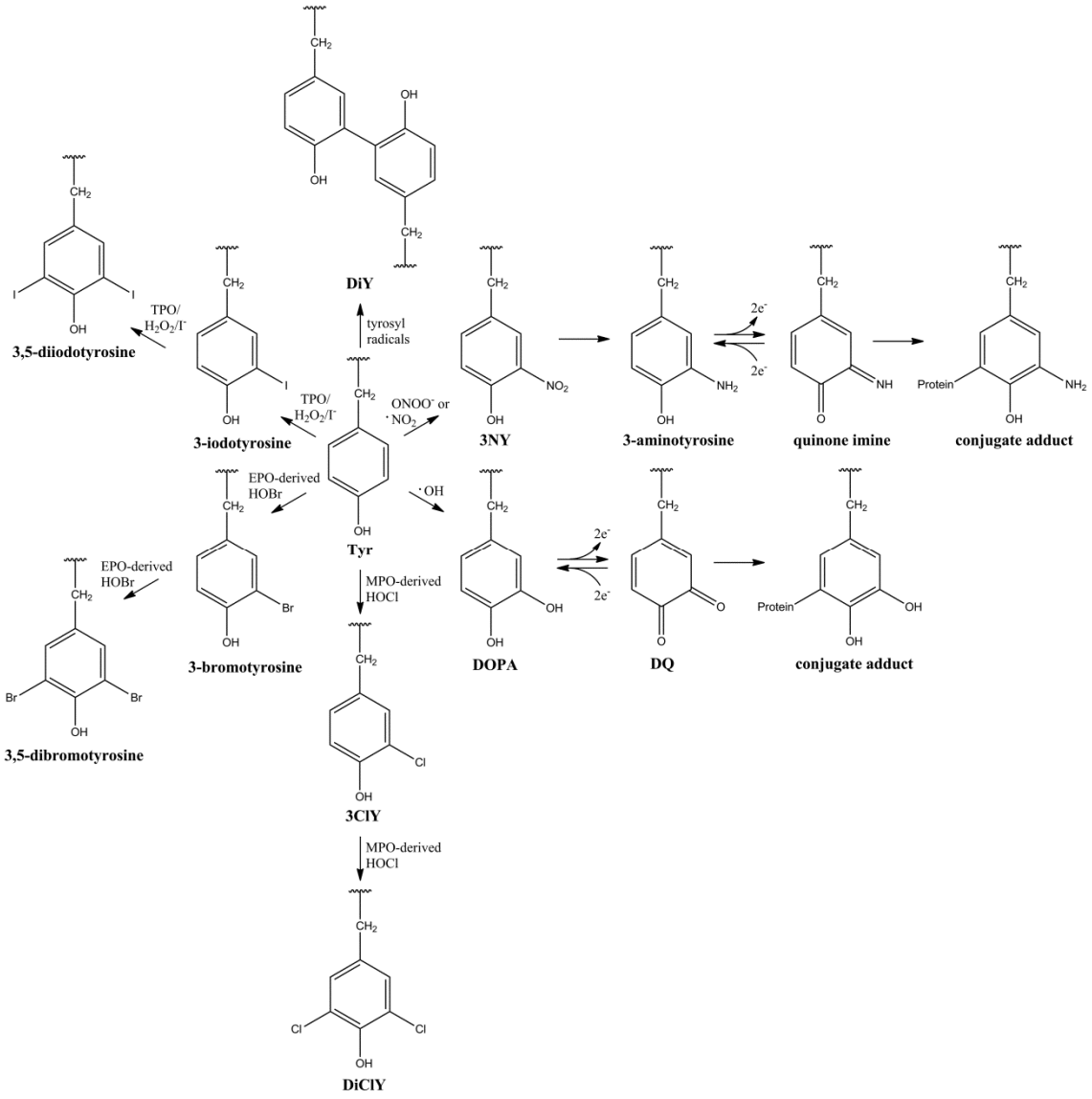

Fig. 1. Endogenous post-translational modifications of protein-bound Tyr. EPO: eosinophil peroxidase; MPO: myeloperoxidase; TPO: thyroid peroxidase.

Consequences of Modification

In many cases, oxidation targets proteins for degradation, perhaps due to the increased surface hydrophobicity that results from unfolding or misfolding (13,19,67,81). However, after extensive oxidative modification and/or when cross-links and aggregates form, proteins can

become resistant to and even inhibit proteolysis, leading to pathological accumulation and deposition (13,19,81). Proteolysis by both proteasomal and lysosomal pathways also tends to decline with aging and certain disease states, which may further contribute to cellular senescence and to pathologies characterized by protein deposition, such as atherosclerosis, cataract, macular degeneration, rheumatoid arthritis, and neurodegenerative diseases like Alzheimer's disease (AD), Parkinson's disease (PD), and amyotrophic lateral sclerosis (ALS) (13,19,36,67,81).

The introduction of modified residues within proteins and any associated structural changes can create neo-epitopes for antibody recognition, and cross-reactivity with unmodified self-proteins can induce autoimmune disorders. This is particularly relevant for modified proteins that are absent during early development but accumulate with age (2,52,67).

In addition to these general consequences for proteins, oxidation can have specific effects on the function of a particular protein. For example, it can modify an active site, block a phosphorylation site, or disrupt a binding site for substrates, cofactors or partner proteins. If a particular modification is reversible by either repair or protein turnover, it may serve a regulatory function and/or participate in cellular signaling pathways [(2,52,67) and references cited therein].

Importance of Site Specificity

While overall levels of a particular Tyr modification (e.g. protein-bound 3NY or DOPA) may or may not be measurably elevated in a particular tissue or cell sample, specific proteins may carry significant levels of such modifications (52,67). When these proteins are of low abundance, the absolute quantity of the modification will not contribute significantly to the overall yield in the sample. Nevertheless, the modification may be physiologically important. For this reason, many proteomic studies have been undertaken to identify long lists of Tyr-modified proteins. However, the focus of the present review will be on progress made in

characterizing the effects of specific protein modifications on structure, function, aggregation, and pathogenesis, with an emphasis on implications for aging. The discussion will concentrate on studies published over the last 5 years.

1.1.2 3-Nitrotyrosine

Formation and Significance

3NY is the most commonly measured Tyr oxidation product, due to its relative chemical stability, the availability of anti-3NY antibodies, and its status as a marker of nitric oxide (NO)-dependent protein modifications. 3NY is generated by several pathways, including reactions of peroxynitrite ($ONOO^-$) or nitrogen dioxide ($^{\bullet}NO_2$) and catalysis by heme-containing proteins (52,67). The nitration of Tyr can lead to conformational changes, unfolding, aggregation, immunogenicity, and/or partial or total inactivation of a target protein, although in some cases gain of function has been observed. These consequences may be attributed to changes in steric requirements, electrostatics, pK_a of amino acid side chains, and/or surface hydrophobicity. Going beyond tables of proteomic identifications, there have been significant developments in the study of specific protein nitration sites and their effects on structure and function. The possibility of 3NY as a signaling moiety has also been proposed, and evidence has been presented for pathological roles of 3NY-containing proteins. For a comprehensive review, see (52) and references cited therein.

Inactivation of MnSOD by Nitration of Tyr-34 in the Active Site

The activity of human manganese superoxide dismutase (MnSOD), which protects cells from damage by scavenging superoxide, is largely inhibited by nitration at Tyr-34 in the active site, and this modification has been observed in aging, ALS, AD, PD, and diabetes, among others (42,52). Quint *et al.* (61) determined the crystal structures of both native and nitrated enzyme in

order to investigate the mechanism of this inactivation (Fig. 2). Treatment with peroxynitrite gave 75% yield of 3NY-34 and reduced enzymatic activity to 20% ± 5% compared to that of the wild-type enzyme. Although mass spectrometry identified additional modification sites, 3NY-34 was the only modification present in the crystal structure. While no significant conformational

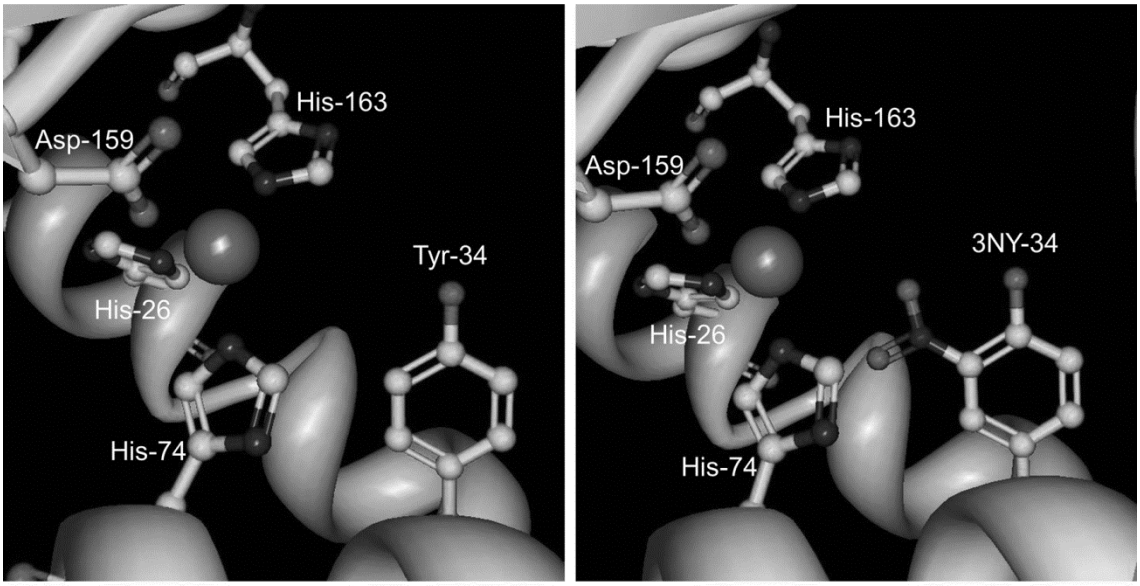

Fig. 2. Active site of native (a) and nitrated (b) human MnSOD, shown with Mn and its ligands, His-26, Tyr-34, His-74, Asp-159, and His-163. Image derived from crystal structures stored in the Protein Data Bank (61); accession codes 2ADQ for native and 2ADP for nitrated. Figure generated using Protein Workshop (45).

changes were evident upon nitration, enzyme inhibition was attributed to steric interference with substrate binding and changes in the hydrogen bonding network. Electrostatic changes due to the lower phenolic pK_a of 3NY relative to Tyr may also alter the finely-tuned redox potential in the active site and/or cause repulsion of the substrate, $O_2^{\bullet -}$, although this hypothesis was not tested. The pK_a of 3NY-34 in MnSOD is expected to be similar to that measured spectroscopically for 3NY-34 of the bacterial iron superoxide dismutase enzyme (FeSOD), which is 7.95, or approximately two units lower than that of Tyr [(61) and references cited

therein]. In this protein environment, this value is higher than the pK_a ~7.2 measured for 3NY in other peptides and proteins and in its free form (78,91).

In order to isolate 3NY-34 from all other modifications that can occur with oxidizing agents, Neumann *et al.* (48) used a genetic approach for site-specific incorporation of the unnatural amino acid 3NY at position 34 in recombinant rat mitochondrial MnSOD. Upon quantitative formation of this nitrated mutant, the enzyme showed 97% decrease in activity.

Nitration Disrupts Catalysis by GAPDH

Glyceraldehyde-3-phosphate dehydrogenase (GAPDH), a crucial protein for cellular metabolism and energy, is a common entry on proteomic lists of nitrated proteins, including studies of aging (33) and AD (82), likely due to its role as a sensor of NO (53). In a mechanistic study, Palamalai *et al.* (53) recently determined that *in-vitro* nitration of Tyr-311 and Tyr-317 in rabbit GAPDH by tetranitromethane resulted in loss of binding to NAD+, thereby destroying all catalytic activity of the enzyme. Computational analysis of the X-ray crystal structure predicted that these nitration sites are located very close to both the catalytic cysteine residue and the NAD+ binding site (Fig. 3). Furthermore, *in silico* nitration resulted in an even shorter predicted distance (1.4 Å) between 3NY-317 and NAD+, such that significant steric interference may occur. Alternatively, the movement of this residue at the

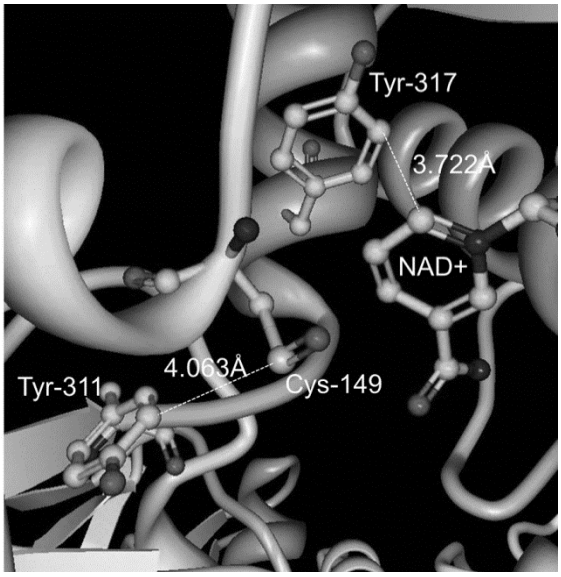

Fig. 3. Nitration sites of rabbit muscle GAPDH, Tyr-311 and Tyr-317, and their proximity to Cys-149 and NAD+ in the active site. Image derived from the crystal structure stored in the Protein Data Bank (12); accession code 1J0X. Figure generated using Protein Workshop (45).

base of an α-helix may disrupt this secondary structure. In fact, circular dichroism shows some loss of secondary structure following *in vitro* nitration.

1.1.3 DOPA, DQ, and Tyr-Mediated Cross-links

DOPA and DQ

Hydroxyl radicals can convert Tyr to DOPA (27), and site-specificity for this reaction can be facilitated by redox-active transition metals bound to proteins or by localized sources of hydroxyl radicals, such as mitochondria (46,95). Through reversible oxidation to DQ, DOPA is part of a redox cycle capable of regenerating the reduced state of redox-active transition metals, particularly iron and copper, and of reducing metalloproteins (14,23,27). This phenomenon can perpetuate oxidative insult but also presents an opportunity for putative signaling functions, such as triggering antioxidant defenses (46). Protein-bound DOPA can also serve a protective role by scavenging radicals and chelating metals, although the latter function can alternatively direct oxidative damage to specific protein sites (46,47,80).

DOPA and DQ can also be formed enzymatically by tyrosinase or tyrosine hydroxylase (54). In addition, DOPA may be incorporated during protein synthesis when free DOPA is available to compete with Tyr, such as in levodopa-treated PD patients (18).

Conjugate Addition

DQ and the related quinone imine (*e.g.* an oxidation product of 3-aminotyrosine) can serve as conjugate acceptors for nucleophilic groups on other amino acid side chains to generate protein cross-links (54). Protein aggregates may result that are resistant to proteolysis and can contribute to protein deposition/plaque formation in aging and various disease states (13,19). Conversely, such cross-links can perform important functions. For example, the cofactor lysine

tyrosylquinone is formed by the intramolecular addition of Lys-314 to the DQ moiety derived from Tyr-349 in lysyl oxidase (88).

3,3'-Dityrosine

Another route to Tyr-mediated protein cross-links involves the combination of two tyrosyl radicals to form DiY (28,81). Various pathways to the formation of tyrosyl radicals exist, mediated by hydroxyl radicals, peroxynitrite-derived species, peroxyl radicals, redox-active metals, γ-radiolysis, UV irradiation, heme, or hemeperoxidase enzymes (5,28,81). In the hydrophobic region of biological membranes, lipid-derived radicals can also play an intermediary role (5). Specificity may arise due to conformational requirements for the interaction of Tyr residues. DiY modification leads to selective proteolysis, and the released DiY is a stable and useful biomarker for oxidative stress, for example as excreted in urine (28).

Although not as widely studied as 3NY, these other modifications have been linked to atherosclerosis (23), cataracts (24,44), levodopa therapy for PD (18), and lysosomal dysfunction (18,19). Some proteomic studies of DOPA, for example, have been published (39,95), but here the focus will be on recent mechanistic studies.

Age-Related Cataracts

The formation of age-related cataracts in humans is associated with up to 15-fold increases in protein-bound DOPA, as well as elevated levels of DiY and other protein-bound amino acid hydroxylation products, which can contribute to the protein cross-linking and browning that characterize cataractous lenses (24). DOPA and DiY formation may result from both Fenton-type, hydroxyl-radical chemistry (24) and reactions photosensitized by protein-bound Trp metabolites (44). The free Trp metabolites kynurenine, 3-hydroxykynurenine, 3-

hydroxykynurenine-*O*-β-D-glucoside, 4-(2-aminophenyl)-4-oxobutanoic acid, and 4-(2-amino-3-hydroxyphenyl)-4-oxobutanoic acid serve as filters for UVA light, as they absorb with high efficiency but are poor sensitizers for the formation of singlet oxygen or radical species. However, with aging, they become increasingly bound to lens proteins, either covalently or non-covalently (Fig. 4). Such protein-filter adducts accumulate in the lens nucleus, due at least in part to a diffusional barrier that develops at middle age. In this state, these compounds may lose their protective function and instead promote direct and indirect photooxidation of proteins, including generation of DOPA and DiY. At the same time, the pool of free, protective filter compounds is depleted, leaving the aging lens more susceptible to photochemical damage (44).

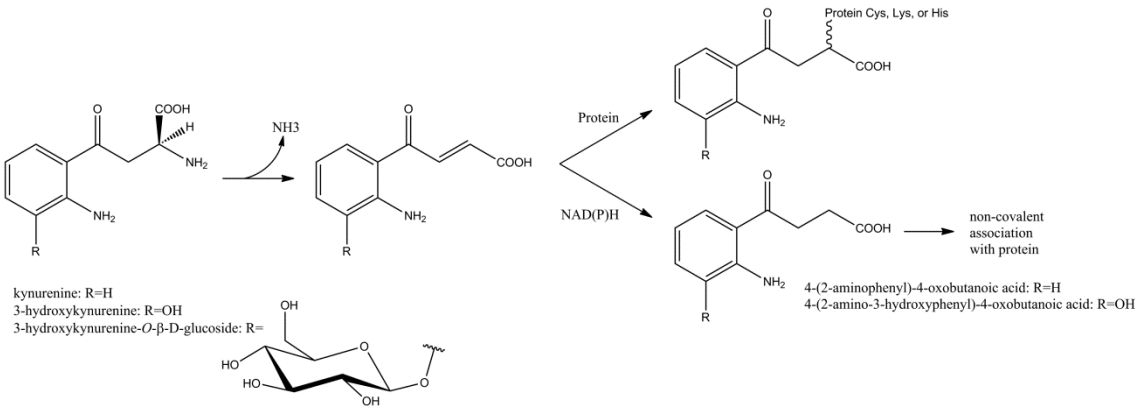

Fig. 4. Trp metabolites can form covalent or non-covalent associations with proteins to become photosensitizers for protein oxidation. Figure based on information from (44).

When tested *in vitro* with soluble bovine lens proteins (44), all but one of these protein-Trp metabolite adducts led to increased peroxide formation (primarily hydrogen peroxide) in a process that is sensitive to D_2O (increased yield) and azide (decreased yield), indicating the involvement of singlet oxygen. However, the levels of DOPA and DiY were metabolite-dependent and insensitive to D_2O. In addition, DOPA formation was independent of illumination and atmospheric oxygen. The authors postulated at least two reaction pathways to account for these differences: 1) the photosensitized formation of singlet oxygen and 2) the

autoxidation of the *o*-aminophenol moiety in 3-hydroxykynurenine or its metabolite, 4-(2-amino-3-hydroxyphenyl)-4-oxobutanoic acid, which generates superoxide. Furthermore, in the light-dependent pathway, the excited states of the filter compounds appear to have competing energy transfer pathways, either to oxygen or to protein-bound Tyr.

Regardless of the pathway, these phenomena generated covalent, non-disulfide protein cross-links and may also contribute to lens browning, two characteristic features of age-related nuclear cataracts (24,44). The DOPA levels in the Trp metabolite study (44) were similar to those found in human type IV nigrescent cataract lenses, while DiY levels were much higher in the model system than in the cataract lenses. Cross-links observed by reducing SDS-PAGE may be due to DiY and/or reaction of nucleophilic side chains with the protein-bound oxidation products of DOPA (*i.e.* DQ) or the *o*-aminophenol moiety of 3-hydroxykynurenine or 4-(2-amino-3-hydroxyphenyl)-4-oxobutanoic acid (*i.e. o*-quinone imine).

Lysosomal Accumulation

Using metabolic incorporation of DOPA into proteins, Dunlop *et al.* (19) showed that such proteins form autofluorescent, SDS-stable, proteolysis-resistant aggregates in J774 murine macrophages, similar to the "aging pigment" lipofuscin or its disease-related counterpart, ceroid. This aggregation is consistent with the ability of DOPA to oxidize to DQ and react with nucleophiles, such as cysteine residues, to form cross-links. The perinuclear punctate pattern of fluorescence and upregulation of the lysosomal proteases cathepsins B and L indicate accumulation of these aggregates in lysosomes. Lysosomes are rich in transition metals due to their role in autophagic degradation of metal-containing proteins, and DOPA redox cycling can continually regenerate these reactive species to fuel oxidative damage to the lysosomal membrane, setting off a lysosomal pathway to apoptosis, as illustrated in Fig. 5 [see (36) for a

review]. Indeed, in a subsequent study (18), the authors repeated this result in THP1 human monocytes and used a variety of fluorescent staining/flow cytometry approaches to demonstrate

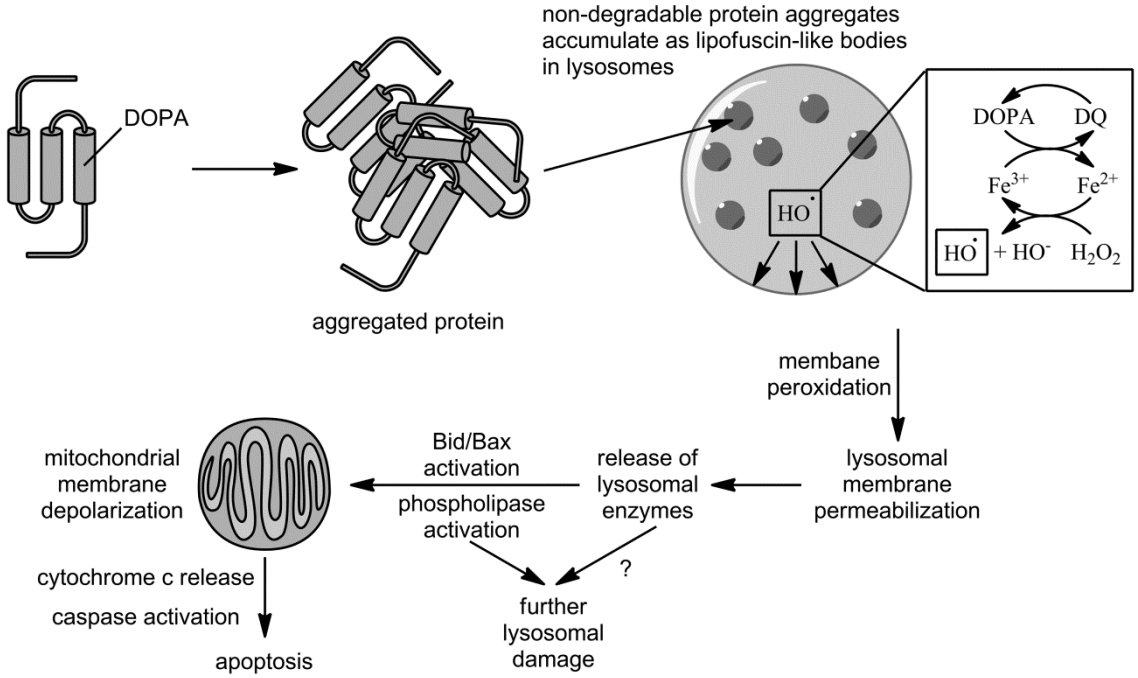

Fig. 5. Lysosomal pathway to apoptosis mediated by the accumulation of aggregated proteins following metabolic incorporation of DOPA. Figure based on information from (18,36).

lysosomal membrane permeabilization, depolarization of mitochondrial membranes, decreased mitochondrial cytochrome *c* levels, and increased apoptosis (measured as phosphatidylserine externalization by Annexin V-FITC, cellular DNA content by propidium iodide, and DNA fragmentation by TUNEL). Lysosomal membrane permeabilization occurred even in the presence of a pan-caspase inhibitor, demonstrating that it is not caused by an early release of caspases and thus indicating that it is the trigger for the apoptotic event. In the absence of the inhibitor, Western blots showed the cleavage of pro-caspase 3 to its active form, which is a key step that commits cells to apoptosis, and the resulting increase in activity was measured using a fluorigenic substrate. Lysosomal membrane permeabilization was also replicated in SH-SY5Y human neuroblastoma cells and MRC5 human lung fibroblasts.

Similar experiments with *o*-Tyr, *m*-Tyr, Tyr, and D-DOPA (a negative control for protein incorporation) showed that these effects are unique to protein-bound DOPA (18,19). While *o*-Tyr did induce lower levels of apoptosis than DOPA, as well as lower levels of caspase 3 activation, it did not aggregate or accumulate, indicating a separate apoptotic pathway (18).

By specifically incorporating DOPA into cellular proteins *in vitro*, the study just described isolates this protein modification from other possible consequences of oxidative stress and defines the subsequent pathway to apoptosis. It also mimics long-term levodopa treatment of PD patients, for whom protein incorporation has been observed (18), and the apoptotic events observed may contribute to the suspected neurotoxicity of this treatment regimen. The lysosome-mediated apoptotic pathway may be particularly relevant for neurons and other post-mitotic cells that are more prone to accumulation of proteolysis-resistant proteins (18). Even without apoptotic events, the accumulation of non-degradable proteins or lipofuscin in lysosomes can lead to mitochondrial dysfunction, a phenomenon observed in long-lived post-mitotic senescent cells that may contribute to aging (36).

It should also be noted that sites of metabolic DOPA incorporation could very well be different from those sites altered by ROS *in vivo*. Perhaps this study is a better indication of events occurring in large-scale oxidative stress events (indeed, aggregation of DOPA-containing proteins occurs only when this oxidized amino acid is incorporated in larger amounts (19)), but not of localized effects that may result from highly specific redox events, such as the metal-catalyzed oxidation of Tyr in an enzyme's active site. Complementary proteomic studies could identify whether there are common sites for metabolic incorporation *versus* oxidative damage and if any of these sites may be functionally significant, especially at lower levels of oxidative

insult. Such proteomic studies and corresponding structural and functional studies for DOPA are currently lacking in the field.

1.1.4 3-Chlorotyrosine

Formation and Significance

The enzyme myeloperoxidase (MPO) is secreted by neutrophils, monocytes, and some macrophages and is a key component of inflammatory response (94). It uses hydrogen peroxide and chloride ions to generate hypochlorous acid (HOCl) as a defense against microorganisms, but it can also inflict oxidative damage on proteins and lipids (59). HOCl can react with protein-bound Tyr, and this is the only known source of 3ClY formation in humans, making this modification a good fingerprint for oxidative damage promoted by MPO (30,59). HOCl can further chlorinate 3ClY to form DiClY (81). In addition, MPO can generate $^{\bullet}NO_2$ from nitrite or $ONOO^-$, which can generate 3NY, as well as tyrosyl radicals, leading to DiY and other Tyr-derived cross-links (52,59).

3ClY has been found in many inflammatory disease states, such as in synovial fluid from rheumatoid arthritis patients (89). In addition, both MPO and its products, particularly 3ClY and 3NY, are known to be enriched in human atherosclerotic plaques and in plasma from patients with cardiovascular disease (9,30,94). Indeed, plasma MPO level has been shown to be an effective predictor of major adverse coronary events in patients presenting with chest pain to the emergency department (9).

Chlorination of HDL May Contribute to Atherogenesis

Studies of specific 3ClY sites in proteins are scarce, but there has been interest in characterizing the role of MPO in the oxidative damage of high-density lipoprotein (HDL), particularly its major protein component, apolipoprotein A-I (apoAI). Fig. 6 shows the locations

of several important oxidation sites. While there is agreement in the literature that MPO selectively targets Tyr-192 (a highly conserved residue) in lipid-free apoAI for both chlorination and nitration, with lower levels observed at the other six Tyr residues (69,97), the functional impact of this specific modification is controversial. There is agreement that MPO-mediated modification, and specifically the 3ClY and 3NY content of apoAI, correlates with loss of cholesterol efflux activity mediated by ATP-binding cassette transporter A1 (ABCA1) (69,96) and that both chlorinated and nitrated apoAI are enriched in human plasma from patients with cardiovascular disease and even more so in atheromas isolated from such patients (96,97). Shao et al. (69) further demonstrated that the specific modification of Tyr-192 to 3ClY shows a strong linear correlation with the loss of ABCA1-dependent cholesterol efflux activity. Additional, contradictory findings are briefly described below, and for recent related reviews from both groups actively researching this subject, see (70,77).

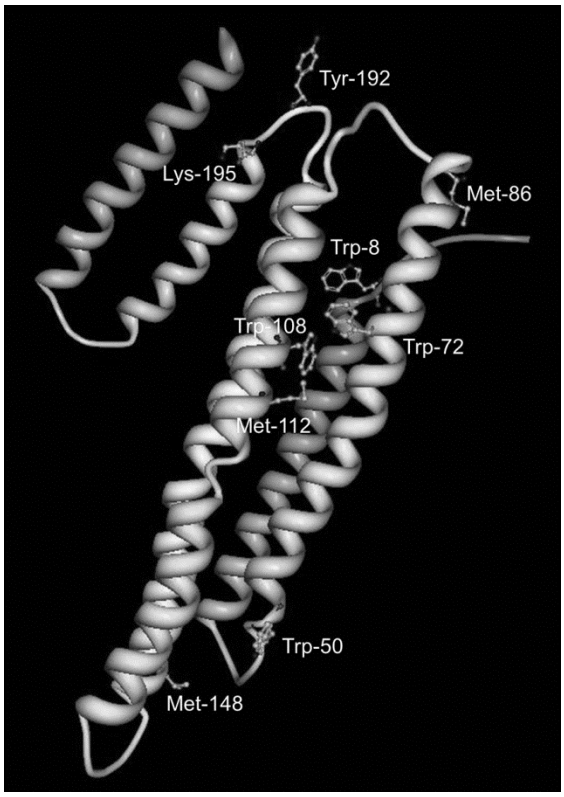

Fig. 6. Oxidation sites of lipid-free human apoAI, many of which are located near hinge regions that may be important for rearrangement upon lipid association and subsequent binding to ABCA1 for reverse cholesterol transport activity. Lys-195 facilitates chlorination of Tyr-192. Image derived from the crystal structure stored in the Protein Data Bank (3); accession code 2A01. Figure generated using Protein Workshop (45).

In a series of studies, the groups of Heinecke and Oram described roles for Tyr, Lys, and Met residues in the MPO-mediated inactivation of apoAI cholesterol efflux activity *via* ABCA1.

While Tyr-192 was the major target for both chlorination and nitration by MPO (and also nitration by $ONOO^-$), the latter modification did not significantly affect the biological activity (69). Nearby Lys residues on the same face of the amphipathic helix as Tyr, specifically in YXXK motifs, regiospecifically directed Tyr chlorination *via* chloramine intermediates formed on the ε-amino group of Lys (6,71). Point mutations designed to add or remove Met residues near target Tyr residues showed their capacity to act as intramolecular antioxidants to inhibit the chlorination (71), as also demonstrated in a later study by Peng *et al.* (55).

Paradoxically, Shao *et al.* (71) presented evidence that Met oxidation, along with Tyr-192 chlorination, was required to impair cholesterol transport activity of apoAI. Mutation of Tyr-192 to the more MPO-oxidation-resistant Phe (Y192F) gave a functional apoAI that was protected slightly from chlorination-dependent loss of activity. Following quantitative oxidation of all three native Met residues to Met sulfoxide by the MPO system, their complete conversion back to Met by the methionine sulfoxide reductase enzyme PilB resulted in partial recovery of activity. While neither of these strategies led to full recovery on its own, the combination of the Y192F mutation and PilB treatment almost completely restored the activity to that of unmodified, wild-type apoAI, leading to the conclusion that both Tyr-192 chlorination and Met oxidation contribute to MPO-mediated functional impairment.

Toward an understanding of the mechanism underlying impaired reverse cholesterol transport, Shao *et al.* (72) showed that while both unmodified and nitrated apoAI were able to compete with ^{125}I-labeled apoAI for binding to ABCA1, the MPO-treated protein could not. Furthermore, their data indicated that the lipid-binding ability of the protein was not compromised by MPO treatment. Since Tyr-192 and all three oxidized Met are in or near hinge regions of apoAI (Fig. 6), their modification may interfere with the rearrangement of its hairpin

loops that is required for interaction with ABCA1. The resulting impairment of cholesterol removal from lipid-laden macrophages or foam cells would promote formation of atherosclerotic plaque (70).

Other researchers have also independently identified Tyr-192 in apoAI as a major target for chlorination by MPO, but their data has not supported a significant functional impact for this particular modification in murine macrophages. Rather, their mutation of all seven Tyr residues to Phe conferred no protective effect for cholesterol efflux activity following MPO treatment of apoAI (56). On the other hand, mutation of all four Trp residues to Phe did make apoAI resistant to MPO-mediated oxidation, leading to the conclusion that mono- and di-hydroxylated Trp is responsible for loss of apoAI's ABCA1-dependent cholesterol efflux activity (55).

Acknowledging these discrepancies, Shao *et al.* (71) suggest that different cell culture models may behave differently, specifically proposing that since their ABCA1-transfected baby hamster kidney cells express higher levels of ABCA1 than murine macrophages, the modest protective effect of replacing Tyr-192 with Phe is more easily detected. Furthermore, Shao and Heinecke (70) point to structural changes in the Trp-free mutant that may explain its resistance to MPO-mediated inactivation, rather than the absence of oxidizable Trp. They specifically cite the increase in α-helical content from 56% for the wild-type to 71% in the Trp-free mutant (55,70).

There are likely many factors that contribute to HDL dysfunction in atherosclerosis [see (77) for a useful discussion], of which modification of Tyr and other amino acids is only one. Even so, specific characterization of the residues involved in oxidation-mediated protein damage may open new diagnostic and therapeutic avenues, both through the use of modified residues as biomarkers and the development of oxidation-resistant forms of apoAI as more effective anti-atherogenic agents for possible therapeutic use (70,71,76). In particular, the specificity of 3ClY

as a marker for MPO activity and the link between MPO and disease progression may make it an important diagnostic and/or therapeutic tool.

1.1.5 Conclusions

Tyr modification has been demonstrated to have important consequences for protein function and structure in many cases. In others, there is still an opportunity to learn what impact these PTMs may have on particular proteins and what role they may play. As the work of identifying, isolating, and characterizing modified proteins under conditions relevant to biological aging and age-related diseases continues, novel insights and deeper understanding of physiological and pathological processes can ultimately lead to improved diagnostic methods and therapeutic

1.2 Proteomic Approaches to Analyze Protein Tyrosine Nitration

This section has previously been published as a review article (21).

1.2.1 Introduction

Nitrative Stress Leads to 3-Nitrotyrosine Formation

Under conditions of nitrative stress, particularly when nitric oxide combines with superoxide to form peroxynitrite, protein Tyr residues can undergo nitration to 3-nitrotyrosine (3NY), and increases in 3NY have been correlated to aging and numerous disease states, including cardiovascular disease, neurodegeneration, and autoimmune diseases (52). Tyr nitration can alter protein structure and function and may play a role in redox signaling (2,22,62).

In order to understand the biological impact of Tyr nitration, protein targets must be identified, most often by mass spectrometry (MS)–based proteomics. Because many reviews of nitroproteomic methods exist (2,15,17,34,50,87,92), including several dedicated to MS techniques (7,58,67,68), the present review will focus on recent improvements in the field.

Some Considerations for the Development of Nitroproteomic Methods

The field of nitroproteomics has long been dominated by two-dimensional polyacrylamide gel electrophoresis (2D-PAGE), followed by Western blotting with antibodies against 3NY and analysis of in-gel-digested spots by MS. This remains the most sensitive technique available, routinely indicating endogenous nitration. However, it is laborious and suffers from problems with specificity, background signals, and reproducibility, due in part to variations among antibody batches and suppliers (2,34,90). Antibodies may be either too specific, depending on the antigen used to raise them, or not specific enough, as cross-reactivity can occur, for instance, with the Trp derivative 5-hydroxy-6-nitrotryptophan (51). Methods for enrichment by immunoprecipitation can suffer from some of the same limitations. Furthermore, 2D-PAGE can be biased against proteins on the extremes of size, isoelectric point, and hydrophobicity. Finally, unambiguous identification of nitrated proteins and residues is difficult because a single gel spot may contain multiple proteins, and tandem mass spectrometry (MS/MS) data are often not obtained for the tryptic peptides containing 3NY (2,34).

Multi-dimensional chromatography, either on-line or off-line, can partially automate the pre-fractionation process for 3NY proteomics. However, specifically offline pre-fractionation can be time-consuming and generate large amounts of samples for MS analysis, thus requiring significant instrument time. Due to the large dynamic range required for proteomic analysis, as well as concerns about column capacity and ion suppression of low-abundance species by an overwhelming matrix of high-abundance species, detection of low endogenous levels of 3NY [on the order of one to five residues per 10,000 Tyr residues in samples under inflammatory conditions (62)] depends upon sufficient simplification and/or purification of the sample.

To address these limitations, many methods for chemical derivatization of 3NY have been developed, mostly to enrich 3NY-containing proteins and/or peptides. These methods often involve several derivatization steps, almost always including the reduction of 3NY to 3-aminotyrosine (3AY) by sodium dithionite (SDT) (78), followed by reaction of the aromatic amine with a labeling reagent, along with one or more cleaning steps. Derivatization methods also present opportunities for relative and absolute quantitation using isotopic labeling and/or fluorogenic tagging. Some derivatization strategies have focused on simplification and avoidance of sample losses that inevitably accompany derivatization and cleaning.

The reduction of 3NY to 3AY can be a challenging step. The most popular method uses SDT (78), but concomitant 3AY and Tyr sulfation can interfere with MS analysis (25,26). An alternative method using thiols and heme yields 3AY as a single product but is more sensitive to conditions and difficult to automate (4,25,26). An electrochemical 3NY reduction has not yet been widely applied in the field of nitroproteomics (2). 3AY may also form inadvertently during sample processing, as observed for the *Arabidopsis thaliana* proteome (41), and may even form *in vivo* (2). These phenomena should be accounted for in proteomic database searches.

Labeling the 3AY aromatic amine with high specificity is crucial, due to the very large excess of aliphatic amine groups (N-termini and Lys ε-amino groups) over low-abundance, endogenous 3NY sites in biological samples, approximated to be *ca.* 28,000-fold molar excess (1). Some groups have attempted to exploit the lower pKa of the aromatic amine, which is 4.75 in the free amino acid (78), relative to aliphatic amines (pKa *ca.* 8-10) to impart specificity in labeling. However, others observed that such pH-based selectivity is insufficient (1,26,93), and most methods have added steps to block reactive amines prior to the reduction of 3NY.

Some Considerations for Mass Spectrometry of Nitrated Peptides and Proteins

When matrix-assisted laser desorption ionization (MALDI) is used for ionization, 3NY photodegradation can occur with a loss of one or two oxygen atoms or reduction of 3NY to 3AY (10,38,40,58,66). While some studies use this characteristic pattern to aid in 3NY identification, it raises limits of detection because the MS signal intensity is shared among three or four peaks. Electrospray ionization (ESI) avoids this problem but does have some disadvantages, such as a lower tolerance for sample contaminants and matrix components. Regardless of the ionization source, both 3NY- and 3AY-containing peptides can have low ionization efficiency and/or poor MS/MS fragmentation (1,26,35,38,58,85). 3AY may give deviating isotopic envelopes for fragment ions, possibly due to chemical rearrangements, which can interfere with protein database searching and prevent proper identification (26). Derivatization of 3AY can overcome these problems (26,60). Removal of the nitro group, an "electron predator," enables the use of electron capture and electron transfer dissociation as complementary fragmentation methods to improve sequence coverage (60); see Refs. (31,43) for further discussion.

1.2.2 Multidimensional Chromatography

Technical and methodological advances have benefited nitroproteomic studies (2,7,8,79). More recent developments are discussed below.

COFRADIC

Ghesquière *et al.* (25) applied combined fractional diagonal chromatography (COFRADIC) to nitroproteomics. Protein digests are separated by reverse-phase (RP) high-performance liquid chromatography (HPLC) and fractions collected over one-minute intervals. After reduction of 3NY to 3AY with SDT, samples are again fractionated using the same RP-HPLC conditions, and peaks showing a hydrophilic shift are collected for MS identification. While this method requires tedious fraction collection, it successfully identified six *in-vivo*

nitration sites in four different proteins from serum in a mouse model of sepsis, specifically female C57BL6/J mice injected intravenously with pathogenic *Salmonella enteritidis*. Likewise, 3NY sites were identified from *in-vitro* nitration models, such as bovine serum albumin (BSA) treated with tetranitromethane (TNM) and Jurkat cell lysate exposed to peroxynitrite.

The authors also observed sulfated 3AY as a side product of reduction of Jurkat cell samples by SDT, where *ca.* 84% of peptides were partially sulfated. Thus, it is important to include sulfation when searching MS data against proteomic databases in experiments that use SDT.

Larsen *et al.* (37) combined COFRADIC with off-line nano-HPLC-MALDI-MS with tandem time-of-flight detection in a study that was limited to BSA nitrated *in vitro*, for which this method identified five 3NY sites. Advantages include the small amount of sample required and the potential for automation.

1.2.3 Fluorescent Labels

Incorporation of fluorescent moieties into nitropeptides or nitroproteins can provide a powerful tool for detection, with high signal-to-noise ratios, as well as for absolute and/or relative quantitation and for visualization in gels, Western blots, or tissue samples.

6-Substituted 2-Phenylbenzoxazoles

Several studies have demonstrated fluorogenic labeling of 3NY by reduction to 3AY with SDT followed by reaction with benzylamine (57,74) or benzylamine derivatives, 4-(aminomethyl)benzenesulfonic acid (ABS) (73) or (3*R*,4*S*)-1-(4-(aminomethyl)phenylsulfonyl)pyrrolidine-3,4-diol (APPD) (16) (Fig. 7). A major advantage of this strategy is the selectivity for the *o*-aminophenol moiety of 3AY, which precludes the need to block other reactive amines in the peptide or protein. The products are highly fluorescent 6-

substituted 2-phenylbenzoxazoles. For each reagent, three products have been characterized that differ in the substituent at the 6-position of the benzoxazole ring system but maintain similar fluorescent properties. Labeling can be followed by fluorescence detection and identification by MS. The method has also been applied for histochemical staining (75).

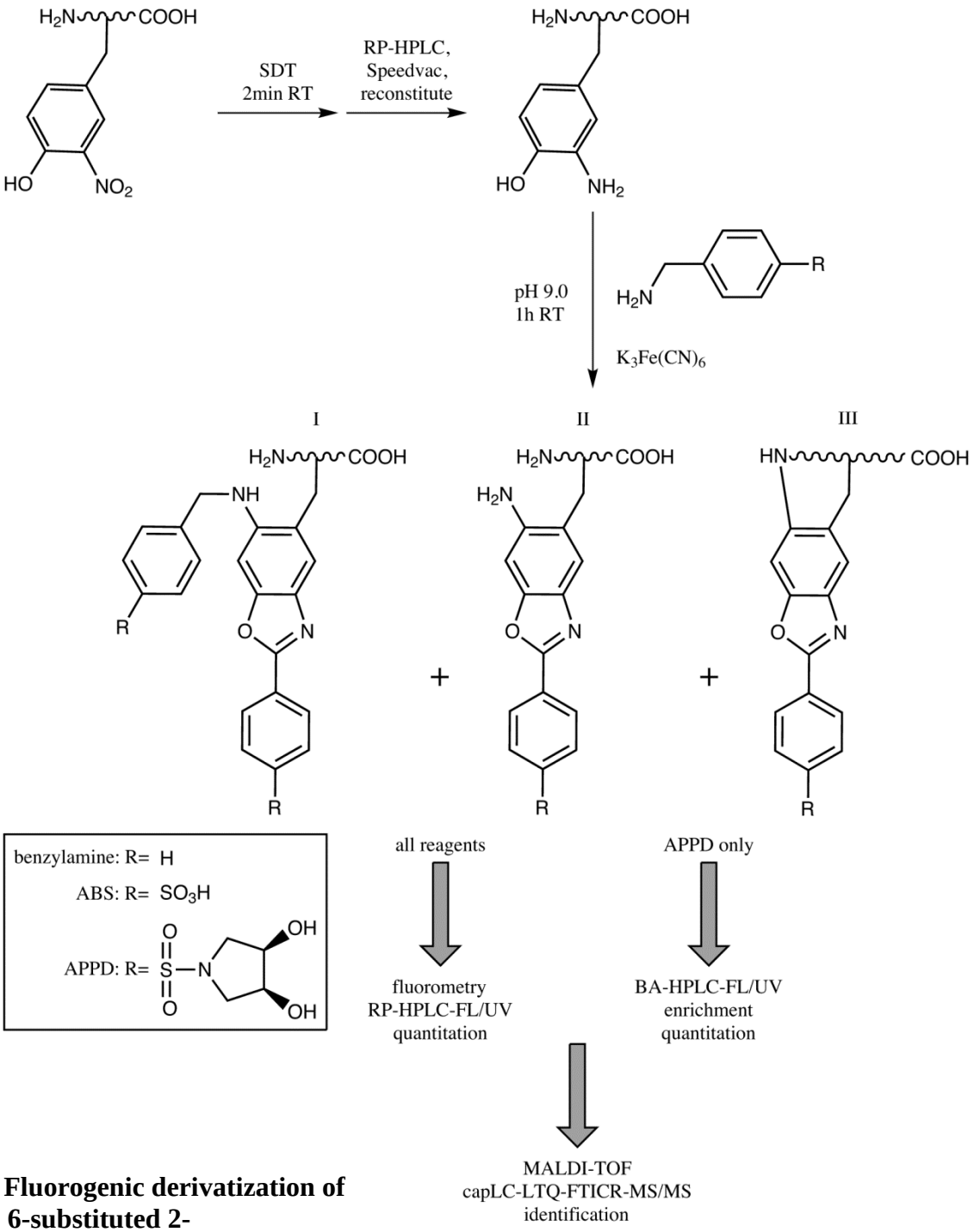

Fig. 7. Fluorogenic derivatization of 3NY to 6-substituted 2-phenylbenzoxazoles. Adapted and modified from Refs. (16,73,74). RT = room temperature, FL = fluorescence detection, UV = ultraviolet absorbance detection, TOF = time-of-flight, capLC = capillary liquid chromatography, LTQ = linear trap quadrupole (linear ion trap), FTICR = Fourier transform ion cyclotron resonance.

For a synthetic nitropeptide, FSA(3NY)LER, tagged with ABS, the fluorescence quantum yield was determined as 0.77 ± 0.08 (73), and limits of detection by fluorescence spectrometry were measured as 12pmol and 40pmol for the nitropeptide alone and in the presence of 100µg digested proteins from C2C12 murine myoblasts, a model background matrix, respectively. Each of the reagents is amenable to isotopic coding for MS-based relative quantitation (57,74).

Notably, 3,4-dihydroxyphenylalanine and 5-hydroxytryptophan can also be labeled by this method, without reduction by SDT (73). The identity of the detected post-translational modification (PTM) can thus be deduced using controls not treated with SDT.

1.2.4 Affinity Labels

In order to avoid ion suppression of low-abundance nitropeptides, as well as to address chromatographic capacity limits, specific and efficient labeling of 3NY for affinity-based enrichment is a promising strategy for nitroproteomics. There has been great interest in developing antibody-free methods to overcome disadvantages of specificity, reproducibility, and throughput.

Boronate Affinity

In the most recent development of a fluorogenic labeling strategy (57,73,74), Dremina *et al.* (16) describe a new benzylamine-derived reagent for derivatization and affinity enrichment of 3NY using boronate-affinity HPLC (BA-HPLC) (Fig. 7). The reagent APPD contains a benzylamine moiety for reaction with 3AY and a *cis*-diol moiety for pH-dependent coordination with boronic acid.

Both fluorescence spectrometry and BA-HPLC data (with fluorescence detection) can be used for quantitation of 3NY by this method, with limits of detection calculated as 19nmol and

13pmol, respectively, for a digest of rabbit phosphorylase *b* nitrated *in vitro* by peroxynitrite, alone or in a matrix of digested C2C12 murine myoblast proteins. Side product(s) can increase background and detection limits, but enrichment by BA-HPLC attenuates this problem.

Biotin

The high-affinity interaction of biotin with avidin and streptavidin makes it an attractive labeling moiety. As reviewed elsewhere (2,50), several groups have developed methods for biotinylation followed by enrichment on immobilized avidin or streptavidin.

The method of Abello *et al.* (1), summarized in Fig. 8, reduces the need for cleaning steps and pH changes, thus minimizing sample losses. Aliphatic amines are acetylated by N-hydroxysuccinimide (NHS) ester, 3NY is reduced to 3AY using the dithiothreitol/hemin system, and a large excess of biotinyl NHS ester completes the derivatization. Following both NHS-based reactions, heating in a bath of boiling water degrades remaining reagent and reverses any

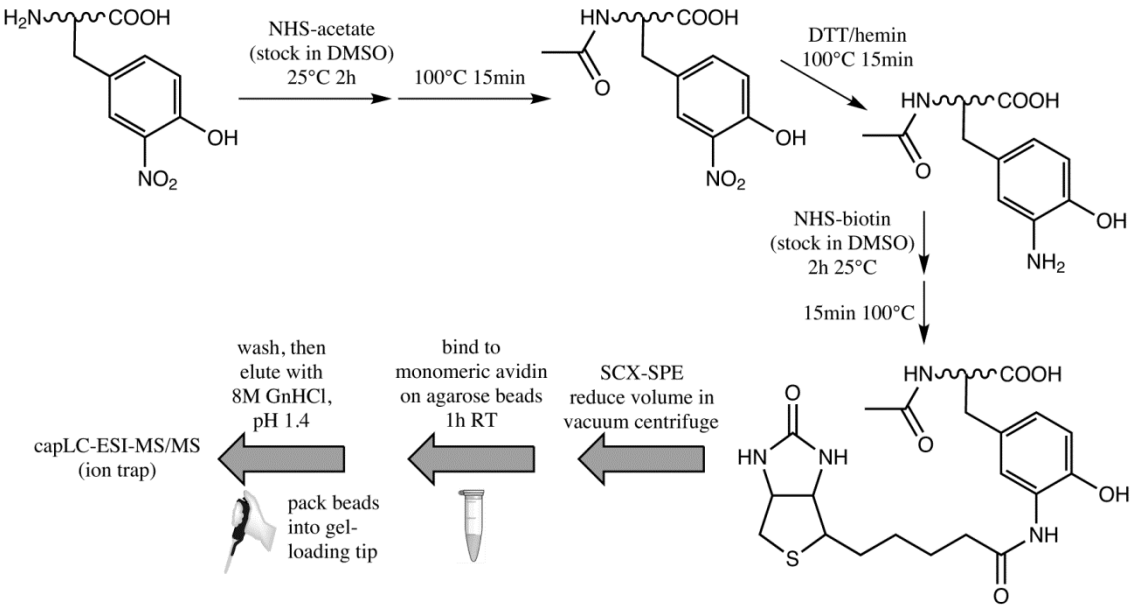

Fig. 8. Method for biotinylation of 3NY for affinity-based enrichment. This particular method minimizes sample cleaning steps. Adapted and modified from Ref. (1). NHS-acetate = acetic acid NHS ester, DMSO = dimethyl sulfoxide, DTT = dithiothreitol, NHS-biotin = biotinyl NHS ester, SCX = strong cation exchange, GnHCl = guanidinium hydrochloride.

undesirable O-acetylation or O-biotinylation. The single cleaning step required, a strong cation exchange solid-phase extraction (SPE) used to remove remaining biotin reagent, has poor recovery. After cleaning, the biotinylated peptides are enriched using a monomeric avidin resin and elution by guanidinium hydrochloride under acidic conditions.

The peptide angiotensin II (Ang II) was nitrated *in vitro* by peroxynitrite and spiked into a tryptic digest of BSA as a model system. Although the peptide was successfully labeled and recovered, the SPE cleaning step is a major source of sample loss. Therefore, the authors propose future work to perform all derivatization reactions on intact proteins, such that size-based separation methods (*e.g.*, gel filtration or dialysis) can be used instead.

Metal Chelation

A new adaption of immobilized metal affinity chromatography (IMAC) has been developed by Lee *et al.* (38) for the enrichment of 3NY-containing peptides (Fig. 9). Primary amines are blocked by acetylation with sulfo-NHS-acetate prior to SDT reduction of 3NY to 3AY, after which the latter undergoes Schiff base formation and reductive amination with a large excess of pyridine-2-carboxaldehyde and sodium cyanoborohydride to give peptides that are bispyridinylated at the original nitration sites, with small amounts of monopyridinylation. Desalting steps are required following each of these reactions. The labeled peptides now chelate nickel (II) attached to magnetic agarose beads. After binding and washing, peptides are released with imidazole or ethylenediaminetetraacetic acid, desalted, and identified by MALDI-MS with time-of-flight detection.

This approach was applied to synthetic nitrated Ang II and to BSA nitrated by TNM. The authors demonstrate detection of as little as 100fmol of nitropeptide spiked into a matrix of 10µg HeLa cell lysate. As absolute signal intensity values are not presented with the MS data, it

is unclear whether significant peptide losses occur during derivatization and cleaning steps. Also, while the mass shifts are generally in accord with expected values for each reaction step, all of the observed *m/z* values for Ang II and its derivatives appear higher than the corresponding theoretical values, with mass errors of 580-1080ppm, a phenomenon also seen in the data of Kim *et al.* (35) (described below).

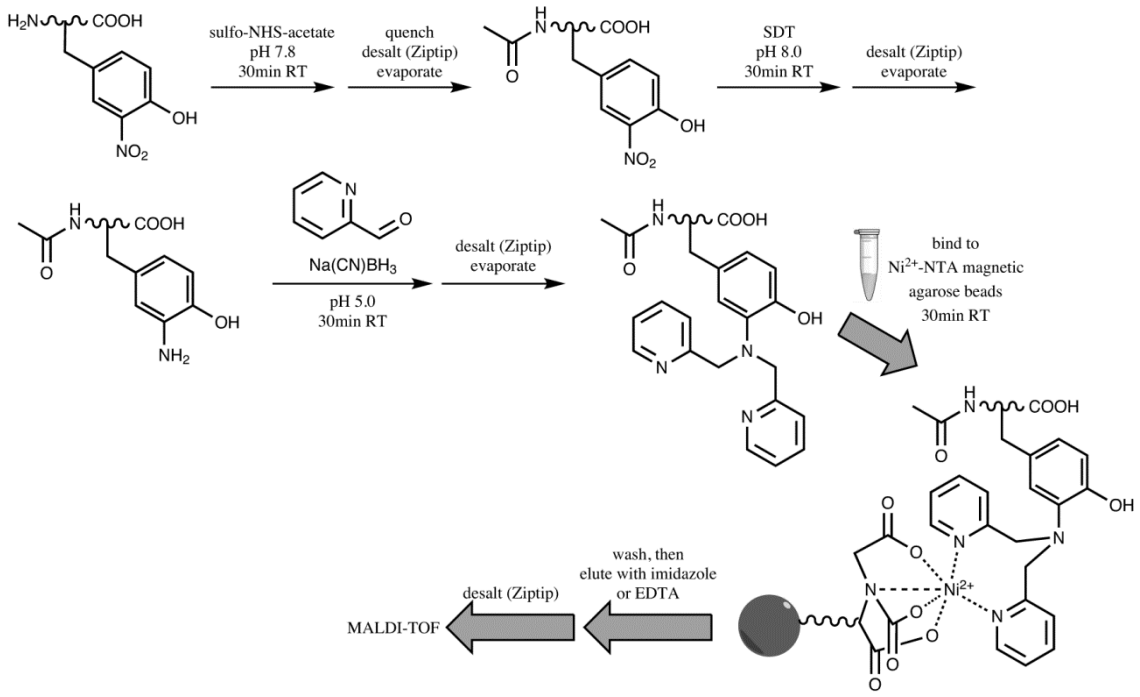

Fig. 9. IMAC method for enrichment of 3NY-containing peptides, by bispyridinylation of 3NY. Adapted and modified from Ref. (38). NTA = nitrilotriacetic acid, EDTA = ethylenediaminetetraacetic acid.

Fluorine Affinity

Some of the same researchers have also developed a strategy to derivatize 3NY with highly fluorinated moieties for enrichment by fluorinated SPE (FSPE) (35) (Fig. 10). After acetylation of aliphatic amines with sulfo-NHS-acetate and reduction of 3NY to 3AY with SDT, peptides are tagged with *N*-succinimidyl 3-(perfluorobutyl)propionate, with cleaning steps after each reaction. Labeled peptides are enriched using FSPE, and the eluates are analyzed by MS.

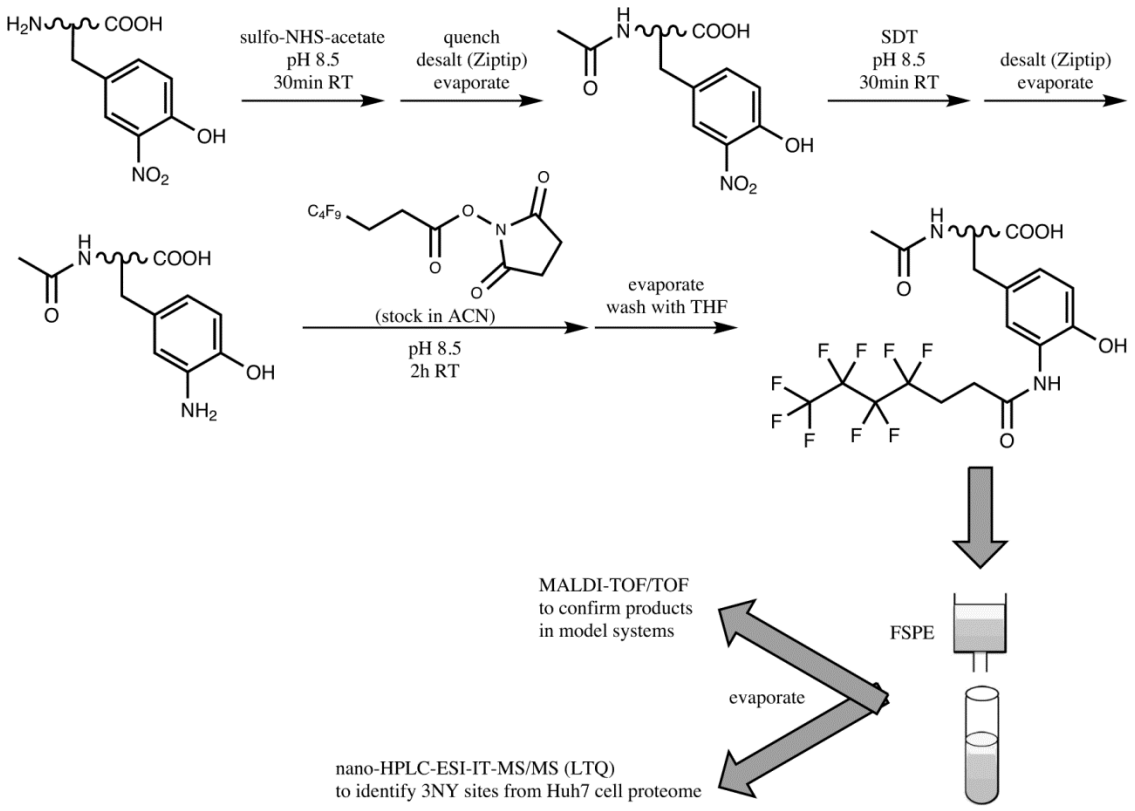

Fig. 10. Method for fluorination of 3NY for purification by FSPE. Adapted and modified from Ref. (35). ACN = acetonitrile, THF = tetrahydrofuran, TOF/TOF = tandem time-of-flight, IT = ion trap.

Using this strategy for synthetic nitrated Ang II mixed with its non-nitrated counterpart, successful derivatization and enrichment are demonstrated by MALDI-MS. Interestingly, the absolute MS intensity for the tagged peptide is much greater after FSPE than before, and, while not discussed in the article, this may be an indication of ion suppression in the crude sample that is overcome by the affinity purification step.

However, as in the IMAC study (38), there are systematic deviations of observed *m/z* values from the theoretical values, especially for nitrated Ang II and its derivatives, which show large mass errors of +580-1038ppm. The mass shifts after each reaction are generally as expected, except for $\Delta m/z$=46.1 between native and nitrated Ang II (the expected value is 45.0).

Inadequate instrument calibration is one possible explanation for this combination of phenomena, but the article does not discuss it. Also, there are some additional peaks in the final product spectrum that are not explained. Among them is a small peak near 1100 *m/z*, which could represent amino-Ang II (1104 *m/z*), but the absence of annotation for this peak precludes a definitive determination. At the characteristically low ionization efficiency of the amino-peptide, even a small peak can represent a significant amount of peptide that was not tagged.

The decrease in absolute intensity of the MALDI peak for the non-nitrated, acetylated peptide following subsequent steps probably results from sample losses due to cleaning, or perhaps due to reaction conditions (*e.g.*, possible side products or peptide degradation). These losses can become very important when looking for low-abundant PTMs, like 3NY.

The method was able to tag, enrich, and detect 100pmol of nitrated Ang II in a background of 10µg of a BSA tryptic digest. More notably, 28 endogenously nitrated peptides from 28 proteins were identified in the Huh7 human hepatoma cell line, and the 3NY sites were confirmed by MS/MS with manual validation. Some of the peptide spectra show XCorr scores [cross-correlation values generated by the SEQUEST algorithm (20)] that are lower than ideal, possibly indicating a poor fit to the theoretical spectra for the assigned peptide sequences. The most intense peaks in the MS/MS spectra are assigned, but only one spectrum shown has backbone cleavages on both sides of the tagged Tyr, which is stronger evidence for nitration site assignment. Not all of the Lys residues are acetylated, even though the text listed this modification as a requirement for acceptance of the identification. In contrast, all of the N-termini are acetylated in the identified peptides. For two of the identifications, the nitration site is located in a specific functional domain.

1.2.5 Solid-Phase Chemistry

Several methods have used covalent reactions between the peptide of interest and a solid-phase reagent, followed by chemical cleavage to recover the peptide with a vestigial tagging moiety that can be identified during MS analysis. Recent studies have endeavored to improve upon the earlier methods of Zhang *et al.* (93) and Nikov *et al*. (49).

Chemoprecipitation Using Solid-Phase Activated Ester Reagent

In order to simplify the derivatization procedure and avoid sample losses incurred by cleaning steps, Prokai-Tatrai *et al.* (60) developed a chemoprecipitation technique in which amine groups are blocked by reductive methylation, 3NY is reduced to 3AY, and the latter reacts with a solid-phase active ester reagent (SPAER) on glass beads, followed by washing and gentle acid-catalyzed hydrolysis to remove the peptides, which retain a 4-formylbenzoylamido group (Fig. 11). By solution methods, the dimethylation step requires clean-up by SPE, but a one-pot method using solid-phase reagents is also reported. Importantly, dimethylation prevents non-selective labeling of amine groups while retaining their ability to ionize for facile detection in positive-mode HPLC-ESI-MS/MS.

In addition to identifying tagged derivatives of three synthetic nitropeptides in a BSA tryptic digest matrix (>200-fold molar excess of unmodified over nitrated peptides), 32 unique tagged peptides were identified from 12 different proteins in a tryptic digest of human plasma samples that were nitrated *in vitro* by TNM, some of which were previously found nitrated in aging and disease states. Eight contaminating, unmodified peptides from plasma proteins were also identified. This is attributed to non-specific adsorption to the beads, which the authors propose to address by more thorough washing with organic solvents.

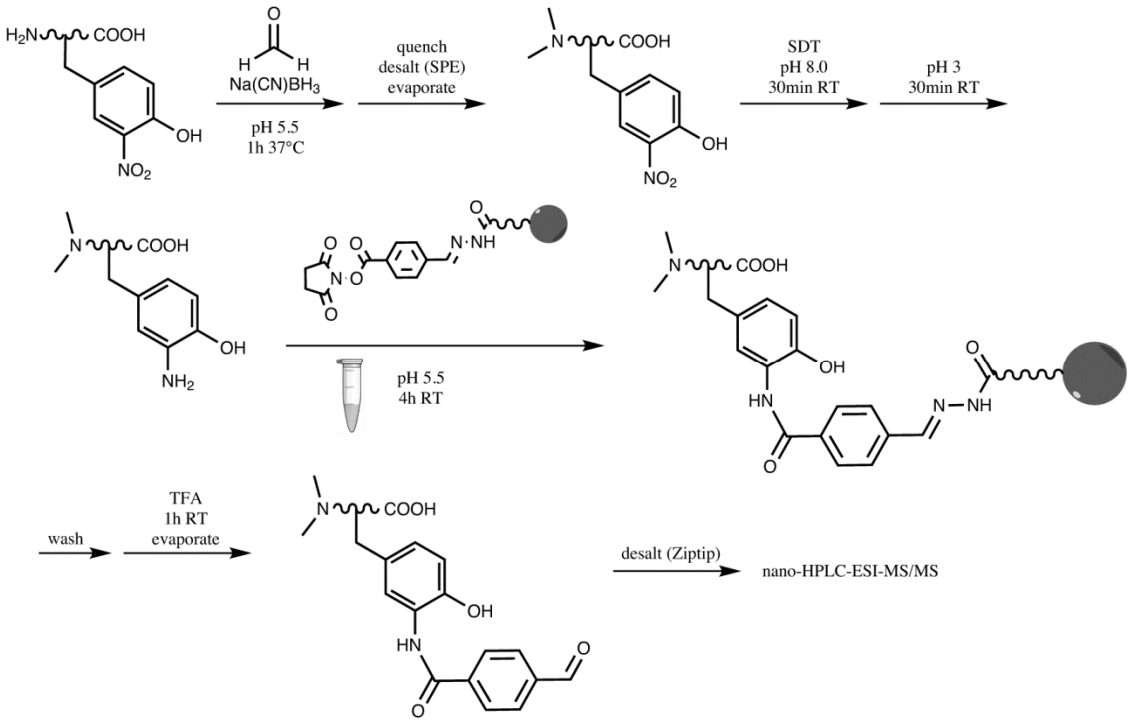

Fig. 11. SPAER method for enrichment of 3NY by chemoprecipitation. This represents the solution-phase method, but a solid-phase method was also tested. Adapted and modified from Ref. (60). Incorporation of isotopic labels for relative quantitation is further described in Ref. (29). TFA = trifluoroacetic acid.

Building upon this work, Guo *et al.* (29) developed a method for relative quantitation by using isotopically labeled formaldehyde for reductive methylation, which did not alter the chromatographic properties of the products. This method was successfully applied to two model systems: synthetic nitropeptides spiked into a matrix containing the tryptic digest of human serum albumin and the model protein ubiquitin nitrated *in vitro* and spiked into a matrix of human plasma (29).

1.2.6 Quantitation

An important strategy for quantitation of 3NY consists of using isotopically coded reagents for differential labeling of samples from two (or more) experimental conditions and mixing these samples prior to MS analysis, thus allowing for quantitative comparisons of ion

peak areas. While this is largely applied to relative quantitation, there are ways to achieve absolute quantitation by including an isotopically labeled internal standard. Isobaric tagging strategies have also emerged, which maintain a single *m/z* value for precursor ions but yield specific reporter ions after fragmentation, with the latter used for quantitation. These include tandem mass tags (TMT) (83) and isobaric tags for relative and absolute quantitation (iTRAQ) (64).

iTRAQ

The iTRAQ method was developed based on labeling primary amines for profiling whole proteomes (64). By acetylating primary amines with acetic acid NHS ester, then reducing 3NY to 3AY with SDT, and finally labeling 3AY with iTRAQ reagents, with some cleaning procedures required, Chiappetta *et al.* (10) have adapted the iTRAQ methodology for identification and quantitation of 3NY sites (Fig. 12). Nano-HPLC-ESI-MS/MS was performed in the precursor ion scanning mode for specific reporter ions, which enabled the use of the mass spectrometer's duty cycle for analyzing only peptides of interest and thus enhanced the limit of detection without the need for affinity purification/enrichment.

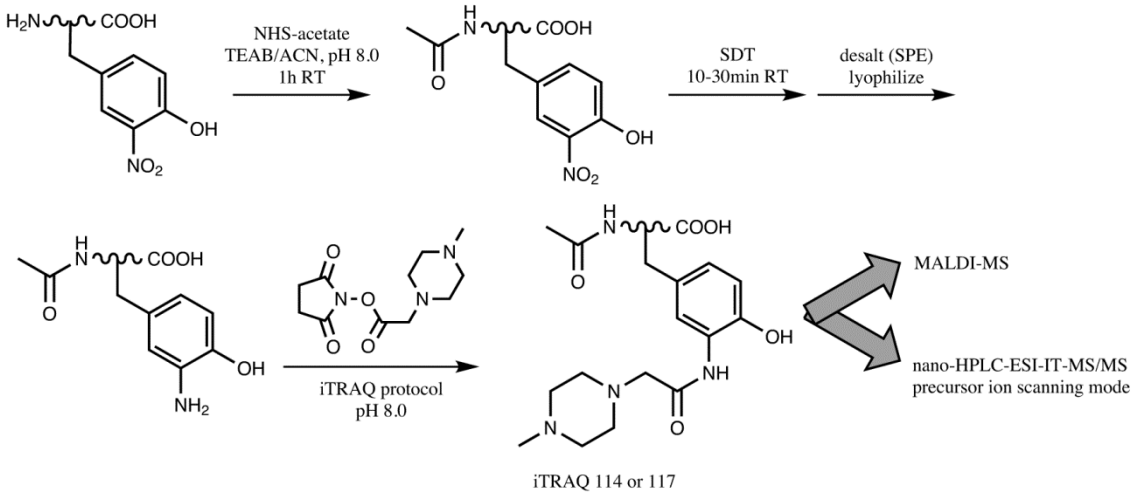

Fig. 12. Relative quantitation of 3NY with an adaptation of the iTRAQ method. Adapted and modified from Ref. (10). TEAB = tetraethylammonium bicarbonate.

This method was applied to BSA nitrated *in vitro* by TNM, alone or in the presence of 30mg of *E. coli* protein extract, and to bovine milk proteins nitrated *in vitro* with TNM. For the latter, nine 3NY sites were identified, which were found in both high- and low-abundance proteins, with accurate relative quantitation for seven of them.

Two-Dimensional Isotopic Coding

Building on previous work (84), Tsumoto *et al.* (85) developed a method to increase the ionization efficiency of tryptic nitropeptides, prevent their photodecomposition during MALDI experiments, and incorporate isotopic labels (Fig. 13). Due to the two-dimensional nature of this isotopic labeling strategy, with the first dimension applied to all peptides and the second dimension applied only to 3NY, both non-nitrated and nitrated peptides are quantitatively compared between two samples in a single experiment. This feature was used to quantify the degree of nitration achieved by *in-vitro* methods for specific Tyr residues. Although not explicitly discussed, it could also be very useful to control for protein expression levels, an important concern for comparative proteomic profiling of PTMs. Any 3NY labeling strategy that includes a step to block aliphatic amines could likely be adapted to take advantage of this feature.

Following acetylation of aliphatic amines with light or heavy acetic anhydride, 3NY is reduced to 3AY by SDT for subsequent tagging with 1-(6-methyl[D_0/D_3]nicotinoyloxy)succinimide, with appropriate cleaning procedures, followed by MS analysis.

Two model systems were used, synthetic nitrated Ang II and BSA nitrated *in vitro* with peroxynitrite. Ionization efficiency of tagged peptides was greatly improved compared to their 3NY- or 3AY-containing counterparts, recovering to about the same level as the acetylated, non-

nitrated peptide. Since no absolute intensities are shown for the mass spectra, it is not possible to compare samples for peptide losses during derivatization and cleaning steps.

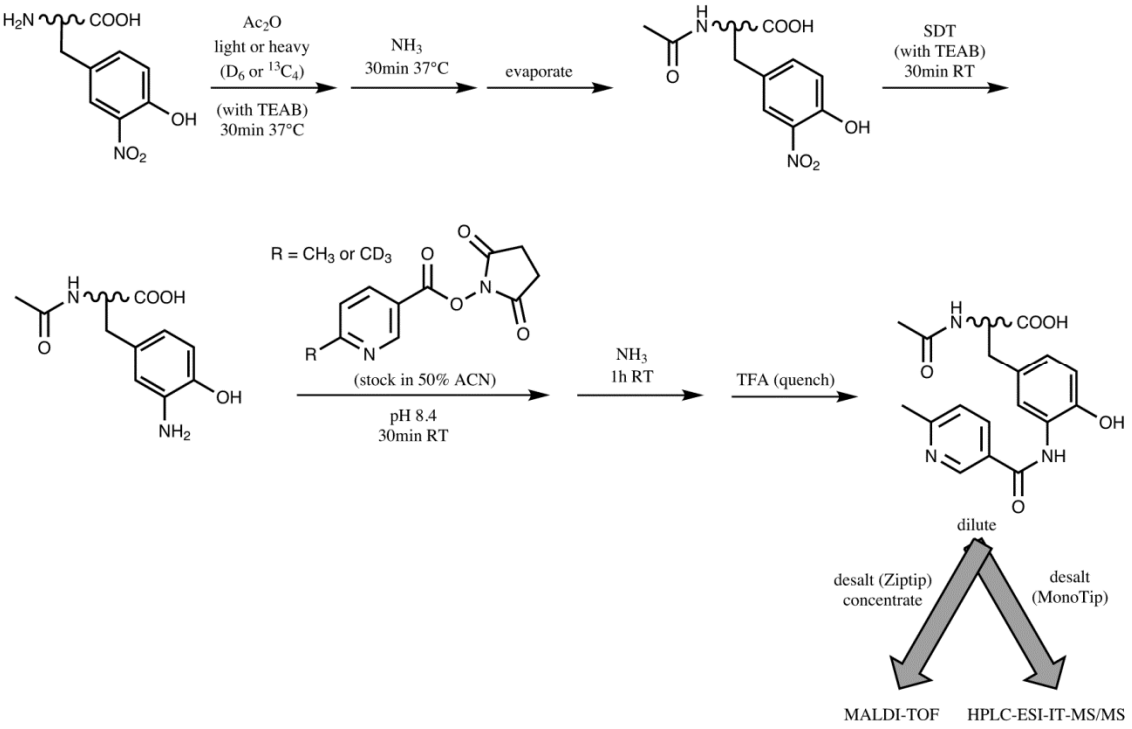

Fig. 13. Method for isotopic coding of 3NY for quantitation. Adapted and modified from Ref. (85). Ac_2O = acetic anhydride.

cPILOT

Robinson *et al.* (63) developed the method of combined precursor isotopic labeling and isobaric tagging (cPILOT) in order to multiplex as many as 16 samples, using the previously reported isobaric tagging methods TMT (83) and iTRAQ (64) (Fig. 14). This allows for simultaneous comparison of numerous biological samples, which is more cost-efficient. After acetylating amines with light or heavy N-acetoxysuccinimide to give duplexed samples, SDT reduces 3NY to 3AY, and sets of either TMT or iTRAQ reagents complete the derivatization, with up to 16-plex experiments possible in theory and no cleaning steps required until immediately prior to MS.

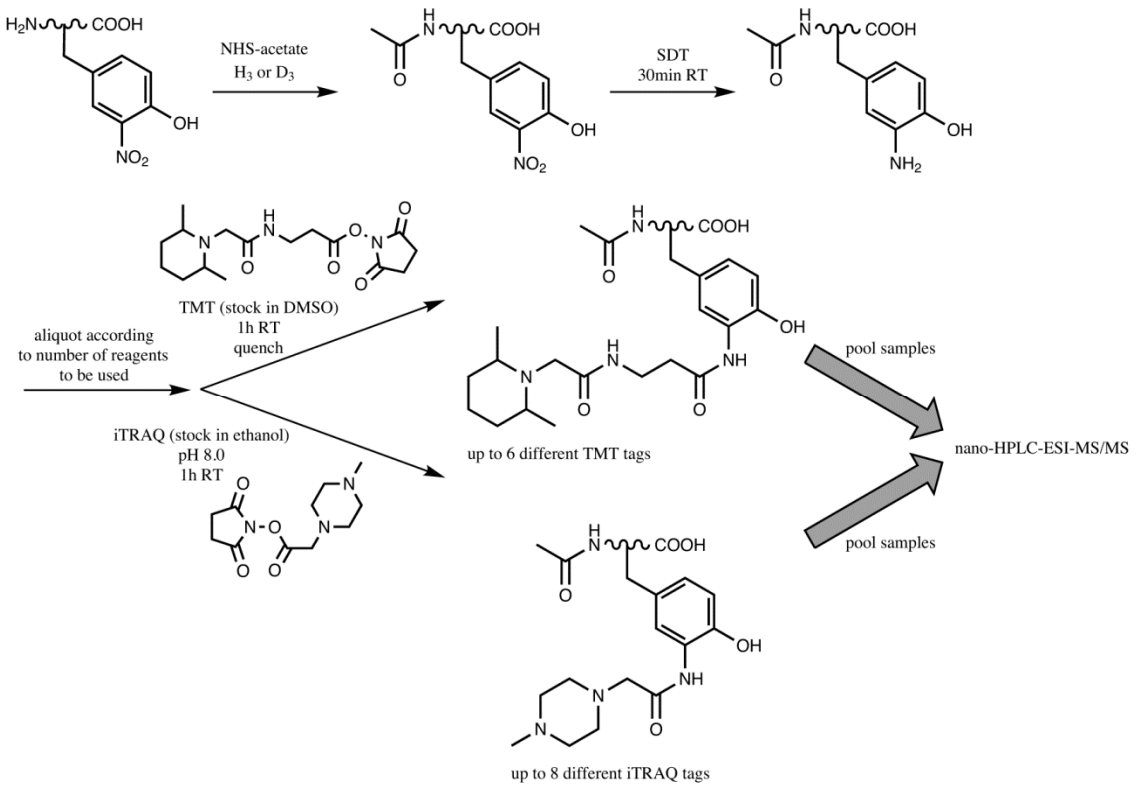

Fig. 14. Multiplexed method for relative quantitation of 3NY in up to 16 samples. Adapted and modified from (63).

Using BSA nitrated *in vitro* by peroxynitrite as a model, a 12-plex experiment (duplexed acetylation combined with 6-plex TMT) showed overlap in the precursor ion isolation, causing inaccurate quantitation (63). For investigation of unknown, *in-vivo* nitration sites in the mouse spleen proteome, scaling back to 4-plex still resulted in some overlap, but the relative quantitation was accurate nevertheless. Notably, five endogenous nitration sites were identified from five unique proteins. Possible improvements include enrichment strategies prior to labeling to increase proteomic identifications and an increase in the mass shift for the first dimension of isotopic labeling to overcome the problem of precursor ion overlap.

1.2.7 Conclusions

Despite many successful proof-of-concept studies with model systems, detection of endogenous 3NY remains a significant challenge. At present, most endogenous 3NY assignments are still based on 2D-PAGE/Western blot and immunoprecipitation methods (2). Of the recent studies covered in this review, only three (25,35,63) successfully identified *in-vivo* nitration sites, for a total of 39 sites in 37 different proteins. Other successful studies (65,95) did not derivatize 3NY but used pre-fractionation and advanced HPLC-MS equipment, most notably capillary columns that were 65cm in length, compared to 10-15cm for most other studies.

This difficulty may be due to a combination of very low levels of endogenous 3NY and sample losses during derivatization and cleaning steps. Many studies (1,10,16,29,35,38,85) rely on the disappearance of mass spectral peaks for the starting materials to demonstrate "complete" conversion for each reaction. However, this is not a truly quantitative technique, especially when MALDI is used, and furthermore this data cannot account for sample losses (*e.g.*, due to adsorption on plastic or glassware) or undetected side products.

Successful nitroproteomics requires selective separation and/or purification of nitropeptides from the matrix of non-modified peptides in order to reduce ion suppression and remain within limits of column capacity for HPLC-MS/MS. This must be done with a minimum of sample losses, especially considering the low abundance of 3NY *in vivo* and the small amounts of biological material that are often available from precious specimens. Indeed, several of the most successful methods to date have either avoided 3NY derivatization completely (65,95) or kept it to a minimum (25).

1.3 Specific Aims

Toward the goals of labeling, enrichment, identification, and relative quantitation of the protein oxidation products 3,4-dihydroxyphenylalanine (DOPA) and 3-nitrotyrosine (3NY), this thesis project applies benzylamine-dependent chemistry to model peptides, model proteins, and cardiac tissue samples from a rat model for aging. This project encompasses method optimization, the effect of primary structure on tagging properties, and the search for potential age-dependent differences in cardiac protein modification. Based on previous evidence of 3NY accumulation in cardiac proteins during aging (32), as well as other conditions of oxidative stress like diabetes (86), this tissue was selected for application of the novel labeling method. Many challenges of translating such a method from simple model systems to complex biological sample are explored, and a variety of optimization efforts are described. In addition, the model protein glycogen phosphorylase *b* (Ph-b) is used to measure the method's limit of detection by fluorescence spectrometry and to study the effect of the cardiac homogenate matrix on 3NY residues. Finally, a series of model peptides are labeled and quantitatively analyzed to determine fluorescence quantum yields, molar absorptivities, and chemical reaction yields of labeled products and to compare these properties in peptides of varying sequence and physicochemical properties.

1.4 References

1. Abello N, Barroso B, Kerstjens HAM, Postma DS, Bischoff R. Chemical labeling and enrichment of nitrotyrosine-containing peptides. *Talanta* 80: 1503-1512, 2010.
2. Abello N, Kerstjens HAM, Postma DS, Bischoff R. Protein tyrosine nitration: selectivity, physicochemical and biological consequences, denitration, and proteomics methods for the identification of tyrosine-nitrated proteins. *J Proteome Res* 8: 3222-3238, 2009.

3. Ajees AA, Anantharamaiah GM, Mishra VK, Hussain MM, Murthy HMK. Crystal structure of human apolipoprotein A-I: Insights into its protective effect against cardiovascular diseases. *Proc Natl Acad Sci U S A* 103: 2126-2131, 2006.

4. Balabanli B, Kamisaki Y, Martin E, Murad F. Requirements for heme and thiols for the nonenzymatic modification of nitrotyrosine. *Proc Natl Acad Sci U S A* 96: 13136-13141, 1999.

5. Bartesaghi S, Wenzel J, Trujillo M, López M, Joseph J, Kalyanaraman B, Radi R. Lipid peroxyl radicals mediate tyrosine dimerization and nitration in membranes. *Chem Res Toxicol* 23: 821-835, 2010.

6. Bergt C, Fu X, Huq NP, Kao J, Heinecke JW. Lysine residues direct the chlorination of tyrosines in YXXK motifs of apolipoprotein A-I when hypochlorous acid oxidizes high density lipoprotein. *J Biol Chem* 279: 7856-7866, 2004.

7. Bigelow DJ, Qian WJ. Quantitative proteome mapping of nitrotyrosines. *Methods Enzymol* 440: 191-205, 2008.

8. Bischoff R, Schlüter H. Amino acids: chemistry, functionality and selected non-enzymatic post-translational modifications. *J Proteomics* 75: 2275-2296, 2012.

9. Brennan M-L, Penn MS, Van Lente F, Nambi V, Shishehbor MH, Aviles RJ, Goormastic M, Pepoy ML, McErlean ES, Topol EJ, Nissen SE, Hazen SL. Prognostic value of myeloperoxidase in patients with chest pain. *N Engl J Med* 349: 1595-1604, 2003.

10. Chiappetta G, Corbo C, Palmese A, Marino G, Amoresano A. Quantitative identification of protein nitration sites. *PROTEOMICS* 9: 1524-1537, 2009.

11. Coval ML, Taurog A. Purification and iodinating activity of hog thyroid peroxidase. *J Biol Chem* 242: 5510-5523, 1967.

12. Cowan-Jacob SW, Kaufmann M, Anselmo AN, Stark W, Grütter MG. Structure of rabbit-muscle glyceraldehyde-3-phosphate dehydrogenase. *Acta Crystallogr D Biol Crystallogr* 59: 2218-2227, 2003.

13. Davies KJA, Shringarpure R. Preferential degradation of oxidized proteins by the 20S proteasome may be inhibited in aging and in inflammatory neuromuscular diseases. *Neurology* 66: S93-S96, 2006.

14. Dean RT, Fu S, Stocker R, Davies MJ. Biochemistry and pathology of radical-mediated protein oxidation. *Biochem J* 324: 1-18, 1997.

15. Deeb R, Nuriel T, Gross SS. Untargeted discovery of nitric oxide-modified proteins. In: *Nitric Oxide: Biology and Pathobiology*. edited by Ignarro LJ. San Diego, CA: Academic Press; 2010. pp. 327-389.

16. Dremina ES, Li X, Galeva NA, Sharov VS, Stobaugh JF, Schöneich C. A methodology for simultaneous fluorogenic derivatization and boronate affinity enrichment of 3-nitrotyrosine-containing peptides. *Anal Biochem* 418: 184-196, 2011.

17. Duncan MW. A review of approaches to the analysis of 3-nitrotyrosine. *Amino Acids* 25: 351-361, 2003.

18. Dunlop RA, Brunk UT, Rodgers KJ. Proteins containing oxidized amino acids induce apoptosis in human monocytes. *Biochem J* 435: 207-216, 2011.

19. Dunlop RA, Dean RT, Rodgers KJ. The impact of specific oxidized amino acids on protein turnover in J774 cells. *Biochem J* 410: 131-140, 2008.

20. Eng JK, McCormack AL, Yates III JR. An approach to correlate tandem mass spectral data of peptides with amino acid sequences in a protein database. *J Am Soc Mass Spectrom* 5: 976-989, 1994.

21. Feeney MB, Schöneich C. Proteomic Approaches to Analyze Protein Tyrosine Nitration. *Antioxid Redox Signal* in press, 2012.

22. Feeney MB, Schöneich C. Tyrosine modifications in aging. *Antioxid Redox Signal* 17: 1571-1579, 2012.

23. Fu S, Davies MJ, Stocker R, Dean RT. Evidence for roles of radicals in protein oxidation in advanced human atherosclerotic plaque. *Biochem J* 333: 519-525, 1998.

24. Fu S, Dean R, Southan M, Truscott R. The hydroxyl radical in lens nuclear cataractogenesis. *J Biol Chem* 273: 28603-28609, 1998.

25. Ghesquière B, Colaert N, Helsens K, Dejager L, Vanhaute C, Verleysen K, Kas K, Timmerman E, Goethals M, Libert C, Vandekerckhove J, Gevaert K. In vitro and in vivo protein-bound tyrosine nitration characterized by diagonal chromatography. *Mol Cell Proteomics* 8: 2642-2652, 2009.

26. Ghesquière B, Goethals M, Van Damme J, Staes A, Timmerman E, Vandekerckhove J, Gevaert K. Improved tandem mass spectrometric characterization of 3-nitrotyrosine sites in peptides. *Rapid Commun Mass Spectrom* 20: 2885-2893, 2006.

27. Gieseg SP, Simpson JA, Charlton TS, Duncan MW, Dean RT. Protein-bound 3,4-dihydroxyphenylalanine is a major reductant formed during hydroxyl radical damage to proteins. *Biochemistry* 32: 4780-4786, 1993.

28. Giulivi C, Traaseth NJ, Davies KJA. Tyrosine oxidation products: analysis and biological relevance. *Amino Acids* 25: 227-232, 2003.

29. Guo J, Prokai-Tatrai K, Prokai L. Relative quantitation of protein nitration by liquid chromatography–mass spectrometry using isotope-coded dimethyl labeling and chemoprecipitation. *J Chromatogr A* 1232: 266-275, 2012.

30. Hazen SL, Heinecke JW. 3-Chlorotyrosine, a specific marker of myeloperoxidase-catalyzed oxidation, is markedly elevated in low density lipoprotein isolated from human atherosclerotic intima. *J Clin Invest* 99: 2075-2081, 1997.

31. Jones AW, Mikhailov VA, Iniesta J, Cooper HJ. Electron capture dissociation mass spectrometry of tyrosine nitrated peptides. *J Am Soc Mass Spectrom* 21: 268-277, 2010.

32. Kanski J, Behring A, Pelling J, Schöneich C. Proteomic identification of 3-nitrotyrosine-containing rat cardiac proteins: effects of biological aging. *Am J Physiol Heart Circ Physiol* 288: H371-H381, 2005.

33. Kanski J, Hong SJ, Schöneich C. Proteomic analysis of protein nitration in aging skeletal muscle and identification of nitrotyrosine-containing sequences in vivo by nanoelectrospray ionization tandem mass spectrometry. *J Biol Chem* 280: 24261-24266, 2005.

34. Kanski J, Schöneich C. Protein nitration in biological aging: proteomic and tandem mass spectrometric characterization of nitrated sites. *Methods Enzymol* 396: 160-171, 2005.

35. Kim JK, Lee JR, Kang JW, Lee SJ, Shin GC, Yeo W-S, Kim K-H, Park HS, Kim KP. Selective enrichment and mass spectrometric identification of nitrated peptides using fluorinated carbon tags. *Anal Chem* 83: 157-163, 2011.

36. Kurz T, Terman A, Gustafsson B, Brunk U. Lysosomes in iron metabolism, ageing and apoptosis. *Histochem Cell Biol* 129: 389-406, 2008.

37. Larsen T, Bache N, Gramsbergen J, Roepstorff P. Identification of nitrotyrosine containing peptides using combined fractional diagonal chromatography (COFRADIC) and off-line nano-LC-MALDI. *J Am Soc Mass Spectrom* 22: 989-996, 2011.

38. Lee JR, Lee SJ, Kim TW, Kim JK, Park HS, Kim D-E, Kim KP, Yeo W-S. Chemical approach for specific enrichment and mass analysis of nitrated peptides. *Anal Chem* 81: 6620-6626, 2009.

39. Lee S, Chen Y, Luo H, Wu AA, Wilde M, Schumacker PT, Zhao Y. The first global screening of protein substrates bearing protein-bound 3,4-Dihydroxyphenylalanine in Escherichia coli and human mitochondria. *J Proteome Res* 9: 5705-5714, 2010.

40. Lee SJ, Lee JR, Kim YH, Park YS, Park SI, Park HS, Kim KP. Investigation of tyrosine nitration and nitrosylation of angiotensin II and bovine serum albumin with electrospray ionization mass spectrometry. *Rapid Commun Mass Spectrom* 21: 2797-2804, 2007.

41. Lozano-Juste J, Colom-Moreno R, León J. In vivo protein tyrosine nitration in Arabidopsis thaliana. *J Exp Bot* 62: 3501-3517, 2011.

42. MacMillan-Crow LA, Crow JP, Thompson JA. Peroxynitrite-mediated inactivation of manganese superoxide dismutase involves nitration and oxidation of critical tyrosine residues. *Biochemistry* 37: 1613-1622, 1998.

43. Mikhailov VA, Iniesta J, Cooper HJ. Top-down mass analysis of protein tyrosine nitration: comparison of electron capture dissociation with “slow-heating” tandem mass spectrometry methods. *Anal Chem* 82: 7283-7292, 2010.

44. Mizdrak J, Hains PG, Truscott RJW, Jamie JF, Davies MJ. Tryptophan-derived ultraviolet filter compounds covalently bound to lens proteins are photosensitizers of oxidative damage. *Free Radic Biol Med* 44: 1108-1119, 2008.

45. Moreland J, Gramada A, Buzko O, Zhang Q, Bourne P. The Molecular Biology Toolkit (MBT): a modular platform for developing molecular visualization applications. *BMC Bioinformatics* 6: 21, 2005.

46. Nelson M, Foxwell AR, Tyrer P, Dean RT. Protein-bound 3,4-dihydroxy-phenylanine (DOPA), a redox-active product of protein oxidation, as a trigger for antioxidant defences. *Int J Biochem Cell Biol* 39: 879-889, 2007.

47. Nelson M, Foxwell AR, Tyrer P, Dean RT. Radical sequestration by protein-bound 3,4-dihydroxyphenylalanine. *Int J Biochem Cell Biol* 42: 755-761, 2010.

48. Neumann H, Hazen JL, Weinstein J, Mehl RA, Chin JW. Genetically Encoding Protein Oxidative Damage. *Journal of the American Chemical Society* 130: 4028-4033, 2008.

49. Nikov G, Bhat V, Wishnok JS, Tannenbaum SR. Analysis of nitrated proteins by nitrotyrosine-specific affinity probes and mass spectrometry. *Anal Biochem* 320: 214-222, 2003.

50. Nuriel T, Deeb RS, Hajjar DP, Gross SS. Protein 3-nitrotyrosine in complex biological samples: quantification by high-pressure liquid chromatography/electrochemical detection and emergence of proteomic approaches for unbiased identification of modification sites. *Methods Enzymol* 441: 1-17, 2008.

51. Nuriel T, Hansler A, Gross SS. Protein nitrotryptophan: formation, significance and identification. *J Proteomics* 74: 2300-2312, 2011.

52. Pacher P, Beckman JS, Liaudet L. Nitric oxide and peroxynitrite in health and disease. *Physiol Rev* 87: 315-424, 2007.

53. Palamalai V, Miyagi M. Mechanism of glyceraldehyde-3-phosphate dehydrogenase inactivation by tyrosine nitration. *Protein Sci* 19: 255-262, 2010.

54. Pattison DI, Dean RT, Davies MJ. Oxidation of DNA, proteins and lipids by DOPA, protein-bound DOPA, and related catechol(amine)s. *Toxicology* 177: 23-37, 2002.

55. Peng D-Q, Brubaker G, Wu Z, Zheng L, Willard B, Kinter M, Hazen SL, Smith JD. Apolipoprotein A-I tryptophan substitution leads to resistance to myeloperoxidase-mediated loss of function. *Arterioscler Thromb Vasc Biol* 28: 2063-2070, 2008.

56. Peng D-Q, Wu Z, Brubaker G, Zheng L, Settle M, Gross E, Kinter M, Hazen SL, Smith JD. Tyrosine modification is not required for myeloperoxidase-induced loss of apolipoprotein A-I functional activities. *J Biol Chem* 280: 33775-33784, 2005.

57. Pennington JP, Schöneich C, Stobaugh J. Selective fluorogenic derivatization with isotopic coding of catechols and 2-amino phenols with benzylamine: a chemical basis for the relative determination of 3-hydroxy-tyrosine and 3-nitro-tyrosine peptides. *Chromatographia* 66: 649-659, 2007.

58. Petersson A-S, Steen H, Kalume DE, Caidahl K, Roepstorff P. Investigation of tyrosine nitration in proteins by mass spectrometry. *J Mass Spectrom* 36: 616-625, 2001.

59. Podrez EA, Abu-Soud HM, Hazen SL. Myeloperoxidase-generated oxidants and atherosclerosis. *Free Radic Biol Med* 28: 1717-1725, 2000.

60. Prokai-Tatrai K, Guo J, Prokai L. Selective chemoprecipitation and subsequent release of tagged species for the analysis of nitropeptides by liquid chromatography–tandem mass spectrometry. *Mol Cell Proteomics* 10: M110.002923, 2011.

61. Quint P, Reutzel R, Mikulski R, McKenna R, Silverman DN. Crystal structure of nitrated human manganese superoxide dismutase: mechanism of inactivation. *Free Radic Biol Med* 40: 453-458, 2006.

62. Radi R. Nitric oxide, oxidants, and protein tyrosine nitration. *Proc Natl Acad Sci U S A* 101: 4003-4008, 2004.

63. Robinson RAS, Evans AR. Enhanced sample multiplexing for nitrotyrosine-modified proteins using combined precursor isotopic labeling and isobaric tagging. *Anal Chem* 84: 4677-4686, 2012.

64. Ross PL, Huang YN, Marchese JN, Williamson B, Parker K, Hattan S, Khainovski N, Pillai S, Dey S, Daniels S, Purkayastha S, Juhasz P, Martin S, Bartlet-Jones M, He F, Jacobson A, Pappin DJ. Multiplexed protein quantitation in Saccharomyces cerevisiae using amine-reactive isobaric tagging reagents. *Mol Cell Proteomics* 3: 1154-1169, 2004.

65. Sacksteder CA, Qian W-J, Knyushko TV, Wang H, Chin MH, Lacan G, Melega WP, Camp DG, Smith RD, Smith DJ, Squier TC, Bigelow DJ. Endogenously nitrated proteins in mouse brain: links to neurodegenerative disease. *Biochemistry* 45: 8009-8022, 2006.

66. Sarver A, Scheffler NK, Shetlar MD, Gibson BW. Analysis of peptides and proteins containing nitrotyrosine by matrix-assisted laser desorption/ionization mass spectrometry. *J Am Soc Mass Spectrom* 12: 439-448, 2001.

67. Scaloni A. Mass spectrometry approaches for the molecular characterization of oxidatively/nitrosatively modified proteins. In: *Redox Proteomics: From Protein Modifications to Cellular Dysfunction and Diseases*. edited by Dalle-Donne I, Scaloni A, Butterfield DA. Hoboken, NJ: Wiley-Interscience; 2006. pp. 59-99.

68. Schöneich C, Sharov VS. Mass spectrometry of protein modifications by reactive oxygen and nitrogen species. *Free Radic Biol Med* 41: 1507-1520, 2006.

69. Shao B, Bergt C, Fu X, Green P, Voss JC, Oda MN, Oram JF, Heinecke JW. Tyrosine 192 in apolipoprotein A-I is the major site of nitration and chlorination by myeloperoxidase, but only chlorination markedly impairs ABCA1-dependent cholesterol transport. *J Biol Chem* 280: 5983-5993, 2005.

70. Shao B, Heinecke JW. Impact of HDL oxidation by the myeloperoxidase system on sterol efflux by the ABCA1 pathway. *J Proteomics* 74: 2289-2299, 2011.

71. Shao B, Oda MN, Bergt C, Fu X, Green PS, Brot N, Oram JF, Heinecke JW. Myeloperoxidase impairs ABCA1-dependent cholesterol efflux through methionine oxidation and site-specific tyrosine chlorination of apolipoprotein A-I. *J Biol Chem* 281: 9001-9004, 2006.

72. Shao B, Tang C, Heinecke JW, Oram JF. Oxidation of apolipoprotein A-I by myeloperoxidase impairs the initial interactions with ABCA1 required for signaling and cholesterol export. *J Lipid Res* 51: 1849-1858, 2010.

73. Sharov V, Dremina E, Galeva N, Gerstenecker G, Li X, Dobrowsky R, Stobaugh J, Schöneich C. Fluorogenic Tagging of Peptide and Protein 3-Nitrotyrosine with 4-(Aminomethyl)benzenesulfonic Acid for Quantitative Analysis of Protein Tyrosine Nitration. *Chromatographia* 71: 37-53, 2010.

74. Sharov VS, Dremina ES, Pennington J, Killmer J, Asmus C, Thorson M, Hong SJ, Li X, Stobaugh JF, Schöneich C. Selective fluorogenic derivatization of 3-nitrotyrosine and 3,4-dihydroxyphenylalanine in peptides: a method designed for quantitative proteomic analysis. *Methods Enzymol* 441: 19-32, 2008.

75. Sharov VS, Pal R, Dremina ES, Michaelis EK, Schöneich C. Fluorogenic tagging of protein 3-nitrotyrosine with 4-(aminomethyl)benzene sulfonate in tissues: A useful alternative to immunohistochemistry for fluorescence microscopy imaging of protein nitration. *Free Radic Biol Med* 53: 1877-1885, 2012.

76. Smith JD. Dysfunctional HDL as a diagnostic and therapeutic target. *Arterioscler Thromb Vasc Biol* 30: 151-155, 2010.

77. Smith JD. Myeloperoxidase, inflammation, and dysfunctional high-density lipoprotein. *J Clin Lipidol* 4: 382-388, 2010.

78. Sokolovsky M, Riordan JF, Vallee BL. Conversion of 3-nitrotyrosine to 3-aminotyrosine in peptides and proteins. *Biochem Biophys Res Commun* 27: 20-25, 1967.

79. Spickett C, Pitt A. Protein oxidation: role in signalling and detection by mass spectrometry. *Amino Acids* 42: 5-21, 2012.

80. Stadtman ER. Oxidation of free amino acids and amino acid residues in proteins by radiolysis and by metal-catalyzed reactions. *Annu Rev Biochem* 62: 797-821, 1993.

81. Stadtman ER, Levine RL. Chemical modification of proteins by reactive oxygen species. In: *Redox Proteomics: From Protein Modifications to Cellular Dysfunction and Diseases*. edited by Dalle-Donne I, Scaloni A, Butterfield DA. Hoboken, NJ: Wiley-Interscience; 2006. pp. 3-23.

82. Sultana R, Poon HF, Cai J, Pierce WM, Merchant M, Klein JB, Markesbery WR, Butterfield DA. Identification of nitrated proteins in Alzheimer's disease brain using a redox proteomics approach. *Neurobiol Dis* 22: 76-87, 2006.

83. Thompson A, Schäfer J, Kuhn K, Kienle S, Schwarz J, Schmidt G, Neumann T, Hamon C. Tandem mass tags: a novel quantification strategy for comparative analysis of complex protein mixtures by MS/MS. *Anal Chem* 75: 1895-1904, 2003.

84. Tsumoto H, Murata C, Miyata N, Kohda K, Taguchi R. Efficient identification and quantification of proteins using isotope-coded 1-(6-methylnicotinoyloxy)succinimides by matrix-assisted laser desorption/ionization time-of-flight mass spectrometry. *Rapid Commun Mass Spectrom* 21: 3815-3824, 2007.

85. Tsumoto H, Taguchi R, Kohda K. Efficient identification and quantification of peptides containing nitrotyrosine by matrix-assisted laser desorption/ionization time-of-flight mass spectrometry after derivatization. *Chem Pharm Bull (Tokyo)* 58: 488-494, 2010.

86. Turko IV, Li L, Aulak KS, Stuehr DJ, Chang J-Y, Murad F. Protein Tyrosine Nitration in the Mitochondria from Diabetic Mouse Heart: Implications to Dysfunctional Mitochondria in Diabetes. *Journal of Biological Chemistry* 278: 33972-33977, 2003.

87. Tyther R, McDonagh B, Sheehan D. Proteomics in investigation of protein nitration in kidney disease: technical challenges and perspectives from the spontaneously hypertensive rat. *Mass Spectrom Rev* 30: 121-141, 2011.

88. Wang SX, Mure M, Medzihradszky KF, Burlingame AL, Brown DE, Dooley DM, Smith AJ, Kagan HM, Klinman JP. A crosslinked cofactor in lysyl oxidase: redox function for amino acid side chains. *Science* 273: 1078-1084, 1996.

89. Whiteman M, Chu SH, Siau JL, Rose P, Sabapathy K, Schantz J-T, Cheung NS, Spencer JPE, Armstrong JS. The pro-inflammatory oxidant hypochlorous acid induces Bax-dependent mitochondrial permeabilisation and cell death through AIF-/EndoG-dependent pathways. *Cell Signal* 19: 705-714, 2007.

90. Wisastra R, Poelstra K, Bischoff R, Maarsingh H, Haisma HJ, Dekker FJ. Antibody-free detection of protein tyrosine nitration in tissue sections. *ChemBioChem* 12: 2016-2020, 2011.

91. Yee CS, Seyedsayamdost MR, Chang MCY, Nocera DG, Stubbe J. Generation of the R2 subunit of ribonucleotide reductase by intein chemistry: insertion of 3-nitrotyrosine at residue 356 as a probe of the radical initiation process. *Biochemistry* 42: 14541-14552, 2003.

92. Yeo WS, Lee SJ, Lee JR, Kim KP. Nitrosative protein tyrosine modifications: biochemistry and functional significance. *BMB Rep* 41: 194-203, 2008.

93. Zhang Q, Qian WJ, Knyushko TV, Clauss TR, Purvine SO, Moore RJ, Sacksteder CA, Chin MH, Smith DJ, Camp DG, 2nd, Bigelow DJ, Smith RD. A method for selective enrichment and analysis of nitrotyrosine-containing peptides in complex proteome samples. *J Proteome Res* 6: 2257-68, 2007.

94. Zhang R, Brennan M-L, Fu X, Aviles RJ, Pearce GL, Penn MS, Topol EJ, Sprecher DL, Hazen SL. Association between myeloperoxidase levels and risk of coronary artery disease. *JAMA* 286: 2136-2142, 2001.

95. Zhang X, Monroe ME, Chen B, Chin MH, Heibeck TH, Schepmoes AA, Yang F, Petritis BO, Camp DG, Pounds JG, Jacobs JM, Smith DJ, Bigelow DJ, Smith RD, Qian W-J. Endogenous 3,4-dihydroxyphenylalanine and dopaquinone modifications on protein tyrosine: links to mitochondrially derived oxidative stress via hydroxyl radical. *Mol Cell Proteomics* 9: 1199-1208, 2010.

96. Zheng L, Nukuna B, Brennan M-L, Sun M, Goormastic M, Settle M, Schmitt D, Fu X, Thomson L, Fox PL, Ischiropoulos H, Smith JD, Kinter M, Hazen SL. Apolipoprotein A-I is a selective target for myeloperoxidase-catalyzed oxidation and functional impairment in subjects with cardiovascular disease. *J Clin Invest* 114: 529-541, 2004.

97. Zheng L, Settle M, Brubaker G, Schmitt D, Hazen SL, Smith JD, Kinter M. Localization of nitration and chlorination sites on apolipoprotein A-I catalyzed by myeloperoxidase in human atheroma and associated oxidative impairment in ABCA1-dependent cholesterol efflux from macrophages. *J Biol Chem* 280: 38-47, 2005.

Chapter 2: Searching for Endogenous 3-Nitrotyrosine (3NY) and 3,4-Dihydroxyphenylalanine (DOPA) Modifications in Aging Rat Cardiac Tissue

2.1 Introduction

2.1.1 Significance of and Evidence for Protein Oxidation in Aging Rat Cardiac Tissue

As discussed extensively in Chapter 1, oxidative post-translational modifications (PTMs) of proteins can significantly alter protein structure and function and thus lead to dysfunction in cells and tissues. Of particular interest is the accumulation of modifications on specific Tyr residues within specific proteins during biological aging, as well as age-related diseases (3). By identifying proteins affected by such modifications, pathological mechanisms can be uncovered and used to inform development of therapeutic, diagnostic, and/or preventative measures.

Previous studies have shown age-dependent increases in Tyr-nitrated proteins in cardiac tissue from rats (4). Both 3NY and DOPA have been identified in a proteomic study of mouse brain and heart tissue (12). Notably, both studies identified endogenous modifications, which is substantially more difficult – and more biologically relevant – than identifying modification sites following treatment with nitrating or oxidizing agents *in vitro*.

2.1.2 Proteomics: Promise and Challenges

Before studying the effect of specific Tyr modifications on the function of particular proteins that may be involved in pathological processes, it is first necessary to discover where these modifications occur to an extent large enough to effect meaningful changes in biological processes. This challenge is part of the field of proteomics.

Section 1.2 describes in detail the most current strategies in proteomic studies of 3NY, most of which involve derivatization of this modified residue to aid in its enrichment, detection, and quantitation (2). DOPA is a much less-studied modification, and there is a scarcity of proteomic studies focused on it. A major challenge in this field is the low abundance of modified residues within the bulk proteome of a sample. However, this low abundance does not

preclude the capacity for significant biological effects. Since modifications can accumulate on specific proteins and at specific sites within those proteins, a 3NY or DOPA concentration that is dwarfed by the total protein concentration of a bulk sample can still exist on a high percentage of copies of a specific protein and thus significantly affect protein activity. This is especially true for proteins that have large biological effects even at low concentrations, such as signaling proteins.

The complexity of "real," biological samples presents many challenges when adapting a method that has been developed with model systems of relatively pure peptides, proteins, and small molecules. These include interfering species in the biological matrix, unknown (and typically very low) amounts of the analyte of interest (here, 3NY and DOPA), and the effects of a variety of sample preparation conditions on protein integrity and recovery. Furthermore, while the goal of proteomics is to identify as wide a range of protein targets as possible, the physicochemical and structural properties of these targets vary widely and can affect the results of labeling reactions and of behavior in mass spectrometry studies. Thus, it is nearly impossible to find one set of "optimal" conditions for all of the proteins in a sample.

2.1.3 Novel Fluorogenic Derivatization Chemistry with Benzylamine

This project aims to contribute to the field of 3NY and DOPA proteomics by employing a novel strategy for labeling these oxidative PTMs with fluorogenic and affinity moieties to enable their detection, identification, and ultimately quantitation. Sections 1.2.3 and 1.2.4 describe this method, which relies on benzylamine (BA)-based chemistry to convert 3-aminotyrosine (3AY) to a fluorescent 2-phenylbenzoxazole. In addition to the parent benzylamine reagent, which is commercially available, derivatives have been prepared to either enhance aqueous solubility (and thus improve chromatographic properties) or to incorporate an affinity label. For the former

purpose, 4-(aminomethyl)benzenesulfonic acid (ABS) was synthesized and tested with model systems (8). For the latter purpose, (3*R*,4*S*)-1-(4-(aminomethyl)phenylsulfonyl)pyrrolidine-3,4-diol (APPD) was synthesized and used to label model peptides and proteins prior to affinity-based enrichment with a boronate-affinity HPLC method (1). Benzylamine was the primary focus of the current project, which aimed to develop this method to label and identify endogenous modifications that accumulate in cardiac tissue during aging.

2.2 Experimental Methods

2.2.1 Materials

Sodium dithionite (SDT), synonym sodium hydrosulfite, was purchased from Sigma-Aldrich (St. Louis, MO, USA) as one of two product types: purified ≥86% (Riedel-de Haën) or technical grade, 85% (Sigma-Aldrich). Ammonium bicarbonate; sodium iodoacetate, SigmaUltra; sodium phosphate dibasic ACS reagent (anhydrous); benzylamine, redistilled, 99.5%+, which was stored in a sealed container protected from air, moisture and light and retrieved under positive pressure of argon to protect the stock from air exposure; trichloroacetic acid, electrophoresis reagent, minimum 99%; 2-mercaptoethanol; methanol, CHROMASOLV grade; acetone, CHROMASOLV®, for HPLC, ≥99.9%; albumin bovine serum, Fraction V, ≥96%; Triton X-100; glycerol; a kit for molecular weights 12,000-200,000 for gel filtration chromatography; and potassium ferricyanide were all obtained from Sigma-Aldrich, St. Louis, MO, USA.

Sodium dodecyl sulfate (SDS), electrophoresis grade; sodium hydroxide, certified ACS; sodium phosphate monobasic, certified ACS (monohydrate); sodium sulfate, certified ACS (anhydrous); tris(hydroxymethyl)aminomethane hydrochloride, for molecular biology; tris(hydroxymethyl)aminomethane crystallized free base, molecular biology grade; hydrochloric

acid, Certified ACS Plus; and urea, electrophoresis grade were all obtained from Fisher Scientific, Pittsburgh, PA, USA.

Complete, EDTA-free protease inhibitor cocktail was purchased from Roche Diagnostics, Indianapolis, IN, USA.

Ethanol, 99.90-100.00%, was from Decon Laboratories, Inc., King of Prussia, PA, USA.

CHAPS 3-[(3-cholamidopropyl)dimethylamonio]-1-propanesulfonate; bicinchoninic acid (BCA) protein assay kit; zeba spin desalting columns, 7kDa molecular-weight cutoff, 0.5mL; and Coomassie Colloidal Blue stain were all from Thermo Scientific (Rockford, IL, USA).

DL-dithiothreitol (DTT), molecular biology grade; and sequencing grade modified trypsin, porcine, specific activity >5,000U/mg were from Promega, Madison, WI.

2X Laemmli sample buffer; 10X tris/glycine/SDS buffer for SDS-PAGE applications; Ready Gel® Tris-HCl, 4-20% precast linear gradient polyacrylamide gel, 10-well, 50µL, 8.6 x 6.8 cm; and Precision Plus Protein Dual Color Standards were from Bio-Rad, Hercules, CA, USA.

2.2.2 Extraction and Preparation of Cardiac Proteins

The research protocol for treatment of animals was approved by the University of Kansas Institutional Animal Care and Use Committee. Fisher 344/BN F1 rats, an established model for biological aging, were housed under a 12:12 light-dark cycle and provided with food and water *ad libitum*. Following decapitation of the young (5-6 months old) and old (34-36 months old) animals, the hearts were quickly harvested and frozen at -70°C until use. Homogenates of this tissue were prepared in a lysis solution composed of 10mM tris(hydroxymethyl)aminomethane buffer with pH 7.4, 1% (v/v) Triton X-100 detergent, 1% glycerol, EDTA-free protease inhibitor cocktail at the manufacturer's recommended concentration, 6M urea, and 8mM dithiothreitol

(DTT). Heart tissue was sliced, added to lysis solution, and homogenized with an Ultra-Turrax T8 homogenizer (Fisher; Pittsburgh, PA). After 10min incubation, with rocking, followed by centrifugation at 5,445×*g* for 30min at 4°C, the pellet of cellular debris was discarded and the protein-rich supernatant was added to an equal volume of reduction buffer, giving final concentrations of 10mM tris(hydroxymethyl)aminomethane buffer with pH 7.4, 1% (v/v) Triton X-100 detergent, 1% glycerol, EDTA-free protease inhibitor cocktail at the manufacturer's recommended concentration, 3M urea, and 10mM dithiothreitol (DTT). For the reductive alkylation of Cys, proteins were incubated in this reduction buffer for 30min at 55°C before adding 25mM sodium iodoacetate and reacting at room temperature for 30min. Aliquots of this protein solution were cleaned by protein precipitation with cold EtOH, as described in section 2.2.3. Re-constitution buffers were typically at pH 7.4 and contained either sodium phosphate or ammonium bicarbonate with either SDS or CHAPS. The exact buffer composition will be indicated in the text for individual experiments. To aid dissolution, sonication by the probe sonicator Sonic Dismembrator 500 (Fisher Scientific, Pittsburgh, PA, USA) was typically performed with three pulses of 10s each at 20% power output and one pulse of 10s at 40% power output, with breaks between pulses lasting a minimum of 10s. Solutions were also typically warmed in a 37°C water bath for at least 30min. Protein concentration in the final cardiac protein stock solution was determined by BCA assay (see section 2.2.4). Stock solutions were aliquotted and stored at -70°C until use.

2.2.3 Protein Precipitation for Removal of Reagents

In order to clean samples from derivatization reagents or other solution components, such as SDT, potassium ferricyanide, BA, and detergent, proteins were precipitated by one of the following methods. For precipitation in cold ethanol (EtOH), ten solution volumes of 100%

ethanol was cooled to -20°C and added to the sample, which was promptly incubated either overnight at -20°C or for a minimum of 4h at -70°C. Protein pellets were collected by centrifugation for 5min, the supernatant discarded, and fresh cold 100% EtOH added to wash the proteins. This process was repeated for a total of three washes.

For precipitation in cold trichloroacetic acid (TCA), ten solution volumes of 22% (w/v) TCA was cooled on ice and added to the sample, giving a final TCA concentration of 20% (w/v). Samples were incubated overnight on ice in a refrigerator maintained at approximately 4°C. Protein pellets were collected by centrifugation at for 5min, the supernatant discarded, and cold (-20°C) 100% acetone added to wash the proteins. This process was repeated for a total of three washes.

In either method, washed proteins were once more collected by 5min centrifugation and then allowed to air dry before re-constituting proteins in the buffer of choice. As needed, the dissolution process was aided with sonication by the probe sonicator Sonic Dismembrator 500 (Fisher Scientific, Pittsburgh, PA, USA) and/or by warming in a 37°C water bath.

2.2.4 BCA Assay for Protein Concentration

Selected for its compatibility with several detergents, the BCA protein assay was conducted largely as recommended by the manufacturer's protocol for the test tube procedure, with only minor adjustments. Protein standards containing 2mg/mL bovine serum albumin (BSA) were prepared in-house in the same buffer as samples and serially diluted, following the manufacturer's protocol, to produce calibration standards with final protein concentrations in the range 25-2,000µg/mL. To 50µL of sample, diluted as needed to give a concentration within the assay's working range, was added 1mL working reagent. Samples were incubated in a water bath at 37°C for 20-30min. This reaction time was periodically adjusted empirically to produce a

calibration curve with the largest possible linear range. Absorbance at 562nm was measured for all calibration standards and samples, and a blank-corrected calibration curve was constructed and used to calculate sample protein concentrations, according to manufacturer's instructions.

2.2.5 Derivatization Reactions

Since the conditions for both 3NY reduction to 3AY and fluorogenic labeling of 3AY and DOPA were the subject of many optimization experiments over time, details will be provided as needed alongside each set of data described.

2.2.6 SDS Polyacrylamide Gel Electrophoresis (SDS-PAGE)

SDS-PAGE (under reducing conditions) was performed using the Bio-Rad Mini-PROTEAN® electrophoresis and blotting system (Hercules, CA, USA). Samples were mixed with an equal volume of 2X Laemmli sample buffer, which had been supplemented with 5% (v/v) 2-mercaptoethanol, and heated in a boiling water bath for 2min. Samples and molecular-weight markers were loaded into pre-cast 4-20% gradient gels and separated by electrophoresis in 1X tris/glycine/SDS run buffer at constant 200V for 38min, with maximum current limited at 400mA. Proteins were visualized by Coomassie Colloidal Blue staining.

2.2.7 Size-Exclusion HPLC (SE-HPLC)

SE-HPLC was performed on a Shimadzu 10A Series High-Performance Liquid Chromatograph (Kyoto, Japan). The optimal method was as follows: an isocratic method using 0.1M sodium phosphate plus 0.1M sodium sulfate, pH 6.8, as a mobile phase at a flow rate of 1.0mL/min separated protein solutions on a Tosoh TSK-GEL G3000SW$_{XL}$ column, 7.8mm ID x 30cm, 5µm particles. The loop volume for the manual injector was 20µL, and 40µL protein solution was loaded in order to ensure complete loop filling. Detection was by UV absorbance at 280nm and fluorescence at excitation 360nm and emission 460nm. This optimal method was

reached over time, and variations in the method used for particular experiments will be described in the text as appropriate. The method was periodically calibrated with protein molecular-weight standards in the range 12-200kDa and showed good linearity for a plots of log(molecular weight) vs. retention volume.

2.2.8 Mass-Spectrometry-Based Proteomics

Proteins were digested with trypsin overnight at 37°C, typically with a 1:20 molar ratio of trypsin:cardiac protein, as calculated using an estimated average molecular weight of 50kDa for cardiac proteins. Samples containing tryptic peptides were analyzed by nano-HPLC-ESI-MS/MS, as described previously (5,10). Briefly, peptides were separated by nano-flow HPLC with columns (300 Å, 10cm × 75µm, 15µm tip size; New Objective, Woburn, MA) packed in-house with BioBasic octadecyl stationary phase (Thermo Electron) and using a linear gradient of water and acetonitrile, both containing 0.1% formic acid, at a flow rate of 0.5µL/min. Chromatography was online with either a ThermoElectron LCQ Duo or a ThermoElectron Classic (San Jose, CA), equipped with a nanoelectrospray source (ThermoElectron).

2.3 Results

2.3.1 Optimal Conditions for Reduction of 3NY to 3AY

Since the amount of endogenous protein-bound 3NY present in cardiac homogenate samples is unknown, empirical evidence was used to determine the amount of SDT required to reduce 3NY to 3AY. Concentrations of 1, 10, or 20mM SDT were reacted with 0.9mg/mL cardiac proteins from a young rat (in 0.1M pH 7.4 sodium phosphate buffer with 4% CHAPS) for 0.75, 1.5, 2, 15, or 30min at room temperature before precipitation by cold ethanol (see section 2.2.3). Derivatization was carried out in 0.1M pH 9 sodium phosphate buffer plus 4% CHAPS with 0.7mg/mL protein, 1mM potassium ferricyanide, and 460mM BA for 2.5h at room

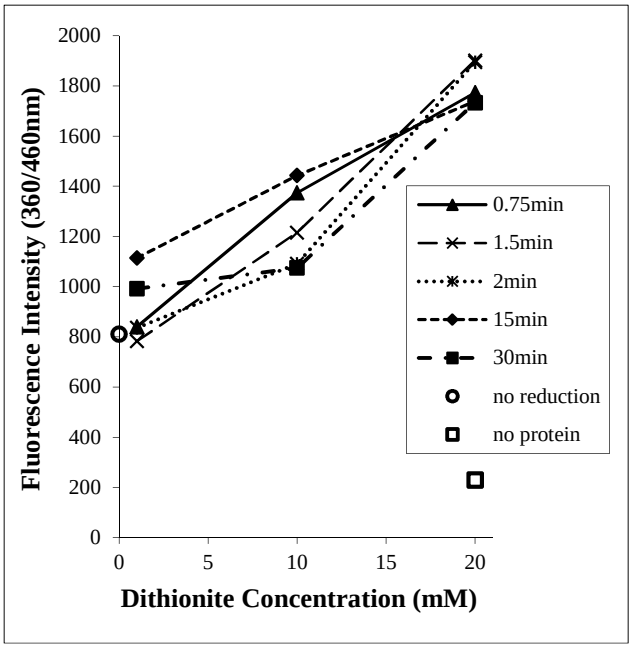

Fig. 2.1 Dithionite concentration dependence for cardiac proteins tagged with BA. Cardiac proteins from a young rat (0.9mg/mL in 0.1M pH 7.4 sodium phosphate buffer with 4% CHAPS) were reduced with 1, 10, or 20mM SDT for 0.75, 1.5, 2, 15, or 30min before precipitation in cold ethanol. Derivatization was carried out in 0.1M pH 9 sodium phosphate buffer plus 4% CHAPS with 0.7mg/mL protein, 1mM potassium ferricyanide, and 460mM BA for 2.5h at room temperature in the dark.

temperature in the dark. Fluorescence measurements at excitation and emission wavelengths of 360 and 460nm, respectively, were conducted using the SpectraMax Gemini XS Dual-Scanning Microplate Spectrofluorometer (Molecular Devices Corporation, Sunnyvale, CA, USA) running SOFTmax® PRO Version 4.0 software for Windows ®, with the following settings: emission cutoff 455nm, 18 reads, PMT sensitivity auto, automix 5s before, and auto calibrate on.

Increasing SDT concentrations consistently increased the yield of fluorescent product, regardless of the reduction reaction time (Fig. 2.1). Importantly, reduced and derivatized samples showed greater fluorescence than controls in which either SDT or protein were omitted. For future experiments, 10-20mM SDT for 1.5-2min was selected as the method of choice, at least when similar protein concentrations were used.

2.3.2 Derivatization Reagent Concentration Dependences

Cardiac proteins from an old rat were prepared at a concentration of 8.0mg/mL in 0.1M pH 7.4 sodium phosphate buffer with 0.5% SDS. For reduction of 3NY to 3AY, proteins were exchanged into 0.1M pH 5 sodium acetate buffer with 0.5% SDS by zeba spin cartridges,

according to the manufacturer's buffer exchange protocol. Reduction with 10mM SDT and ~6.9mg/mL protein was carried out for 37°C for 15min, and the samples remained at room temperature for about an hour during preparation for the next step. Another buffer exchange was performed with zeba cartridges into the tagging buffer, 0.1M pH 9 sodium phosphate with 0.5% SDS. Derivatization of ~3.5mg/mL protein was performed with a range of reagent concentrations, designed as a matrix to test all possible combinations. Potassium ferricyanide was tested in the range 50μM-5mM with either 0-36mM BA or 0-36mM APPD. Reaction progress was followed over time by fluorescence in a plate reader with the following settings: excitation/emission wavelengths 360/510nm with cutoff 495nm (for APPD) and 360/455nm with cutoff 435nm (for BA), 18 readings, PMT sensitivity auto, automix 5s, autocalibrate on. Various control samples were also included, and background correction was performed for labeled protein samples, where indicated, by subtracting the fluorescence intensity of controls lacking protein but containing buffer and all reagents. APPD in particular had rather high background fluorescence in this control.

Fig. 2.2 shows both time course data and reagent concentration dependence curves. BA reactions produced higher fluorescence intensities than APPD samples, but both sets of reactions were largely complete after 60-100min reaction time. Potassium ferricyanide dependence shows a plateau or peak beginning at 1mM. BA dependence is optimal at 18mM for several samples. APPD shows increasing fluorescence intensity throughout the concentration range tested, with the upper limit being 20mM. However, after background correction, this trend reverses, and the greatest fluorescence intensity is observed for 5mM APPD. The sample containing non-reduced proteins with 5mM potassium ferricyanide and 18mM BA seems to be an aberration and may be due to experimental error in sample preparation.

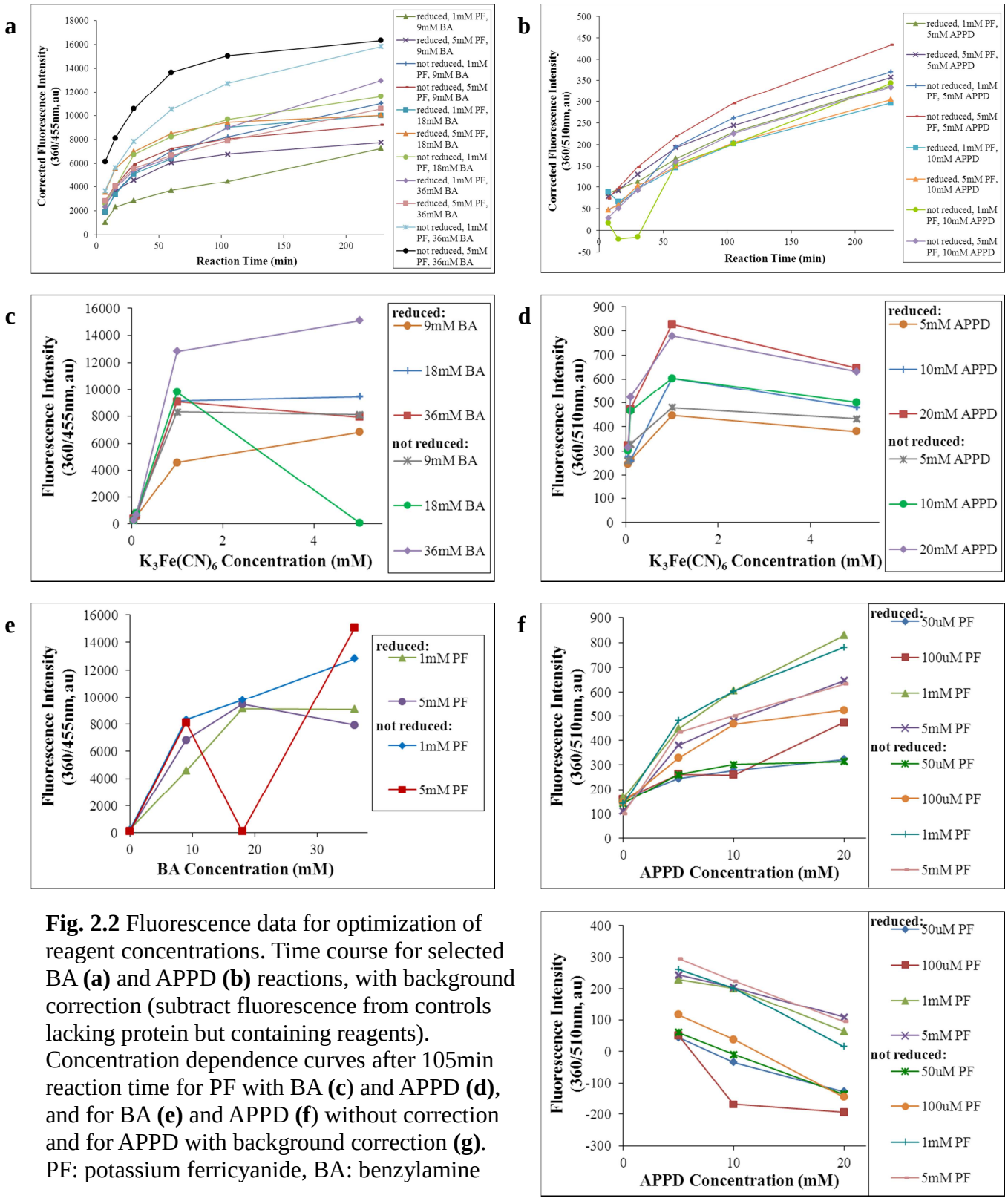

Fig. 2.2 Fluorescence data for optimization of reagent concentrations. Time course for selected BA **(a)** and APPD **(b)** reactions, with background correction (subtract fluorescence from controls lacking protein but containing reagents). Concentration dependence curves after 105min reaction time for PF with BA **(c)** and APPD **(d)**, and for BA **(e)** and APPD **(f)** without correction and for APPD with background correction **(g)**. PF: potassium ferricyanide, BA: benzylamine

The greater solubility of BA in water enabled testing of much larger concentrations, as well. Previous studies with model systems (6,9) supported use of such high excesses of BA over analyte. Cardiac proteins from a young rat were labeled without reduction, thus focusing on labeling DOPA. To 0.7mg/mL protein in 0.1M pH 7.4 sodium phosphate buffer with 4% CHAPS was added potassium ferricyanide in concentrations of the range 10µM-5mM and BA ranging 2-460mM, once again designed as a matrix to test all possible combinations. While the protein remained in a buffer solution at pH 7.4 for this experiment, the alkaline properties of BA [pK_a = 9.32 (7)] are likely to dominate the solution conditions, especially at such high BA concentrations. Reaction progress was followed over time by fluorescence endpoint measurements in a plate reader with the following settings: excitation/emission wavelengths 360/450nm, cutoff 435nm, 18 readings, PMT sensitivity auto, automix 5s, autocalibrate on. Controls lacking protein but containing all buffer and reagents were used for background correction, where indicated, by subtracting their fluorescence intensity from that of their labeled counterparts.

Fig. 2.3 shows most reactions are largely complete after 180min (a), at which time the background-corrected fluorescence intensity shows a maximum at 100µM potassium ferricyanide (b) and a plateau at 100mM BA (c). All data in Fig. 2.3 are background-corrected.

2.3.3 Comparison of Cleaning Procedures

As an optimization effort, variations in SDT reduction time and post-reduction cleaning methods were tested for protein recovery, based on BCA assay (see section 2.2.4), and tagging efficiency, as measured by fluorescence intensity. Cardiac proteins were prepared to 1.2-1.3mg/mL in 0.1M pH 7.4 sodium phosphate buffer with 4% (w/v) CHAPS and reduced with 10mM SDT for either 1.5min or 15min. Non-reduced samples were simultaneously prepared

Fig. 2.3 Fluorescence data for optimization of reagent concentrations. Time course for selected reactions **(a**) and concentration dependence curves for potassium ferricyanide **(b**) and BA **(c**) after 181min reaction time. All data have been background-corrected by subtraction of fluorescence from controls lacking protein but containing reagents.

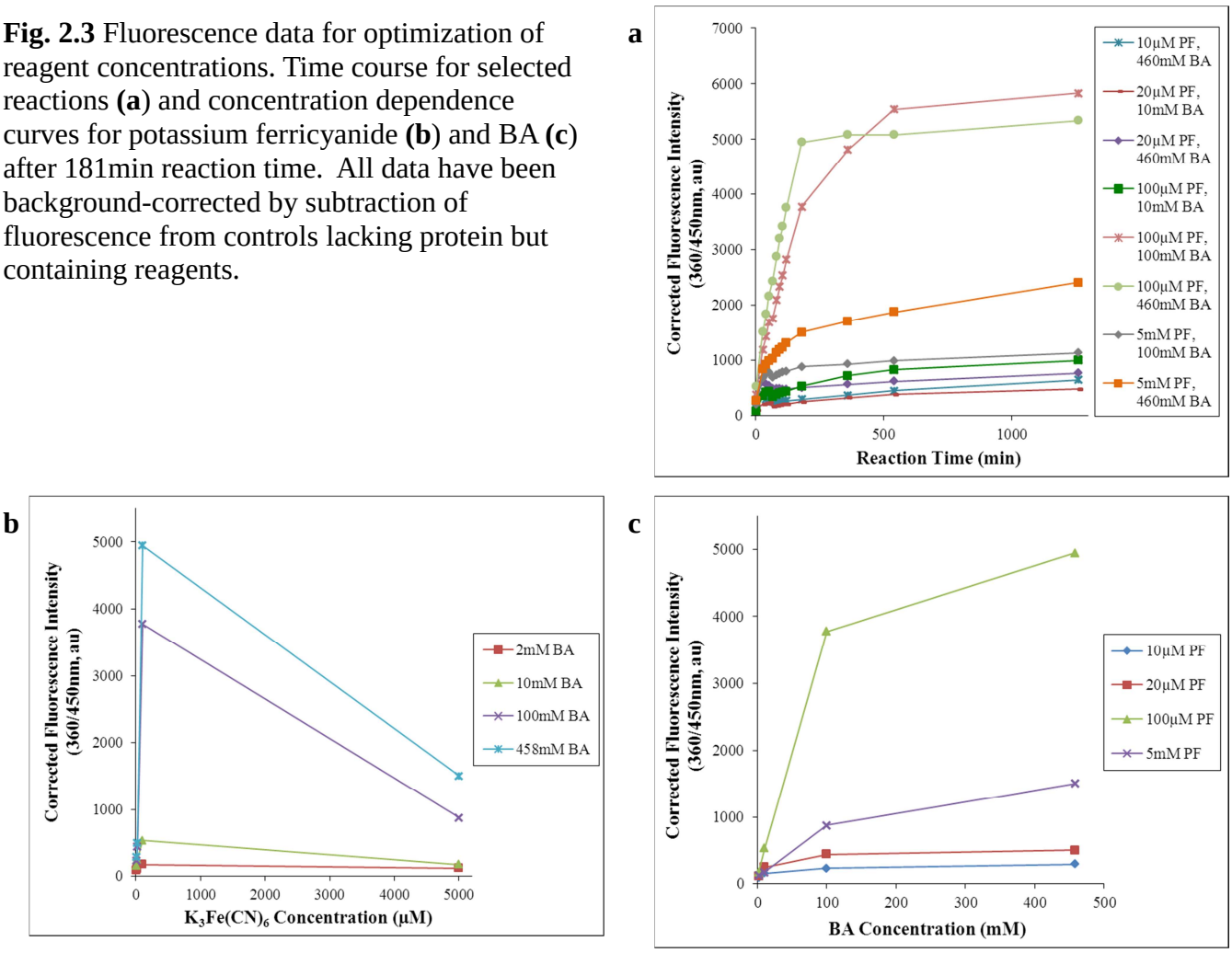

and exposed to all steps of the protocol, except for the omission of SDT. All samples were cleaned by precipitation protocols using either EtOH or TCA (see section 2.2.3) and re-constituted in 0.1M pH 9 sodium phosphate buffer with 4% (w/v) CHAPS, with probe sonication for 5s at 10% power output. For labeling, approximately 0.9mg/mL protein (assuming 100% recovery from reduction and cleaning) was reacted with 1mM potassium ferricyanide and 250mM BA for 1h at room temperature in the dark. Fluorescence was measured by plate reader with the following settings: excitation/emission wavelengths 366/455nm, cutoff 420nm, 6 reads, PMT medium, automix 5s, autocalibrate on. After approximately 2h total reaction time, sample aliquots were taken for analysis by SDS-PAGE (see section 2.2.6), and the remainder of each

sample was again cleaned by precipitation with either the EtOH or TCA protocol, with re-constitution in 0.1M pH 9 sodium phosphate with 4% (w/v) CHAPS. These cleaned samples were analyzed for protein concentration by the BCA assay (see section 2.2.4).

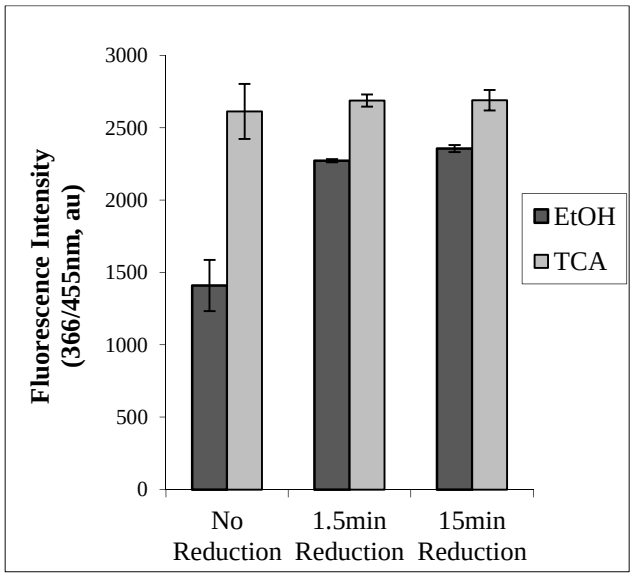

Fig. 2.4 Comparison of protein precipitation methods and reduction reaction times, based on fluorescence intensity of proteins after labeling. Approximately 1mg/mL cardiac protein was reduced with 10mM SDT and cleaned by either EtOH or TCA precipitation protocols. After re-constitution in 0.1M pH 9 sodium phosphate buffer with 4% (w/v) CHAPS, proteins were labeled with 1mM potassium ferricyanide and 250mM BA for 1h before measuring fluorescence using a plate reader.

While reduction time did not have a significant effect on either of these parameters, precipitation by TCA showed superior performance to EtOH, leading to higher fluorescence intensities upon labeling cardiac proteins with BA (Fig. 2.4) and to greater protein recovery (Table 2.1). This experiment was conducted twice, and the fluorescence data was averaged in Fig. 2.4. However, accurate protein recovery data was not obtained from the first sample set due to experimental errors, in particular a poor calibration in the BCA protein concentration

Table 2.1 Protein recovery data and normalization of fluorescence intensities to protein concentrations for comparison of protein precipitation methods and reduction reaction times.

	EtOH			TCA		
	Fluorescence Intensity (366/455nm, au)	protein concentration (µg/mL)	intensity: concen-tration	Fluorescence Intensity (366/455nm, au)	protein concentration (µg/mL)	intensity: concen-tration
No Reduction	1285.932	198	6.5	2748.401	567	4.8
1.5min Reduction	2265.642	354	6.4	2718.041	655	4.1
15min Reduction	2339.766	361	6.5	2740.255	765	3.6

assay. Thus, Table 2.1 presents data from a single experiment, but the results are consistent with similar experiments performed in the course of this project, one of which is described in section 3.2.4. Multiple control samples were also included in this experiment, and the average recovery from all protein-containing samples was 63% ± 27% for the EtOH method and 87% ± 7% for TCA method (n=12 for each method). Controls lacking protein but containing all reagents and buffer components for the labeling reaction contained solid material following EtOH precipitation, indicating the incomplete removal of these substances, which could potentially interfere with subsequent steps.

In order to qualitatively compare protein recovery profiles, samples were separated by SDS-PAGE and visualized using Coomassie Brilliant Blue (Fig. 2.5). Based on protein concentration data from the BCA assay, protein loads were equalized to 15.2µg for each sample. For two samples, this was not possible: lane 6 contains only 8.5µg and lane 10 13.6µg. Each sample shows qualitatively equal amounts of protein (accounting for the lower protein loads in lanes 6 and 10) and a consistent pattern of bands. Thus, the data indicate that the choice of protein precipitation method does not affect the composition or integrity of protein recovered, but rather only the amount. It was surprising to see that the majority of proteins present in all samples, including stock cardiac proteins (lane 2) were of molecular weight less than 50kDa. This may be due to incomplete re-constitution during the

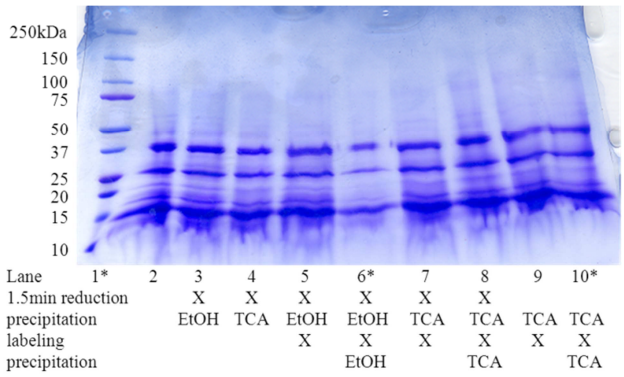

Fig. 2.5 SDS-PAGE stained with Coomassie Blue for comparison of protein precipitation methods and reduction reaction times. Each lane 2-10 contains 15.2µg cardiac protein (based on BCA protein concentration assay), unless marked (*). Lane 1: molecular-weight markers; lane 6: 8.5µg cardiac protein; lane 10: 13.6µg cardiac protein.

preparation of the cardiac homogenate. Particularly, CHAPS is much less efficient than SDS for solubilizing cardiac proteins, as indicated by typical final protein concentrations of 1.0-1.5mg/mL with the former and 10mg/mL with the latter.

Significantly, the EtOH precipitation method seems to be biased against recovery of proteins that are not exposed to SDT (i.e., "no reduction" samples). Such a bias could lead to the inaccurate conclusion that samples reduced by SDT (when cleaned by EtOH precipitation) have increased labeling, presumably representing significant levels of 3NY. However, the ratio of fluorescence intensity to protein concentration is very similar for samples with and without SDT reduction, for both cleaning methods. In addition, controls containing all reaction components except for BA showed higher fluorescence in samples exposed to SDT than in "no reduction" samples, but only when the EtOH precipitation method was used. This may also be connected to poor protein recovery in the latter, suggesting a possible reaction of potassium ferricyanide with protein. Previous work with similar derivatization chemistry has suggested the oxidation of Trp residues to kynurenin and related compounds, leading to background fluorescence (8).

Section 2.3.5 explores further the comparison of samples with and without SDT reduction, and it should be noted that for those experiments, the "no reduction" or "DOPA" samples did not undergo any cleaning procedure and so are not subject to this artifact. The cause of this potential bias remains unknown, and different experimental conditions have given variable results regarding the effect of SDT reduction on the yield of fluorescent product from labeled cardiac proteins. Section 2.3.5 represents the most effective investigation of this topic.

2.3.4 Comparison of Young and Old Rats

Cardiac proteins from young or old rats were prepared to 1.4mg/mL in 0.1M pH 7.4 sodium phosphate buffer with 4% (w/v) CHAPS and acidified with hydrochloric acid to an

estimated pH 5. For each age, one sample was reduced with 20mM SDT for 30min at room temperature and the other was treated similarly, except for the omission of SDT. Desalting by zeba spin cartridges was followed by sonication in a water bath for 10min, which failed to completely solubilize all proteins. Supernatants were collected and labeled with an estimated protein concentration 0.6mg/mL and reagent concentrations 1mM potassium ferricyanide and 460mM BA for 3h at room temperature in the dark. Reaction progress was measured by fluorescence plate reader with the following settings: excitation/emission wavelengths 360/460nm, cutoff 455nm, 18 readings, PMT sensitivity auto, automix 5s, and autocalibrate on. Samples were again desalted with zeba cartridges to avoid fouling the SE-HPLC column with excess reagents. SE-HPLC analysis was conducted as described in section 2.2.7. Both the fluorescence intensity and SE-HPLC data shower greater yields of fluorescently-labeled proteins for old samples compared to young samples and for reduced samples compared to young samples (Fig. 2.6). These results are consistent with increased levels of both DOPA and 3NY in cardiac tissue from old animals and with the successful reduction and labeling of 3NY in reduced samples, while only DOPA is labeled in non-reduced samples.

a

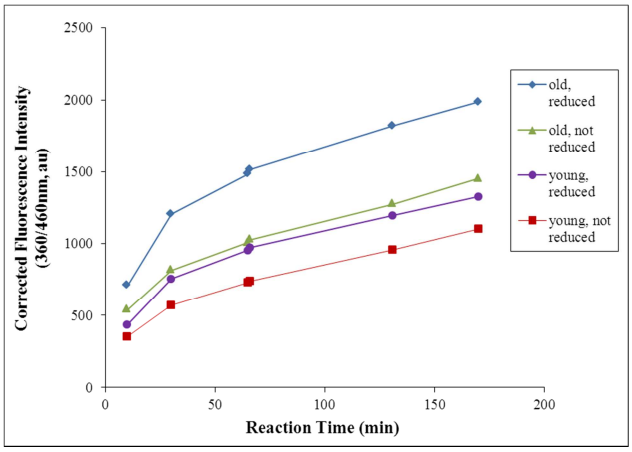

Fig. 2.6 Comparison of cardiac proteins from old and young rats derivatized with BA, with or without prior reduction of 3NY to 3AY by SDT. Reaction time course, with background correction **(a)**, comparisons of SE-HPLC chromatograms for old rat proteins with or without reduction **(b)**, young rat proteins with or without reduction **(c)**, and comparisons of SE-HPLC chromatograms for reduced samples of both ages, **(d)** and non-reduced samples of both ages **(e)**. The dotted lines running through the chromatograms mark the retention volumes of molecular-weight standards.

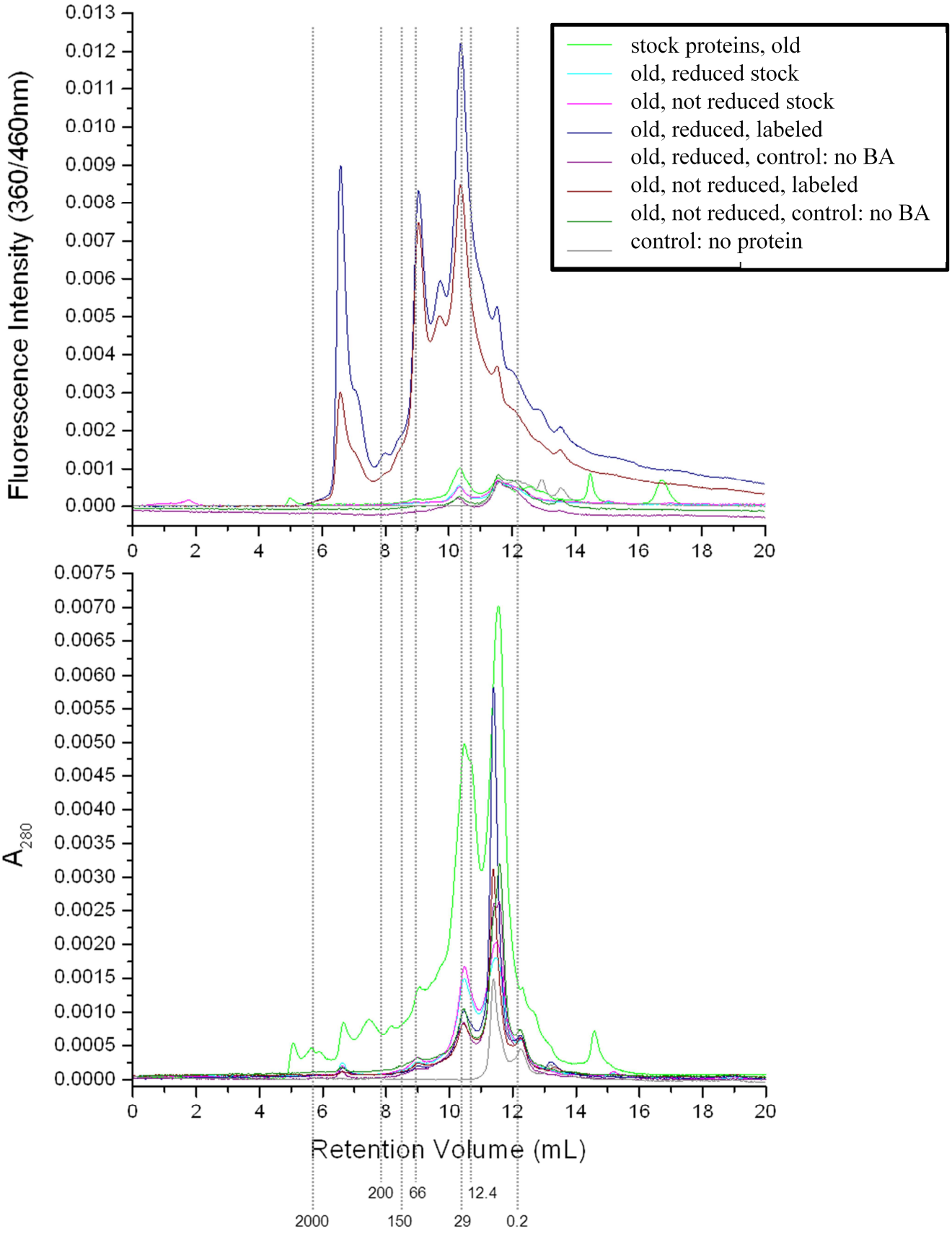
Fluorescence Intensity (360/460nm)
0.013
0.012
0.011
0.010
0.009
0.008
0.007
0.006
0.005
0.004
0.003
0.002
0.001
0.000
0
2
4
6
8
10
12
14
16
18
20
stock proteins, old
old, reduced stock
old, not reduced stock
old, reduced, labeled
old, reduced, control: no BA
old, not reduced, labeled
old, not reduced, control: no BA
control: no protein
A280
0.0075
0.0070
0.0065
0.0060
0.0055
0.0050
0.0045
0.0040
0.0035
0.0030
0.0025
0.0020
0.0015
0.0010
0.0005
0.0000
Retention Volume (mL)
200
66
12.4
2000
150
29
0.2

Fig. 2.6b

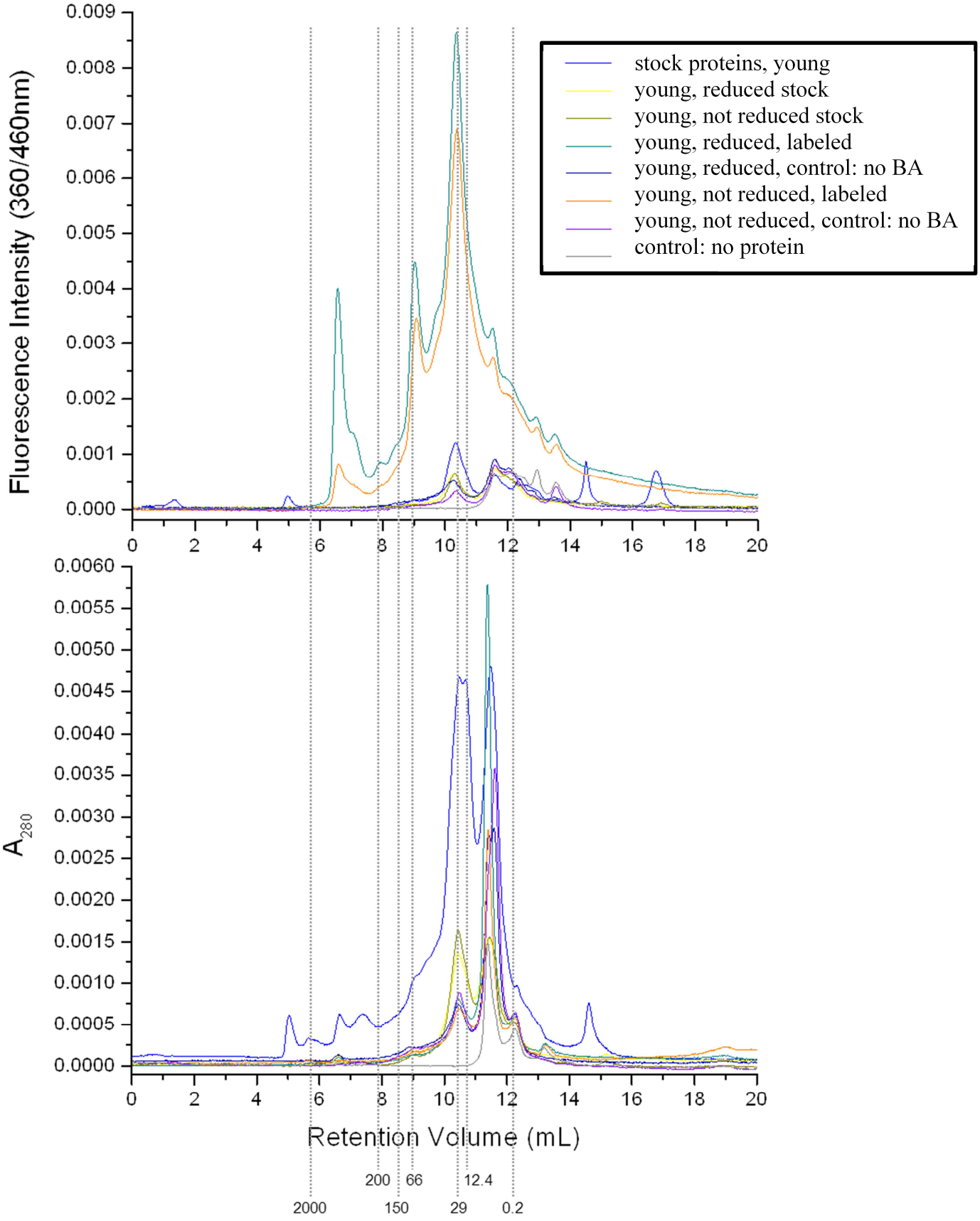
Fluorescence Intensity (360/460nm)
0.009
0.008
0.007
0.006
0.005
0.004
0.003
0.002
0.001
0.000
0 2 4 6 8 10 12 14 16 18 20
stock proteins, young
young, reduced stock
young, not reduced stock
young, reduced, labeled
young, reduced, control: no BA
young, not reduced, labeled
young, not reduced, control: no BA
control: no protein
A280
0.0060
0.0055
0.0050
0.0045
0.0040
0.0035
0.0030
0.0025
0.0020
0.0015
0.0010
0.0005
0.0000
0 2 4 6 8 10 12 14 16 18 20
Retention Volume (mL)
200 66 12.4
2000 150 29 0.2

Fig. 2.6c

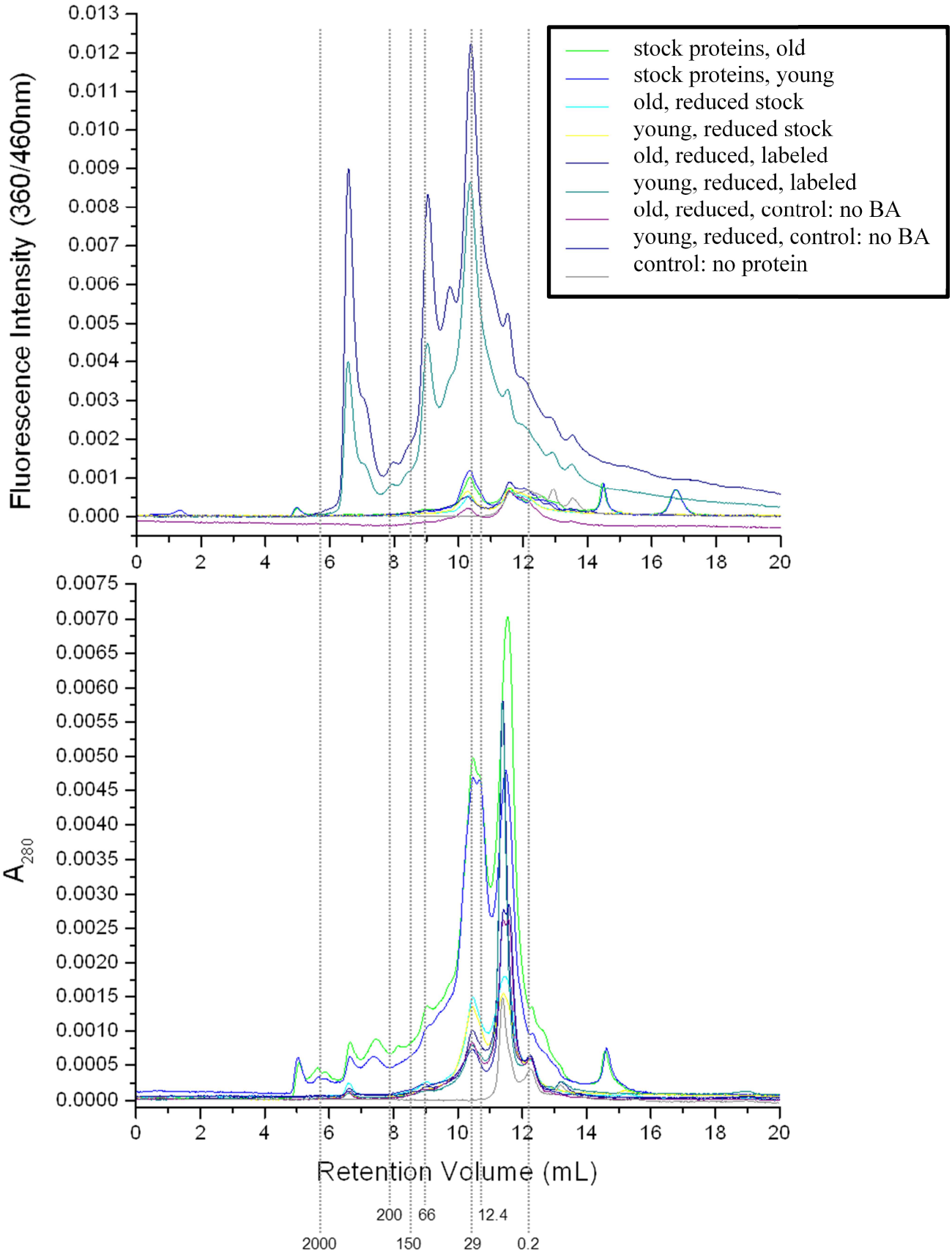
Fluorescence Intensity (360/460nm)
0.013
0.012
0.011
0.010
0.009
0.008
0.007
0.006
0.005
0.004
0.003
0.002
0.001
0.000
0 2 4 6 8 10 12 14 16 18 20
stock proteins, old
stock proteins, young
old, reduced stock
young, reduced stock
old, reduced, labeled
young, reduced, labeled
old, reduced, control: no BA
young, reduced, control: no BA
control: no protein
A280
0.0075
0.0070
0.0065
0.0060
0.0055
0.0050
0.0045
0.0040
0.0035
0.0030
0.0025
0.0020
0.0015
0.0010
0.0005
0.0000
0 2 4 6 8 10 12 14 16 18 20
Retention Volume (mL)
200 66 12.4
2000 150 29 0.2

Fig. 2.6d

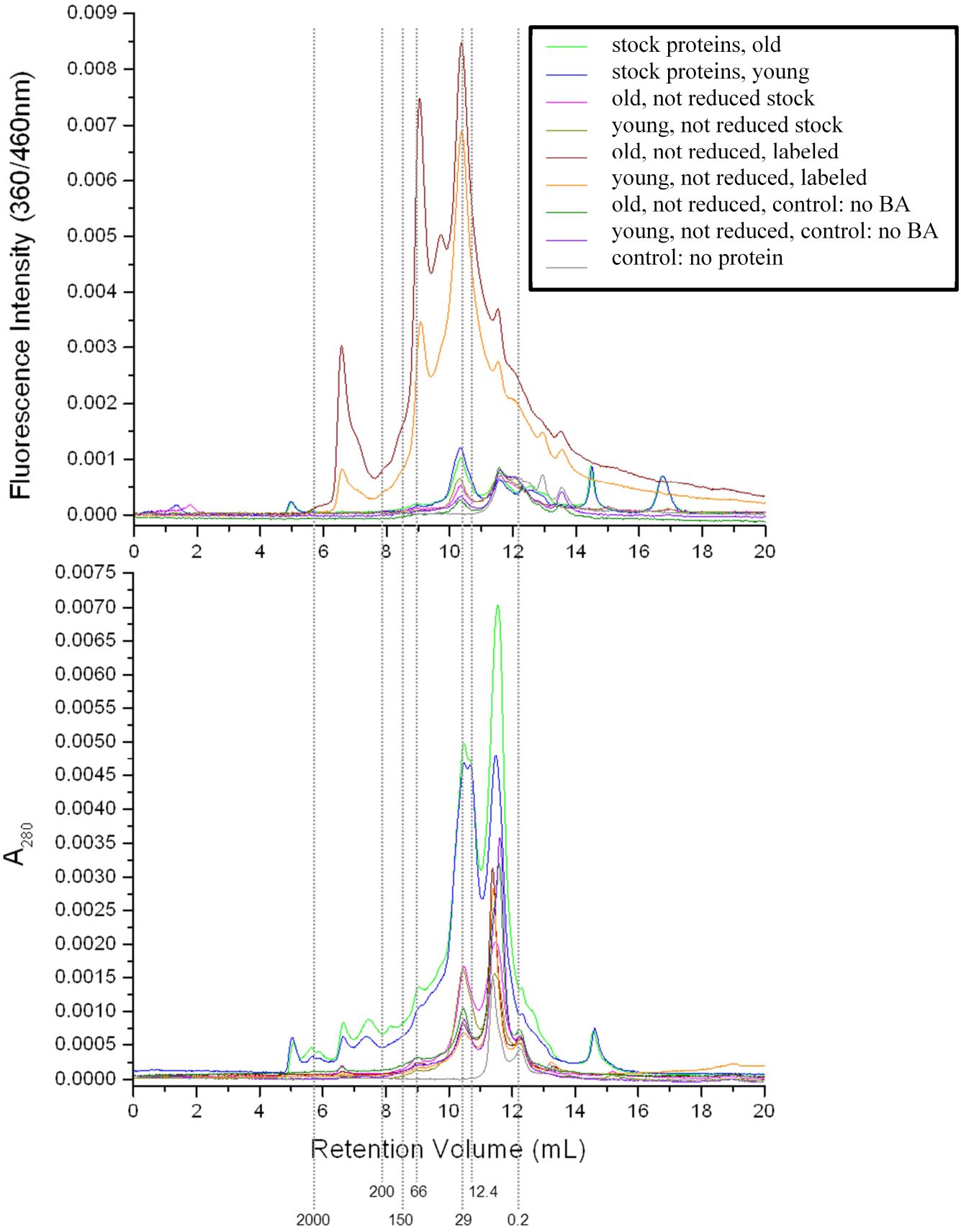
Fluorescence Intensity (360/460nm)
0.009
0.008
0.007
0.006
0.005
0.004
0.003
0.002
0.001
0.000
0 2 4 6 8 10 12 14 16 18 20
stock proteins, old
stock proteins, young
old, not reduced stock
young, not reduced stock
old, not reduced, labeled
young, not reduced, labeled
old, not reduced, control: no BA
young, not reduced, control: no BA
control: no protein
A280
0.0075
0.0070
0.0065
0.0060
0.0055
0.0050
0.0045
0.0040
0.0035
0.0030
0.0025
0.0020
0.0015
0.0010
0.0005
0.0000
0 2 4 6 8 10 12 14 16 18 20
Retention Volume (mL)
2000
200
150
66
29
12.4
0.2

Fig. 2.6e

2.3.5 Comparison of Reduced and Non-Reduced Samples

Proteins from old and young rats were prepared with equal concentrations, 1.4mg/mL, in 0.1M pH 7.4 sodium phosphate buffer with 4% (w/v) CHAPS. To tag only DOPA, samples in the "no reduction" experiment did not undergo any further treatment before benzylamine derivatization. To tag 3NY in addition to DOPA, 1.3mg/mL protein was reduced with 20mM SDT for 30min at room temperature and then cleaned by zeba spin cartridge. For both sample sets, 0.7mg/mL protein was derivatized with 1mM potassium ferricyanide and 460mM BA for 3h at room temperature in the dark. Fluorescence was measured by plate reader with the following settings: excitation/emission wavelengths 360/460nm, cutoff 455nm, 18 reads, PMT sensitivity auto, automix 5s, autocalibrate on.

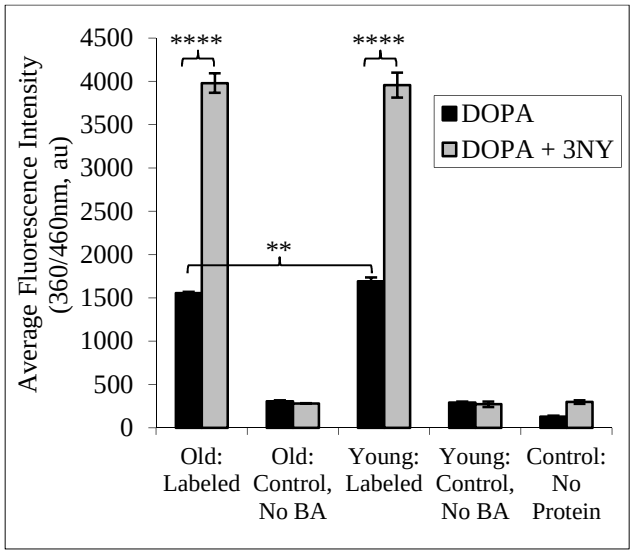

Fig. 2.7 Cardiac proteins from old or young rats, 1.3mg/mL in 0.1M pH 7.4 sodium phosphate with 4% CHAPS, were either untreated (DOPA) or reduced with 20mM SDT for 30min and desalted with zeba spin columns (DOPA + 3NY). All samples were then labeled at concentrations of 0.7mg/mL protein, 1mM potassium ferricyanide, and 460mM benzylamine for 3h in the dark. Fluorescence was measured by plate reader at the excitation/emission wavelengths 360/460nm. **p<0.01, ****p<0.001

As shown in Fig. 2.7, reducing proteins with SDT before tagging produced much higher fluorescence intensities, consistent with labeling of only DOPA in non-reduced samples and both DOPA and 3NY in reduced samples. The age of the rat did not significantly affect the fluorescence intensity for reduced samples in this particular experiment, but there is a statistically significant difference between the ages in the non-reduced samples, with the young sample having greater fluorescence

than the old sample. A two-tailed unpaired Student's t-test was used to calculate all p-values. It is not entirely clear why an age-dependent difference was observed in the previous experiment but not in this one, but the inconsistency may be due to slight changes in experimental conditions and/or different tissue homogenate preparations from different animals. Furthermore, statistical analysis was not performed for the previous experiment, since it represents only a single sample.

Note that in the current experiment, non-reduced samples were not subjected to any cleaning steps before the labeling reaction and thus are not subject to the potential artifact described in section 2.3.3. The SE-HPLC-UV data, described below, provides further analysis of the protein content in both non-reduced and reduced samples. All samples were cleaned with zeba desalting spin columns after approximately 4h total reaction time before SE-HPLC, in order to avoid damaging the column with excess reagents. Sonication was used to help dissolve precipitated proteins after this cleaning step.

The SE-HPLC chromatograms, shown in Fig. 2.8, clearly show the increased fluorescence of reduced samples compared to non-reduced samples, with the major fluorescent peaks eluting in the molecular-weight range >10kDa. In the UV chromatograms, the reduced samples also have slightly higher signals than non-reduced samples. Figures 2.8c and 2.8d show the quantitative comparison based on peak areas, which were integrated only in the molecular-weight region corresponding to protein. Note that retention times shifted slightly between the non-reduced and reduced experiments, likely due to column fouling by sample materials over time. Although SE-HPLC is designed to work only by size-based mechanisms, other interactions between analytes and the stationary phase can occur, particularly hydrophobic interactions (11). This secondary separation mechanism can become more pronounced if hydrophobic sample materials are not completely eluted from the stationary phase. For this

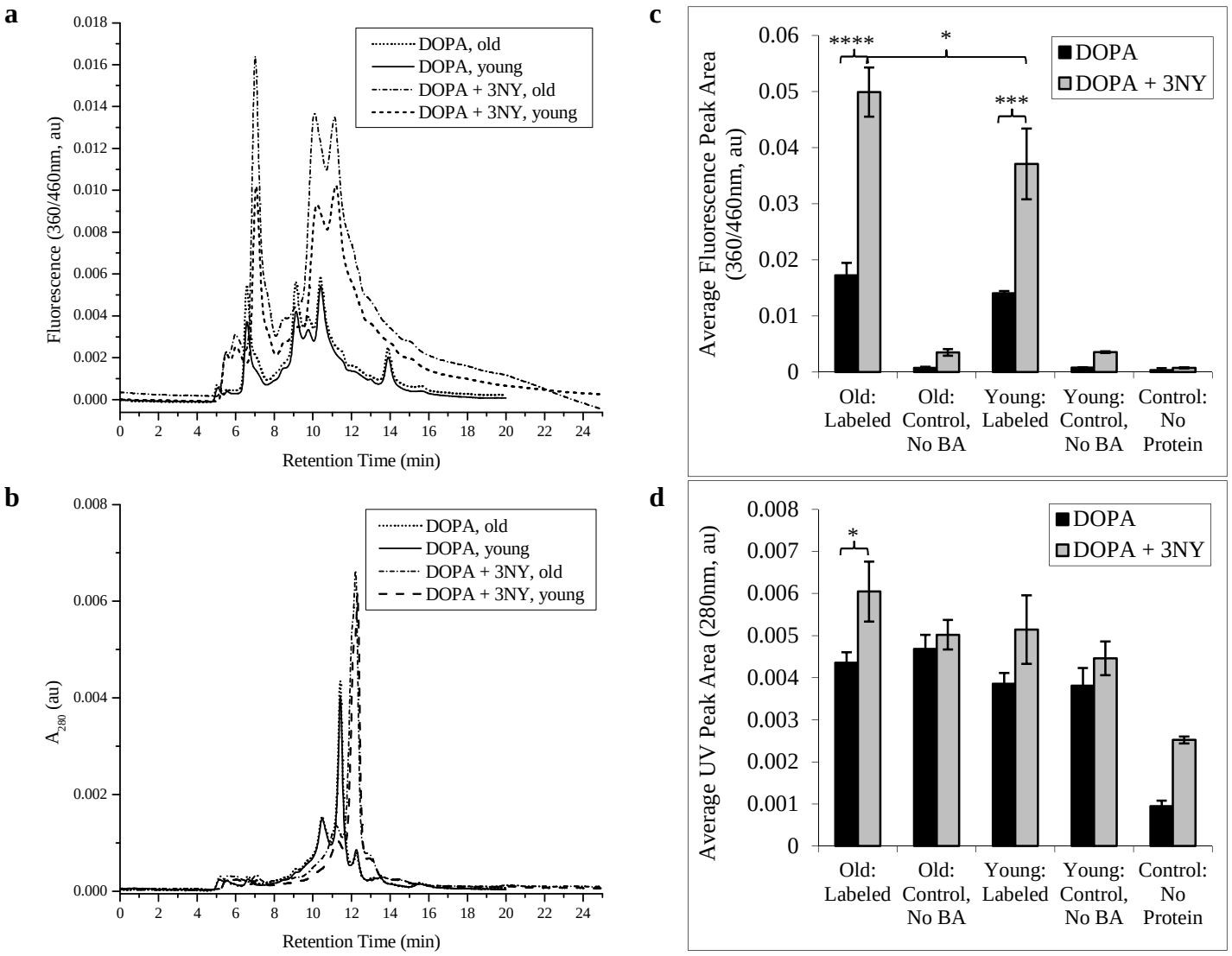

Fig. 2.8 Comparison of SE-HPLC peak areas for labeled cardiac proteins from old and young rats, with (DOPA + 3NY) or without (DOPA) prior reduction by SDT. **(a)** Averaged FL chromatograms (triplicate), **(b)** Averaged UV chromatograms (triplicate), **(c)** FL peak areas, and **(d)** UV peak areas. *p<0.05, ***p<0.005, ****p<0.001

reason, retention time ranges for peak integration were selected based primarily on peak shape, in comparison to previously observed patterns, rather than strictly on the times themselves. Various controls are included, as are peak areas for UV chromatograms (Fig. 2.8d) corresponding to the same retention time ranges that were integrated for the fluorescence data, in order to account for possible differences in protein concentrations. The SE-HPLC peak area data

show much greater fluorescence for cardiac proteins that were reduced before tagging than for those not reduced, once again demonstrating the effect of labeling 3NY in addition to DOPA and suggesting that a significant amount of the former exists in the cardiac samples. A two-tailed unpaired Student's t-test was used to calculate all p-values.

2.3.6 Putative Protein Identifications

Fig. 2.9 shows MS/MS spectra that have been assigned by the proteomic search algorithms to BA- or ABS-labeled tryptic peptides from the rat protein sequence database. While these are putative identifications of endogenous Tyr nitration sites, the spectral quality and assignments are not sufficient to support confident identification.

2.4 Discussion and Conclusions

The effects of various conditions for sample preparation and derivatization reactions have been studied for the fluorogenic labeling of protein-bound 3NY and DOPA in cardiac tissue homogenates. While the multidimensional nature of the optimization process has produced data with sometimes inconsistent results and trends, likely affected by changes of multiple conditions between experiments, several systematic studies have yielded informative results for method development. These include reduction conditions with 10-20mM SDT for 1.5-2min to convert 3NY to 3AY, with the results being more dependent on SDT concentration than on reaction time. Experiments with model systems have indicated side product formation with long reaction times and high SDT concentrations (Victor Sharov, unpublished results). Since this phenomenon is difficult to measure directly in the more complex cardiac samples, it is best to use the minimal SDT concentration and reaction time necessary to give sufficient product yield, as measured by fluorescence intensity. The dependence of fluorescence intensity on derivatization reagent concentrations has also been studied, and the optimized conditions applied to compare samples

Fig. 2.9 MS/MS spectra for putative identifications of 3NY-containing tryptic peptides from rat cardiac protein samples.

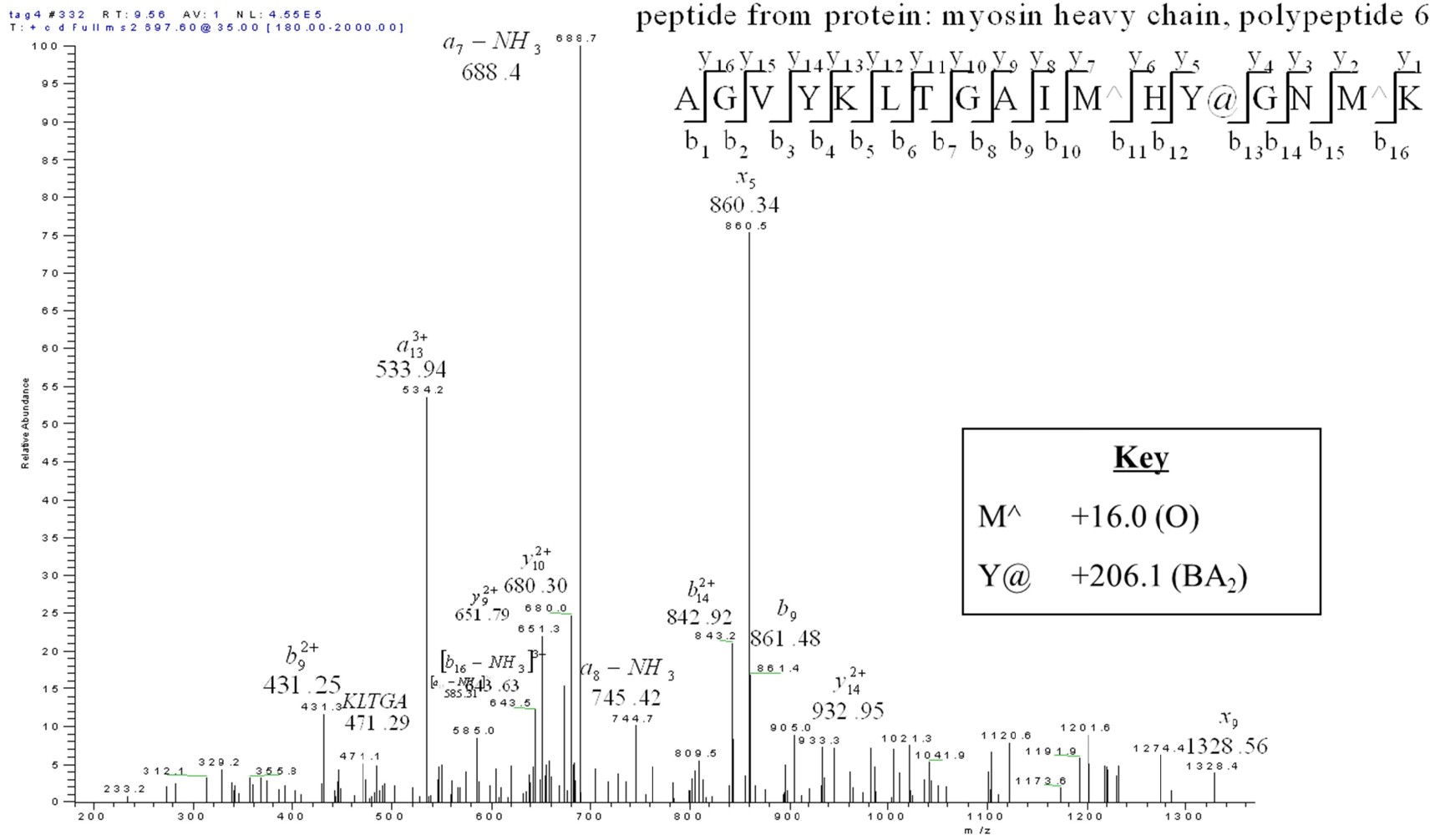

Fig. 2.9a

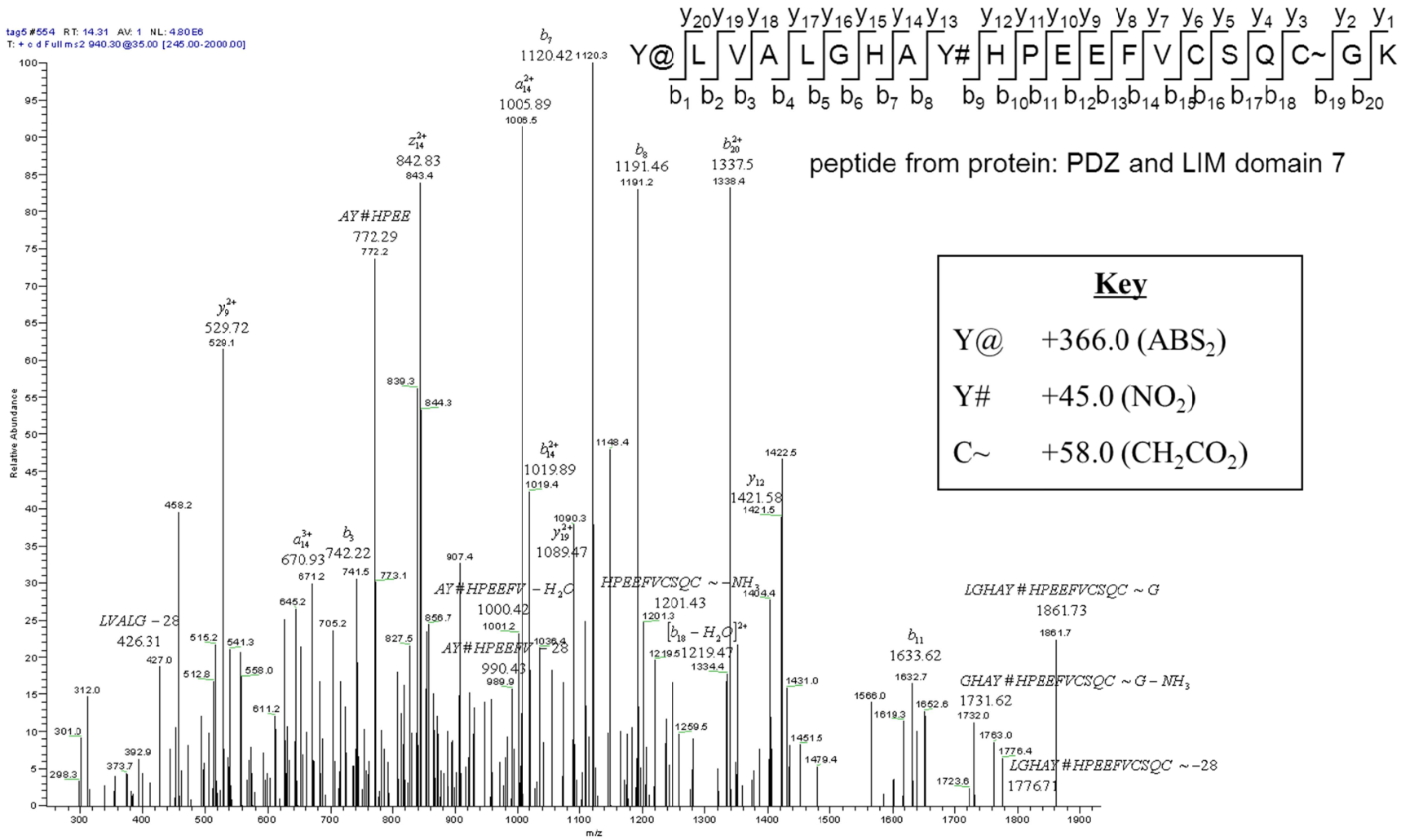
tag5 #554 RT: 14.31 AV: 1 NL: 4.80E6
T: + c d Full ms2 940.30@35.00 [245.00-2000.00]
Y@LVALGHAY#HPEEFVCSQC~GK
peptide from protein: PDZ and LIM domain 7
Key
Y@ +366.0 (ABS2)
Y# +45.0 (NO2)
C~ +58.0 (CH2CO2)
Relative Abundance
m/z

Fig. 2.9b

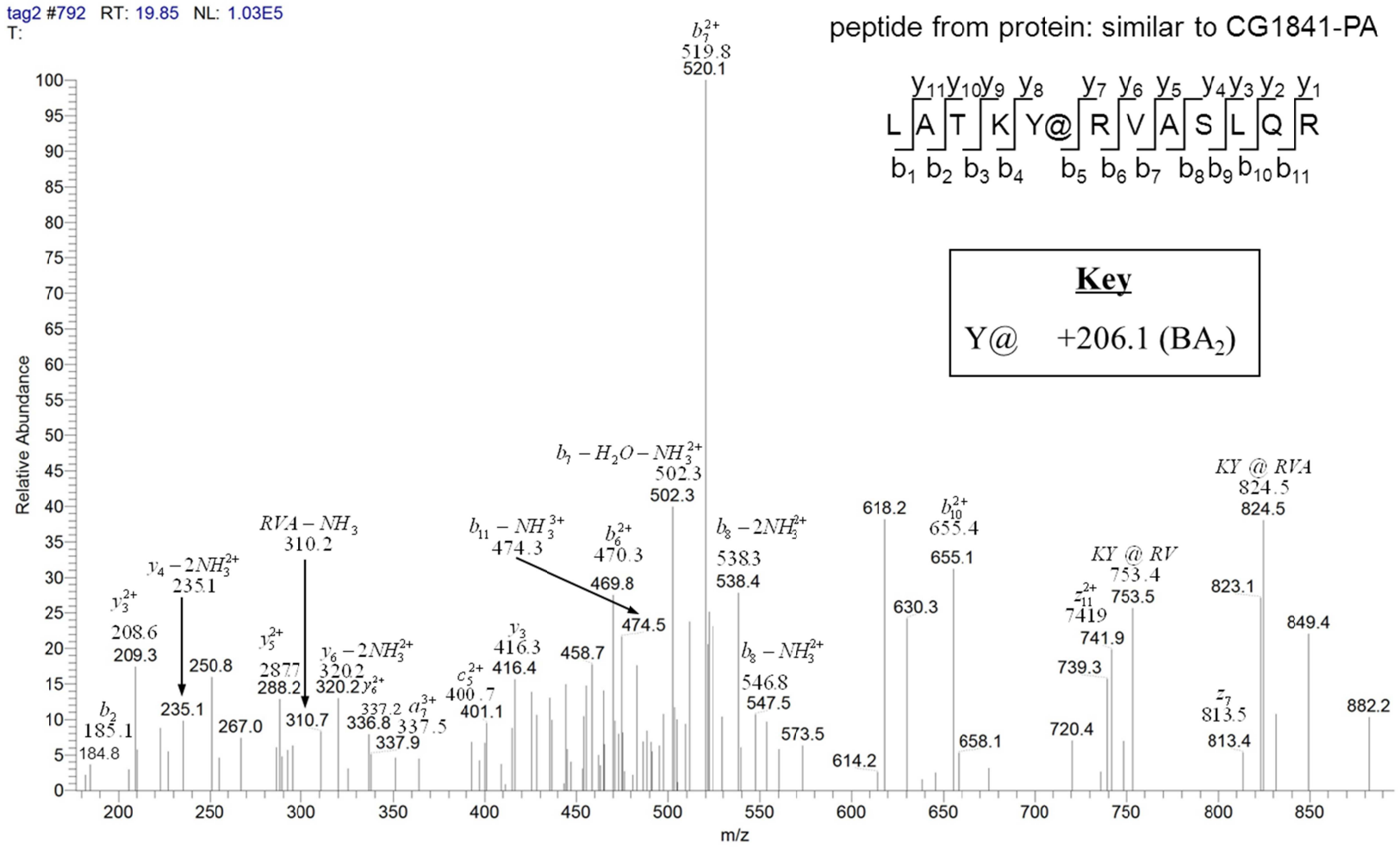
tag2 #792 RT: 19.85 NL: 1.03E5
T:
peptide from protein: similar to CG1841-PA
L A T K Y@ R V A S L Q R
Key
Y@ +206.1 (BA2)
Relative Abundance
m/z

Fig. 2.9c

from old and young rats as well as samples tagged for DOPA only (non-reduced) with those tagged for DOPA plus 3NY (reduced). While several experiments demonstrate significant increases in labeling for reduced samples relative to non-reduced and for old relative to young, these results could not always be reproduced in follow-up experiments. Differences in sample preparation conditions may contribute to this inconsistency. For instance, comparison of protein precipitation methods for cleaning reagents away from cardiac proteins revealed that the EtOH method may have a bias against protein recovery in samples not reduced by SDT, whereas the TCA method has no such bias and does not show a significant difference in fluorescence for these two sample sets, either. Animal-to-animal variability is also an important consideration in working with biological samples, and larger sample sizes, for instance using at least 3 animals in each age group, could provide a more definitive answer to the question of whether PTM accumulation occurs with aging, or at least whether such accumulation is detectable by this method. Tighter quality control for consistency between preparations of cardiac homogenates (for instance, by SDS-PAGE analysis) and for proper function of the HPLC instrument would also help to minimize variability.

Ultimately, the goal of this labeling method is the proteomic identification, by mass spectrometry, of oxidized proteins in aging cardiac tissue. Since these PTMs are in low abundance *in vivo*, it is crucial that the labeling method is as complete and as selective as possible. While searches of nano-HPLC-MS/MS data against the rat proteome database have produced some putative identifications of modified proteins, the sample complexity demands a high standard of spectral quality for confident identification, in order to avoid false positives. Under the current conditions, such confidence has not been achieved. Moving forward, one strategy planned to progress toward this goal is the implementation of ultra-high-performance

liquid chromatography on a 2m-long capillary column on-line with the electrospray source for mass spectrometry. This method is capable of dramatically improving chromatographic column capacity and resolution for tryptic peptides, which in turn reduces ion suppression effects from the overwhelming matrix of unmodified cardiac peptides and thus enhances the signal for low-abundance modified peptides. Another approach to minimize this ion suppression and other interferences is to enrich labeled peptides using the reagent APPD with boronate-affinity HPLC. Finally, in order to overcome limitations due to the suspected low analyte concentrations, nitration of cardiac proteins *in vitro* by peroxynitrite could provide samples with sufficient levels of 3NY to enable effective identification as a proof of concept and to provide a more effective platform for method optimization studies.

2.5 References

1. Dremina ES, Li X, Galeva NA, Sharov VS, Stobaugh JF, Schöneich C. A methodology for simultaneous fluorogenic derivatization and boronate affinity enrichment of 3-nitrotyrosine-containing peptides. *Analytical Biochemistry* 418: 184-196, 2011.
2. Feeney MB, Schöneich C. Proteomic Approaches to Analyze Protein Tyrosine Nitration. *Antioxid Redox Signal* in press, 2012.
3. Feeney MB, Schöneich C. Tyrosine modifications in aging. *Antioxid Redox Signal* 17: 1571-1579, 2012.
4. Kanski J, Behring A, Pelling J, Schöneich C. Proteomic identification of 3-nitrotyrosine-containing rat cardiac proteins: effects of biological aging. *Am J Physiol Heart Circ Physiol* 288: H371-H381, 2005.
5. Kanski J, Hong SJ, Schöneich C. Proteomic analysis of protein nitration in aging skeletal muscle and identification of nitrotyrosine-containing sequences in vivo by

nanoelectrospray ionization tandem mass spectrometry. *J Biol Chem* 280: 24261-24266, 2005.

6. Pennington J, Schöneich C, Stobaugh J. Selective Fluorogenic Derivatization with Isotopic Coding of Catechols and 2-Amino Phenols with Benzylamine: A Chemical Basis for the Relative Determination of 3-Hydroxy-tyrosine and 3-Nitro-tyrosine Peptides. *Chromatographia* 66: 649-659, 2007.
7. Perrin DD. *Dissociation Constants of Organic Bases in Aqueous Solution: By D. D. Perrin*: Butterworths; 1965.
8. Sharov V, Dremina E, Galeva N, Gerstenecker G, Li X, Dobrowsky R, Stobaugh J, Schöneich C. Fluorogenic Tagging of Peptide and Protein 3-Nitrotyrosine with 4-(Aminomethyl)benzenesulfonic Acid for Quantitative Analysis of Protein Tyrosine Nitration. *Chromatographia* 71: 37-53, 2010.
9. Sharov VS, Dremina ES, Pennington J, Killmer J, Asmus C, Thorson M, Hong SJ, Li X, Stobaugh JF, Schöneich C. Selective Fluorogenic Derivatization of 3-Nitrotyrosine and 3,4-Dihydroxyphenylalanine in Peptides: A Method Designed for Quantitative Proteomic Analysis. *Methods in Enzymology* Volume 441: 19-32, 2008.
10. Sharov VS, Galeva NA, Kanski J, Williams TD, Schöneich C. Age-associated tyrosine nitration of rat skeletal muscle glycogen phosphorylase b: characterization by HPLC–nanoelectrospray–Tandem mass spectrometry. *Exp Gerontol* 41: 407-416, 2006.
11. Snyder LR, Kirkland JJ, Glajch JL. Biochemical Samples: Proteins, Nucleic Acids, Carbohydrates, and Related Compounds. In: *Practical HPLC Method Development*. John Wiley & Sons, Inc.; 1997. pp. 479-536.

12. Zhang X, Monroe ME, Chen B, Chin MH, Heibeck TH, Schepmoes AA, Yang F, Petritis BO, Camp DG, Pounds JG, Jacobs JM, Smith DJ, Bigelow DJ, Smith RD, Qian W-J. Endogenous 3,4-dihydroxyphenylalanine and dopaquinone modifications on protein tyrosine: links to mitochondrially derived oxidative stress via hydroxyl radical. *Mol Cell Proteomics* 9: 1199-1208, 2010.

Chapter 3: Derivatization of Glycogen Phosphorylase *b* Protein Nitrated *in vitro*

3.1 Introduction

3.1.1 Glycogen Phosphorylase *b* as a Target of Tyrosine Nitration

Glycogen phosphorylase *b* (Ph-b) has previously been identified as a target of tyrosine nitration both *in vivo* (for instance, as a result of aging) and *in vitro* (2,11,12). With a total molecular weight of 97kDa, it contains 842 amino acids, 36 of which are Tyr (4.3%). This enzyme is an important part of glucose metabolism, converting glycogen to glucose-1-phosphate (2,11). It comprises approximately 5% of total soluble protein in skeletal muscle tissue (11), and its functional impairment leads to deficits in muscle function and metabolic myopathy, such as McArdle's disease (2,11,12). This protein has >95% homology across mammalian species and 98% homology among rabbit, mouse, and human amino acid sequences. In a previous study, Sharov et al. (10) identified by HPLC-MS/MS sequencing 11 unique *in-vitro* nitration sites labeled with the benzylamine derivative 4-(aminomethyl)benzenesulfonic acid. Ph-b nitrated *in vitro* by peroxynitrite was selected as a model nitro-protein to spike into cardiac homogenate samples in order to study the effectiveness of the APPD derivatization strategy within this complex matrix.

3.1.2 "Denitration"

The site-specific accumulation of 3NY in disease and aging results from a combination of processes that generate 3NY and those that repair or remove it (1,9). Both types of processes can be specific or preferential for particular proteins and particular Tyr residue locations. The formation of 3NY can depend on the nitrating agent, cellular localization, protein conformation (especially as it affects the solvent accessibility of Tyr), neighboring amino acids, and interactions of the protein with other proteins or small molecules, particularly metals (1,9). The loss of 3NY can occur by proteolytic degradation (turnover) of damaged proteins or by

"denitration" processes that have been proposed but are not yet clearly understood (1); both of these can have protein or site selectivity. The balance of all of these factors also helps to explain the differences often observed between nitration patterns *in vivo* and *in vitro*.

Incubation of nitrated proteins with various biological matrices has been shown to decrease 3NY levels by a process that is dependent on time, concentration, and temperature, as summarized here based on a review by Abello, et al. (1). This phenomenon persists in the presence of a proteasome inhibitor. It has been reported to be sensitive to heat, trypsin, and peroxynitrite treatments and is inducible by lipopolysaccharide. Filtration with a 10kDa-cutoff membrane did not destroy the activity in one case, but dialysis reduced it by 70% in another. In some cases, denitration is dependent upon oxygen tension. Calcium dependence has been reported in some systems, accompanied by nitrate ion formation. In addition to the hypothesis of an enzymatic system, heme-bound Fe^{3+} plus a reducing agent like dithiothreitol (a common additive in homogenate preparations) is capable of removing 3NY by reducing it to 3AY, as is cobalt-containing cyanocobalamin. No enzymatic system has been identified, and the exact nature of this phenomenon – or, more likely, combination of phenomena – is still unclear.

Products of denitration have been identified as 3AY and native Tyr, but other products are also possible (1,9). Importantly, the formation of 3AY makes these residues undetectable by immunoaffinity methods but does not interfere with fluorogenic derivatization by benzylamine or its derivatives.

3.2 Experimental Methods

3.2.1 Materials

Ammonium bicarbonate; sodium iodoacetate, SigmaUltra; sodium dithionite (SDT), synonym sodium hydrosulfite, technical grade, 85%; sodium phosphate dibasic ACS reagent

(anhydrous); benzylamine, redistilled, 99.5%+, which was stored in a sealed container protected from air, moisture and light and retrieved under positive pressure of argon to protect the stock from air exposure; trichloroacetic acid, electrophoresis reagent, minimum 99%; 2-mercaptoethanol; methanol, CHROMASOLV grade; acetone, CHROMASOLV®, for HPLC, ≥99.9%; albumin bovine serum, Fraction V, ≥96%; and potassium ferricyanide were all obtained from Sigma-Aldrich, St. Louis, MO, USA. Ponceau S was also purchased from Sigma-Aldrich and prepared as a 0.5% (w/v) solution with 5% acetic acid.

Sodium dodecyl sulfate (SDS), electrophoresis grade; sodium hydroxide, certified ACS; sodium phosphate monobasic, certified ACS (monohydrate); sodium sulfate, certified ACS (anhydrous); tris(hydroxymethyl)aminomethane hydrochloride, for molecular biology; sodium chloride, certified ACS; hydrochloric acid, Certified ACS Plus; Millipore Immobilon-P polyvinylidene fluoride (PVDF) transfer membranes, 0.45 μm pore size; Tween 20, enzyme grade; Whatman 3MM Chr chromatography paper; GE Healthcare Amersham ECL Plus Western blotting detection system; and Kodak GBX developer and fixer solutions were all obtained from Fisher Scientific, Pittsburgh, PA, USA.

Phosphorylase b (rabbit muscle), 39.9% protein, balance predominantly lactose was from Prozyme, Hayward, CA.

DL-dithiothreitol (DTT), molecular biology grade; and sequencing grade modified trypsin, porcine, specific activity >5,000U/mg were from Promega, Madison, WI.

Ethanol, 99.90-100.00%, was from Decon Laboratories, Inc., King of Prussia, PA, USA.

CHAPS 3-[(3-cholamidopropyl)dimethylamonio]-1-propanesulfonate; bicinchoninic acid (BCA) protein assay kit; Slide-A-Lyzer MINI dialysis units, 7kDa molecular-weight cutoff; zeba

spin desalting columns, 7kDa molecular-weight cutoff, 0.5mL; and goat anti-mouse HRP secondary antibody were all from Thermo Scientific (Rockford, IL, USA).

Amicon Microcon YM-10 centrifugal concentrators with regenerated cellulose ultrafiltration membranes, 10kDa molecular-weight cutoff, were from EMD Millipore, Billerica, MA, USA.

2X Laemmli sample buffer; 10X tris/glycine/SDS buffer for SDS-PAGE applications; Ready Gel® Tris-HCl, 4-20% precast linear gradient polyacrylamide gel, 10-well, 50µL, 8.6 x 6.8 cm; Precision Plus Protein Dual Color Standards; and 10X TG tris/glycine buffer were from Bio-Rad, Hercules, CA, USA.

Monoclonal antibody to nitrotyrosine, mouse IgG2b, was purchased from GenWay Biotech, Inc., San Diego, CA, USA.

Classic blue autoradiography film BX was from MIDSCI, St. Louis, MO.

3.2.2 Preparation and Nitration of Ph-b

Ph-b was dissolved in 50mM ammonium bicarbonate buffer at pH 8 with 1% (w/v) SDS to a protein concentration of 1mg/mL (approximately 10µM). Cys residues were reduced with 2mM DTT for 30min at 50°C and alkylated with 5mM sodium iodoacetate for 30min at room temperature. Ten volumes of cold 100% ethanol were added and the solution incubated for four hours at -70°C to precipitate the proteins. Following centrifugation for 5min at 5,445×*g*, the supernatant was discarded and the pellet re-constituted in 50mM ammonium bicarbonate buffer at pH 8 with 1% (w/v) SDS. Aliquots of the prepared protein were stored at -20°C until use. "Control" Ph-b proteins were used as is, whereas "3NY-Ph-b" proteins were prepared by treating these aliquots with peroxynitrite.

Peroxynitrite was prepared according to a previously published method for the ozonolysis of sodium azide solutions (7) and stored in alkaline solution at -70°C. Prior to each use, aliquots were thawed on ice, and the peroxynitrite concentration was measured by absorbance of a diluted solution prepared in 0.1% sodium hydroxide, using $\varepsilon_{302} = 1{,}670 M^{-1}cm^{-1}$ (7) in order to account for its gradual degradation during storage. Approximately 3mM final concentration of peroxynitrite was added to 1mg/mL (approximately 10µM) Ph-b by placing a droplet of peroxynitrite solution on the side of the microcentrifuge tube and vortexing quickly. This technique is important for ensuring relatively even distribution of reactive peroxynitrite in the protein solution because it degrades very quickly at pH 8 (7). In order to determine the extent of nitration in each sample, 3NY concentration was determined based on its absorbance at 430nm with $\varepsilon_{430} = 4{,}400 M^{-1}cm^{-1}$ when pH is above 9 (5,10). Specifically, solutions of both control Ph-b and 3NY-Ph-b were prepared in 0.1% sodium hydroxide, and the absorbance value at 430nm for the former was subtracted from that of the latter. This corrected absorbance value was used to calculate 3NY concentration based on Beer's law:

$$A = \varepsilon bc$$

Eq. 3.1

where A is absorbance, ε is molar absorptivity (i.e., extinction coefficient), b is the path length, and c is the concentration of the absorbing species. Aliquots of 3NY-Ph-b were stored at -20°C until use and sometimes required brief sonication to dissolve precipitates that formed upon freezing and storage, typically for 5s at 10-15% power output of the probe sonicator Sonic Dismembrator 500 (Fisher Scientific, Pittsburgh, PA, USA).

3.2.3 Derivatization Reaction

3NY-Ph-b at a concentration of 8µM and carrying approximately 16 mol 3NY per mol of protein (in 50mM ammonium bicarbonate buffer, pH 8, with 1% w/v SDS) was reduced with 10mM SDT for 2min at room temperature and then immediately precipitated by 10 volumes of cold 100% ethanol at -70°C for 3h. After centrifugation at 13,000×*g* for 2min, the supernatant was discarded and the pellet re-constituted in 0.1M sodium phosphate buffer at pH 9 with 4% (w/v) CHAPS detergent, using sonication for 5s at 15% power output. The zwitterionic detergent CHAPS was selected because SDS was found to cause large amounts of precipitation in tagging samples, especially when the pH was decreased in subsequent steps (e.g., size-exclusion HPLC, SE-HPLC). This is presumably due to ion pairing between the negatively charged SDS detergent and the large excesses of protonated benzylamine reagent, $pK_a = 9.32$ (6).

Fluorogenic derivatization was carried out with 0.5µM Ph-b (8µM 3NY), 1mM potassium ferricyanide, and 5% (v/v) benzylamine (= 458mM). Reactions proceeded in the dark at room temperature for various lengths of time. Some experiments monitored reaction progress based on fluorescence emission intensity with excitation and emission wavelengths 360nm and 460nm, respectively, using a Shimadzu RF 5000U Spectrofluorophotometer (Kyoto, Japan) set to high sensitivity. Fluorescence excitation and emission spectra were also collected with this instrument at high sensitivity, using 460nm as the emission wavelength for the former and 360nm as the excitation wavelength for the latter.

Multiple controls were included in these experiments, including 3NY-Ph-b not exposed to SDT (i.e., non-reduced). For both the reduced and non-reduced Ph-b samples, controls omitting either potassium ferricyanide or benzylamine from the derivatization reaction were included. Finally, a sample containing no protein but with all other components of the

derivatization reaction (buffer, potassium ferricyanide, benzylamine) were measured. These samples were also analyzed by SE-HPLC (see section 3.2.5).

3.2.4 Determining the Limit of Detection (LOD) for 3NY-Ph-b in a Background of Cardiac Proteins

After about 1h reaction time, derivatized Ph-b was precipitated by addition of at least 10 volumes 100% ethanol and overnight incubation at -20°C. After centrifugation, the labeled protein was re-constituted in 0.1M sodium phosphate buffer at pH 7.4 with 4% (w/v) CHAPS (protein dissolution was slow). Serial dilutions of labeled Ph-b mixed with a constant amount of cardiac protein solution (see section 2.2.2) were prepared and their fluorescence spectra collected as described in section 3.2.3. These samples were also analyzed by SE-HPLC (see section 3.2.5).

In order to provide a more accurate assessment of the tagging efficiency for proteins within the cardiac homogenate matrix, 3NY-Ph-b and control Ph-b were added to cardiac samples in ratios designed to keep the total Ph-b and cardiac protein concentrations constant while varying the concentration of 3NY on Ph-b. Next, the Ph-b plus cardiac mixtures were subjected to the reduction and derivatization procedures, which will be described below. This experiment was conducted in duplicate to assess variability. A few adjustments to the labeling protocol were made for optimization purposes. Precipitation by ethanol was replaced with trichloroacetic acid (TCA), namely the addition of ten volumes of cold aqueous TCA to give a final acid concentration of 20% (w/v). Samples were incubated overnight on ice in a refrigerator maintained at 4°C. Pellets were collected by centrifugation at 5,445×*g* for 5min and washed three times with 5mL cold acetone to remove any remaining traces of TCA. This precipitation method was shown to improve cardiac protein recovery to 96%, compared to 51% recovery from

ethanol precipitation, based on BCA protein concentration assay (see section 2.2.4). TCA precipitation also showed superior removal of SDT, potassium ferricyanide, and sodium phosphate, based on visual observations of control solutions containing each of these substances individually and subjected to each precipitation protocol. TCA precipitation showed the best performance among all protein clean-up methods tested, which also included dialysis (7kDa molecular-weight cutoff), zeba size-exclusion desalting cartridges (7kDa molecular-weight cutoff), and microcon centrifugal filters (10kDa molecular-weight cutoff). The microcon filters showed nearly equal performance to TCA precipitation but have significantly greater cost. In addition, proteins can clog the filters, especially given the high concentrations that occur during the filtration process. This leads to long centrifugation times and may also adversely affect performance in removal of non-protein solution components. After the TCA precipitation process, proteins were re-constituted in 50mM ammonium bicarbonate buffer at pH 9 with 4% (w/v) CHAPS. This buffer was chosen over sodium phosphate for its compatibility with mass spectrometry, which was the ultimate goal for proteomic analysis of cardiac protein samples labeled by this method.

As each preparation of 3NY-Ph-b has some variability in the extent of nitration, protein concentrations were adjusted to match the 3NY concentration in the previous experiment, while the total Ph-b concentration was different. The stock of 3NY-Ph-b used for this particular experiment contained 2.5mg/mL (approximately 25µM) Ph-b with 6.3mol 3NY per mol Ph-b, giving a stock 3NY concentration of approximately 160µM. Control Ph-b was prepared as described in section 3.2.2, with an estimated final concentration of 2.5mg/mL, or approximately 25µM (assumes no losses during preparation steps). Cardiac proteins were prepared as described in section 2.2.2 from heart tissue harvested from young (5 months old) rats, with a stock protein

concentration of 0.9mg/mL (based on BCA assay, see section 2.2.4) in 50mM ammonium bicarbonate buffer with pH 7.4 and 4% (w/v) CHAPS. Five solutions of 3NY-Ph-b with a range of 3NY concentrations were prepared by serial dilution. To each of these solutions, control Ph-b and cardiac proteins were added to give a total Ph-b concentration of 0.08mg/mL, cardiac protein concentration of 0.45mg/mL, and 3NY concentrations (on Ph-b) in the range 0-5.1µM. SDT, prepared immediately before use as described above, was added to each solution to a final concentration of 10mM, and the reduction reaction was stopped after 1.5min by TCA precipitation, as described above. After re-constitution in 50mM ammonium bicarbonate, pH 9, with 4% (w/v) CHAPS, which required about 30min to complete, samples were derivatized with 1mM potassium ferricyanide and 5% (v/v; approximately 460mM) benzylamine for 1h at room temperature in the dark. Due to a pipetting error, the potassium ferricyanide concentrations in one of the duplicate sample sets was actually 1.8mM, and a slight dilution of other components resulted from the small increase in solution volume. The second set was prepared accurately as planned. Fluorescence spectra were obtained as described in section 3.2.3.

Finally, in order to more closely mimic physiological conditions, a lower 3NY concentration range was tested. As another optimization effort, 4% (w/v) CHAPS was replaced with 1% (w/v) SDS in both the cardiac and derivatization buffers due to its superior performance in solubilizing proteins. In order to avoid ion-pairing and consequent precipitation, pH was maintained at 9 during derivatization and all subsequent analysis. This experiment was conducted in triplicate for purposes of statistical analysis and construction of a calibration curve against which to measure endogenous 3NY levels in cardiac protein samples. 3NY-Ph-b stock was the same as in the previous experiment (2.5mg/mL protein, 160µM 3NY) and was diluted to a protein concentration of 0.5mg/mL and 3NY concentration approximately 32µM. Cardiac

proteins from a young (five months old) rat were prepared as described in section 2.2.2, with re-constitution in 50mM ammonium bicarbonate buffer, pH 7.4, with 1% (w/v) SDS. The stock protein concentration was 10.2mg/mL, as measured by BCA assay (see section 2.2.4), and this was diluted to 0.9mg/mL. The protocol was the same as the previous experiment, with the following changes in concentrations: total Ph-b 0.010mg/mL and 3NY (in Ph-b) 0-0.64µM. Cardiac protein concentration remained 0.45mg/mL, and SDT, potassium ferricyanide, and benzylamine concentrations also remained the same as above. Following the reduction reaction and TCA precipitation procedure, re-constitution in the derivatization buffer was aided by sonication with three pulses of 10s each at 15% power output, with 10s breaks between pulses. After 1h reaction time at room temperature in the dark, fluorescence spectra were measured as described above, and maximal emission intensity near the expected wavelength (440-460nm) was plotted against 3NY concentration. The mean of triplicate sample sets was used to generate a calibration curve and calculate a limit of detection (LOD). In order to account for larger standard deviations in non-blank samples than in the blanks, the LOD was calculated using a pooled standard deviation (13). In addition, samples containing cardiac proteins and control Ph-b (but no 3NY-Ph-b) were compared to samples containing only cardiac proteins that did not undergo reduction by SDT, using a two-tailed Student's t-test (13) to determine whether the difference between these means was statistically significant.

3.2.5 Size-Exclusion HPLC (SE-HPLC)

SE-HPLC was performed on a Shimadzu 10A Series High-Performance Liquid Chromatograph (Kyoto, Japan). An isocratic method using 0.1M sodium phosphate plus 0.1M sodium sulfate, pH 6.8, as a mobile phase at a flow rate of 1.0mL/min separated protein solutions on a Tosoh TSK-GEL G3000SW_{XL} column, 7.8mm ID x 30cm, 5µm particles. The loop volume

for the manual injector was 20µL, and 40µL protein solution was loaded in order to ensure complete loop filling. Detection was by UV absorbance at 280nm and fluorescence at excitation 360nm and emission 460nm.

3.2.6 Western Blots for Nitrotyrosine

SDS polyacrylamide gel electrophoresis (SDS-PAGE) followed by Western blotting for 3NY were performed using the Bio-Rad Mini-PROTEAN® electrophoresis and blotting system (Hercules, CA, USA). Samples were prepared with combinations of 3NY-Ph-b carrying approximately 5.5mol 3NY per mol protein and cardiac proteins [see section 2.2.2 for preparation conditions; buffer was 50mM ammonium bicarbonate at pH 7.4 with 1% (w/v) SDS], with or without treatment with 20mM SDT. After adding SDT (or 18MΩ water for controls), samples were mixed with an equal volume of 2X Laemmli sample buffer and heated in a boiling water bath for 2min. For reducing conditions, 5% (v/v) 2-mercaptoethanol was first added to the stock solution of sample buffer. For non-reducing conditions, the sample buffer was used as received. Samples and molecular-weight markers were loaded into pre-cast 4-20% gradient gels and separated by electrophoresis in 1X tris/glycine/SDS run buffer at constant 200V for 38min, with maximum current limited at 400mA.

Following SDS-PAGE, protein bands were transferred from the gels to PVDF membranes in 1X tris/glycine buffer (25mM tris(hydroxymethyl)aminomethane, 192mM glycine, pH 8.3) with 20% methanol at constant 100V for 2h, with cooling; maximum current was limited at 400mA. Membranes were blocked for 1h with two changes of the blocking buffer, which consisted of 5% (w/v) nonfat dried milk, 20mM tris(hydroxymethyl)aminomethane hydrochloride plus 150mM sodium chloride, pH 7.4, and 0.1% (v/v) Tween 20. Incubation for 2h with anti-3NY primary antibody in blocking buffer at a volume ratio of 1:3,000 was followed

by thorough washing with blocking buffer and incubation for 1h with goat anti-mouse HRP secondary antibody in blocking buffer at a volume ratio of 1:10,000. After thorough washing first with blocking buffer and then with 20mM tris(hydroxymethyl)aminomethane hydrochloride plus 150mM sodium chloride, pH 7.4, with 0.1% (v/v) Tween 20, bands were visualized using the ECL Plus kit according to manufacturer's instructions, with reagents A and B in a 40:1 ratio and film exposition for 10min. Membranes were also stained with 0.5% (w/v) Ponceau S in 5% (v/v) acetic acid to visualize total protein and evaluate loading and transfer consistency.

3.2.7 Mass Spectrometry for Identification of Ph-b Modifications After Mixing with Cardiac Proteins

Protein bands of ca. 100kDa, corresponding to the location of pure Ph-b, were excised from the SDS-PAGE gel (prepared as described in section 3.2.6), washed extensively and digested in-gel with trypsin to extract peptides for HPLC-MS/MS analysis. Samples were separated by capillary HPLC (capLC) with on-line electrospray ionization (ESI) into an LTQ-FT hybrid linear quadrupole ion trap Fourier transform ion cyclotron resonance (FTICR) mass spectrometer (ThermoFinnigan, Bremen, Germany). Sample handling and data analysis methods were analogous to a published procedure (3).

3.3 Results

3.3.1 Protein Derivatization

Under the conditions described in section 3.2.3, the labeling reaction appears to proceed rather quickly, reaching 62% of the final fluorescence intensity after only 8min reaction time and 84% after 25min (Fig. 3.1). After approximately 1h total reaction time, the fluorescence intensity for the tagged Ph-b sample is substantially larger than any background fluorescence in

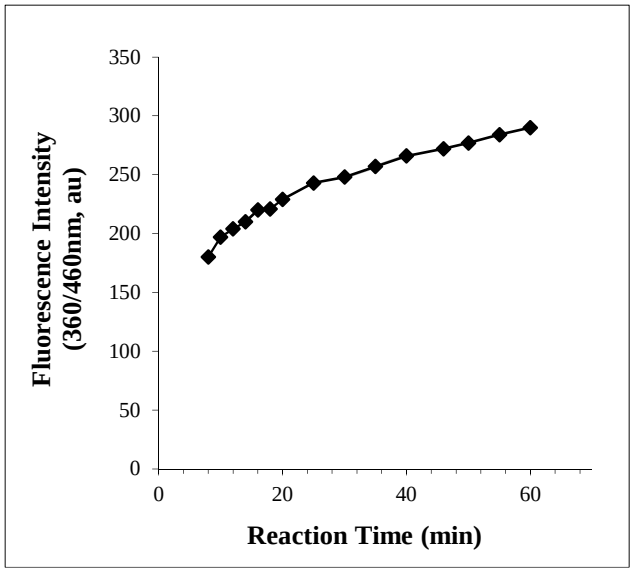

Fig. 3.1 Time course for derivatization of nitrated Ph-b with benzylamine.

the control samples (Fig. 3.2). It is also noteworthy that the wavelengths of maximum intensity shift for controls omitting either potassium ferricyanide or benzylamine.

3.3.2 Derivatization Results in Presence of Cardiac Proteins

3.3.2.1 Linear Dependence of Fluorescence Intensity on Concentration of 3NY-Ph-b

Samples of 3NY-Ph-b that were first derivatized with benzylamine and then mixed with cardiac protein solutions showed a linear response in fluorescence emission intensity with relation to 3NY concentration (Fig. 3.3). The data is corrected by subtracting the baseline fluorescence of a control containing only cardiac proteins and buffer. The SE-HPLC results for these same samples show a correlation that is not as linear as the fluorescence intensity data. Fig. 3.4 shows plots of both fluorescence and UV peak areas, also corrected by

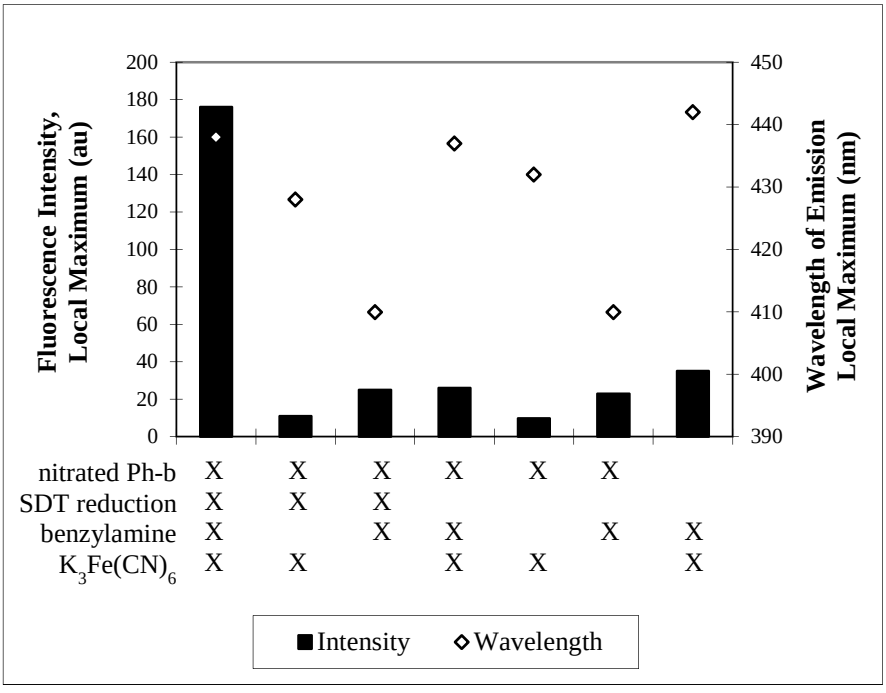

Fig. 3.2 Fluorescence properties of nitrated Ph-b derivatized with benzylamine and controls, approximately 1h reaction time.

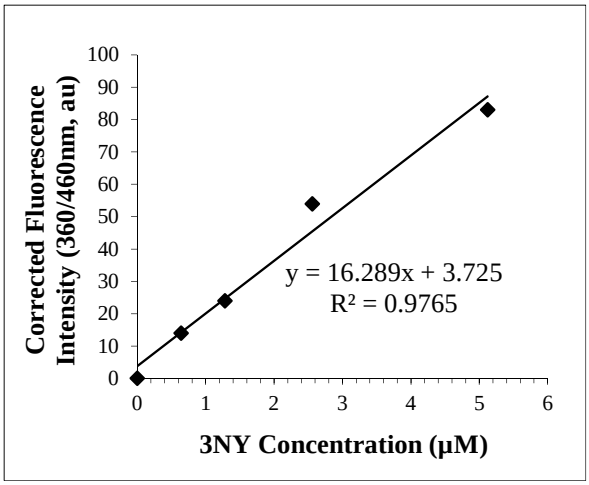

Fig. 3.3 Linear dependence of fluorescence on 3NY concentration in Ph-b derivatized with benzylamine and added to cardiac homogenate solution.

and tagging, a clear linear relationship was observed between the maximal fluorescence intensity near the expected emission wavelength (440-460nm) and the concentration of 3NY in Ph-b. Fig. 3.5 shows data for each of the duplicate sample sets, as well as their mean values, all of which have $R^2 > 0.99$. The variation between the two sample sets may be due to the pipetting error described in section 3.2.4, but the mean nevertheless shows good linearity. The data have been corrected by subtraction of fluorescence from the sample containing no 3NY-Ph-b. subtracting the values for the cardiac protein-only control, against the 3NY concentration. These results are based on a single experiment, and the fluorescence chromatograms were of fairly low intensity.

When 3NY-Ph-b, control Ph-b, and cardiac proteins were mixed prior to reduction

a

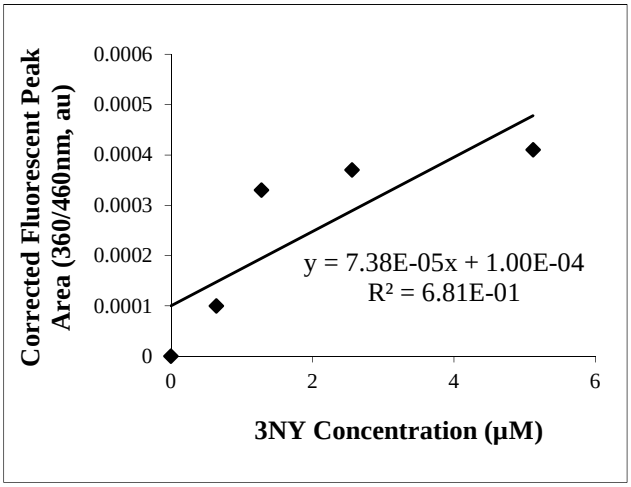

b

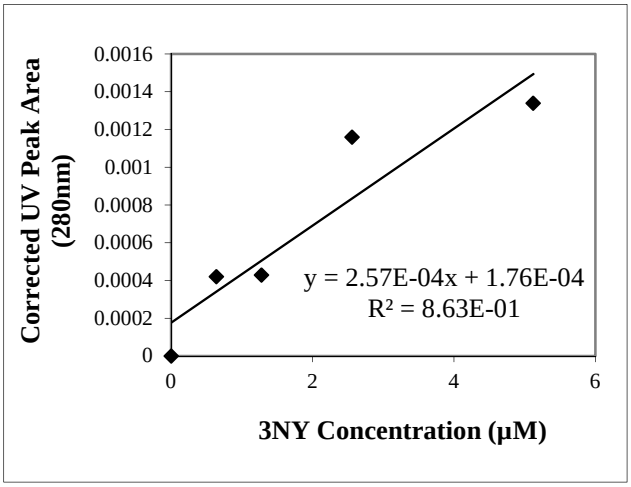

Fig. 3.4 Dependence of fluorescence **(a)** and UV **(b)** SEC-HPLC peak areas on 3NY concentration in Ph-b derivatized with benzylamine and added to cardiac homogenate solution.

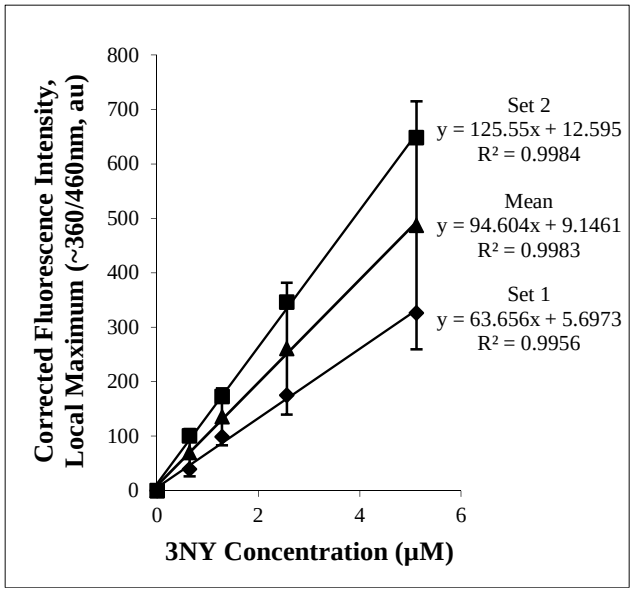

Fig. 3.5 Linear dependence of fluorescence on 3NY concentration in Ph-b mixed with cardiac homogenate solution and derivatized with benzylamine, in duplicate.

Due to the differing experimental conditions introduced by the pipetting error, this calibration curve was not used for any calculations. Instead, a new experiment was designed with several methodological improvements, as described in section 3.2.4.

When 3NY concentrations were decreased in order to test the LOD and come closer to physiological levels, a linear relationship was once again observed between corrected fluorescence intensity and 3NY concentration (Fig. 3.6). Combining data from the higher (i.e., Fig. 3.5 and lower (i.e., Fig. 3.6) 3NY concentration regimes reveals the linearity of this relationship over the entire range tested (Fig. 3.7). Only sample set 2 was used for the higher concentration regime in this plot because of the inadvertent increase in potassium ferricyanide concentrations for sample set 1, which can significantly impact fluorescence intensity. The data for higher 3NY concentrations is thus limited to n=1. Averages and standard deviations were taken for all points available at a given

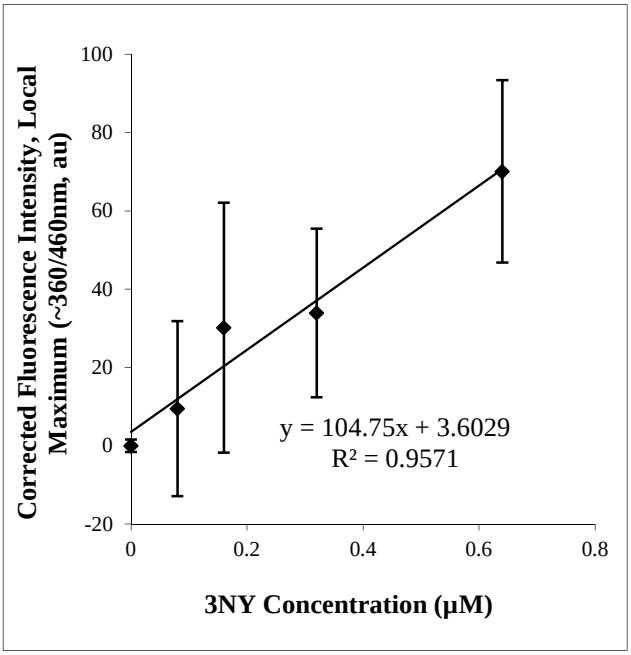

Fig. 3.6 Linear dependence of fluorescence on 3NY concentration (0-0.64µM) in Ph-b mixed with cardiac homogenate solution and derivatized with benzylamine, in triplicate.

concentration: n=4 for 0, 0.64; n=3 for 0.08, 0.16, 0.32; n=1 (no average or standard deviation) for 1.28, 2.56, 5.12. It should also be noted that some experimental parameters were changed between these two experiments, most notably the use of CHAPS in the higher-concentration experiment and SDS in the lower-concentration experiment. Nevertheless, the consistency of the data between these two experiments provides evidence for the linear response of this method over a concentration range spanning a 64-fold difference between the highest and lowest values (0.08-5.12μM).

3.3.2.2 Limit of Detection

The experiment using lower 3NY concentrations was performed in triplicate, and statistical analysis determined the LOD to be 608nM 3NY, according to the equation

$$y_{LOD} = y_{blank} + 3s_{pooled}$$

Eq. 3.2

where y_{LOD} is the fluorescence intensity at the limit of detection, y_{blank} is the fluorescence intensity of the control sample (containing cardiac protein and control Ph-b, but lacking 3NY-Ph-b), and s_{pooled} is the pooled standard deviation of all samples. This method was selected in order to account for larger standard deviations for the non-blank samples than for the blank (13). In order to calculate the 3NY concentration that corresponds to y_{LOD}, the linear regression equation of the calibration curve was solved for x_{LOD}:

$$y_{LOD} = 105x_{LOD} + 300$$

Eq. 3.3

Note that this equation was derived from a plot of uncorrected fluorescence intensities as a function of 3NY concentration (not shown, as the corrected data was selected for presentation). The uncorrected data was used for LOD calculation in order to include deviation values for the

blank sample in the calculation of s_{pooled}. For the sake of comparison, calculation of the LOD by a simpler method, according to the equation

$$y_{LOD} = y_{blank} + 3s_{blank}$$

Eq. 3.4

where s_{blank} is the standard deviation for the blank sample and the other terms are as defined above, gives a value of 8nM 3NY. However, this fails to account for the much greater variability in measurements for samples that contain 3NY-Ph-b.

3.3.2.3 Calibration for Endogenous Cardiac Modifications

Comparison of a sample containing only cardiac protein that was not reduced by SDT to a sample containing cardiac protein and control Ph-b that was reduced by SDT was planned as a method to measure the amount of endogenous 3NY present in the cardiac protein. The non-reduced sample, having been exposed to all aspects of the derivatization protocol other than addition of SDT, should not contain any labeled 3NY, although some background fluorescence is expected, including from the benzylamine-dependent derivatization of any endogenous DOPA or 5-hydroxytryptophan it may contain. On the other hand, the reduced sample would contain labeled 3NY as well as any DOPA or other

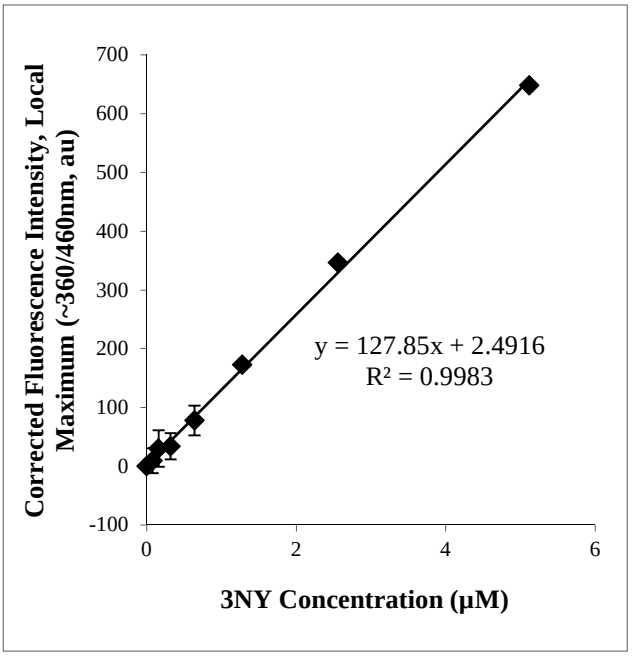

Fig. 3.7 Linear dependence of fluorescence on 3NY concentration in Ph-b mixed with cardiac homogenate solution and derivatized with benzylamine. Data combined from multiple experiments to show the entire 3NY concentration range tested: n=4 for 0µM, 0.64µM; n=3 for 0.08µM, 0.16µM, 0.32µM; n=1 for 1.28µM, 2.56µM, 5.12µM.

background fluorescence present in the non-reduced sample. Contrary to expectations, the non-reduced sample had greater fluorescence intensity than the reduced sample. However, by a two-tailed Student's t test using a pooled standard deviation (13), it was shown that the difference in mean fluorescence intensities for these two samples was not statistically significant. Therefore, it can be concluded that endogenous 3NY in these cardiac samples is below the LOD = 608nM. Using an approximate average molecular weight of 50kDa to estimate the moles of protein in the sample, an estimate of an average 420 amino acid residues per protein (50kDa protein, average molecular weight of the 20 amino acids is 119Da – not weighted for frequency of each amino acid), and the natural abundance of Tyr, which is 3.4%, it was calculated that the LOD of 608nM 3NY translates to nitration of approximately 0.48% of all Tyr residues in the cardiac protein sample. Since 3NY levels around 0.01-0.05% have been observed under inflammatory conditions (8), it is not surprising that 3NY levels in cardiac proteins from young rats are below this LOD.

3.3.3 Observed Loss of 3NY in Ph-b upon Mixing with Cardiac Proteins

3.3.3.1 Detection of Nitrotyrosine Epitope by Western Blotting Diminishes with Addition of Cardiac Proteins

In Fig. 3.8, 3NY-Ph-b was exposed to varying levels of cardiac homogenate, with or without reduction by SDT, which is known to remove the 3NY epitope by converting it to 3AY. Non-reducing conditions were employed in order to avoid any possible artifactual reduction of 3NY to 3AY, for example by DTT or 2-mercaptoethanol and heme. The results of two similar experiments are shown to demonstrate reproducibility and to provide clear visualization of all sample types, as some variation in the blot results are typical for this technique. There is an obvious reduction in size of the immunoreactive 3NY-Ph-b band when it is mixed with

increasing amounts of cardiac homogenate (Fig. 3.8a, 3.8b, 3.8d), even though total protein staining with Ponceau S shows the persistence of a band near 100kDa, corresponding to Ph-b (Fig. 3.8e). In addition, SDT eliminates immunoblot bands for 3NY-Ph-b in each case. Some cardiac proteins above 50kDa show some sensitivity to reduction by SDT, but other bands, especially those near 25kDa and 50kDa, show little or no change upon SDT treatment (Fig. 3.8a, 3.8b). The SDT-insensitive bands likely indicate artifactual detection, and these proteins probably do not contain 3NY. Non-specific binding of the secondary antibody may be to blame, since these bands are absent in experiments that omit the primary antibody or switch to a rabbit polyclonal primary antibody with an anti-rabbit secondary antibody (Elena Dremina, unpublished results).

Fig. 3.9 illustrates the effect of SDT reduction on both 3NY-Ph-b and cardiac proteins, using SDS-PAGE with reducing conditions. There are fewer bands for cardiac proteins than in Fig. 3.8, most likely due to the breakage of sulfide bonds by the reducing conditions of the sample buffer. In parts a and b of Fig. 3.9, lane 8 should contain 50µg of cardiac protein but appears to be empty (by Ponceau staining, Fig. 3.9b), indicating sample loss somewhere in the procedure. Nevertheless, all of the other results provide evidence for the loss of 3NY in Ph-b with SDT treatment, while it has no effect on the few bands observed in the cardiac homogenate.

3.3.3.2 Mass Spectrometric Characterization of Ph-b after Mixing with Cardiac Proteins

For this portion of the project, it seemed prudent to collaborate with Elena Dremina to utilize her experience in preparing gel-based samples for mass spectrometric detection of protein-bound 3NY. Samples of 3NY-Ph-b (5.5mol 3NY per mol Ph-b) and cardiac proteins, prepared as described in sections 3.2.2 and 2.2.2, respectively, along with conditions used for the SDS-PAGE and Western blot experiments illustrated in Figure 3.8, were supplied to her. After

replicating the SDS-PAGE experiment, she extracted tryptic peptides from the Ph-b protein bands and submitted them for HPLC-MS/MS analysis, as described in section 3.2.7. The results

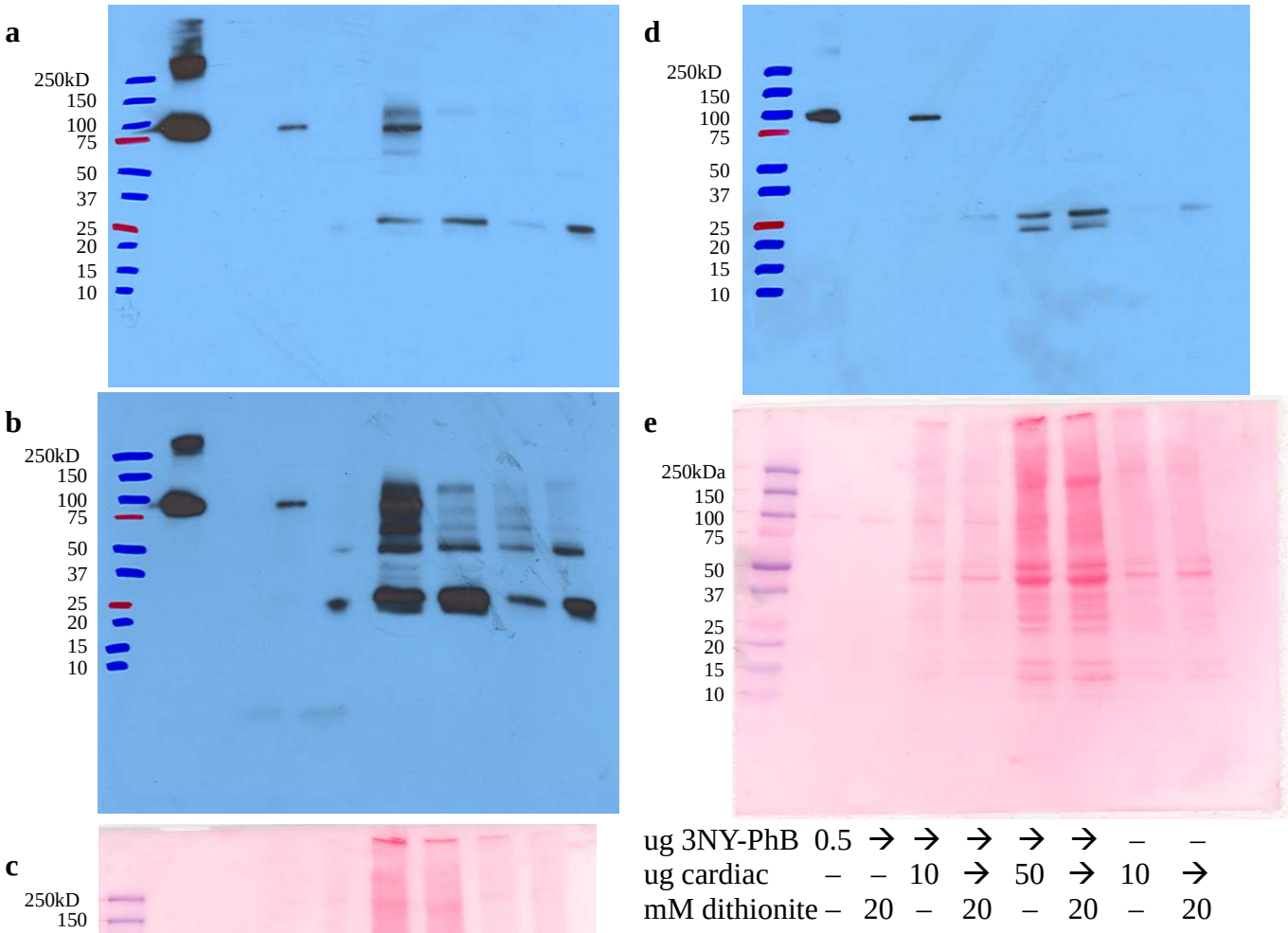

Fig. 3.8 Western blots for 3NY showing the effect of cardiac homogenate solutions and SDT reduction on 3NY epitopes in Ph-b nitrated *in vitro*. SDS-PAGE was performed with non-reducing conditions. Blots and Ponceau-stained membranes are shown from two similar experiments, with sample contents as shown. For the first experiment, the film was exposed for 10s **(a)** or overnight **(b)**, followed by Ponceau staining for total protein **(c)**. For the second experiment, the film was exposed for 10min **(d)** followed by Ponceau staining for total protein **(e)**.

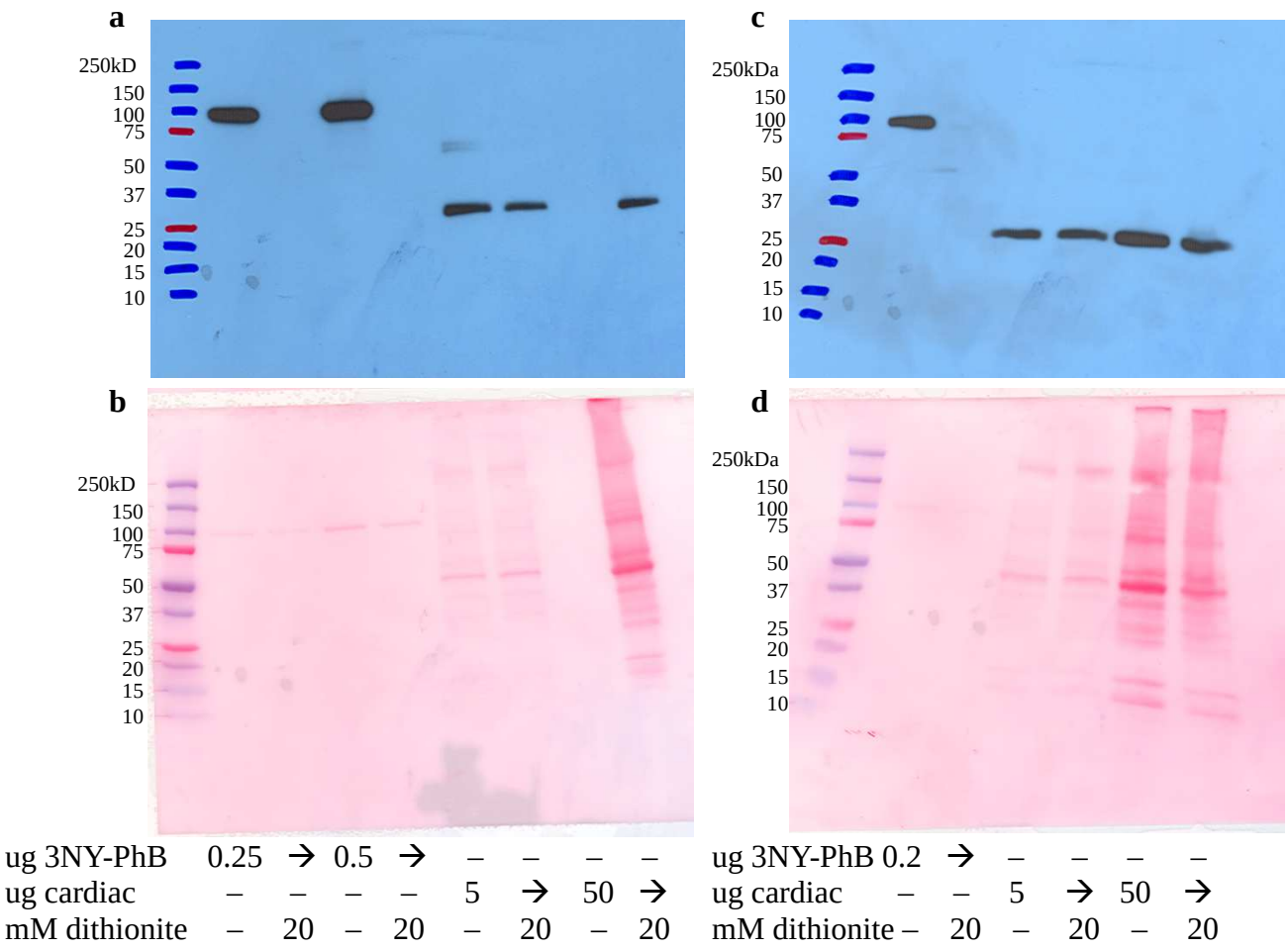

Fig. 3.9 Western blots showing the effect of SDT reduction on 3NY epitopes in both Ph-b nitrated *in vitro* and in cardiac homogenate solutions. SDS-PAGE was performed with reducing conditions. Blots and Ponceau-stained membranes are shown from two similar experiments, with sample contents as shown. For the first experiment, the film was exposed overnight **(a)**, followed by Ponceau staining for total protein **(b)**. For the second experiment, the film was exposed for 10min **(c)** followed by Ponceau staining for total protein **(d)**.

of this analysis show a reduction of mass spectral counts for tryptic peptides of Ph-b containing 3NY (Tyr+45amu) upon addition of increasing amounts of cardiac homogenate (Table 3.1). While a small reduction is also seen in mass spectral counts for unmodified peptides, it is not as great as for 3NY-containing peptides (Table 3.1). [As this data represents a single experiment, additional replicates are currently in preparation in order to assess the reproducibility of this result and to perform statistical analysis.]

In addition, some tryptic peptides containing 3NY were observed to have decreased HPLC-MS peak areas, based on integration in Excalibur software, in the presence of cardiac protein (Table 3.2). For some of these tryptic peptides, the decrease in peak area for the 3NY-containing peptide was accompanied by an increase in peak area for its native Tyr-containing counterpart (Table 3.2).

No peptides containing 3AY were detected in the HPLC-MS/MS search data. Searches with P-Mod software did not find any recognizable Tyr modifications other than 3NY (Tyr+45amu). Thus, the data support the hypothesis that 3NY is converted back to native Tyr when incubated with cardiac homogenate.

Table 3.1 Summary of mass spectrometry results for 3NY-Ph-b in the absence or presence of cardiac proteins. Sequence coverages and spectral counts represent identified tryptic peptides of Ph-b only. For comparison of spectral counts, the value obtained in the absence of cardiac protein is defined as 100% and used as a reference point for values obtained in the presence of cardiac proteins under conditions that are otherwise the same.

Amount 3NY-Ph-b (µg)	Amount cardiac protein (µg)	Ph-b sequence coverage	Total spectrum count for Tyr+45amu	Total spectrum count for unmodified peptides
0.5	0	64%	42 ≡100%	81 ≡100%
0.5	10	63%	37 88%	83 102%
0.5	50	65%	27 64%	67 83%
1.0	0	63%	61 ≡100%	105 ≡100%
1.0	10	66%	58 95%	104 99%
1.0	50	64%	39 64%	81 77%

Table 3.2 HPLC-MS peak areas for selected tryptic peptides of Ph-b, in samples containing 0.5µg 3NY-PhB. [Y+45] indicates 3NY identification. Peptide sequences include in parentheses the identities of residues adjacent to the tryptic cleavage sites.

Peptide sequence	m/z (charge state)	Peak area (au) +0µg cardiac	Peak area (au) +10µg cardiac	Peak area (au) +50µg cardiac
(K)DFNVGG[Y+45]IQAVLDR(N)	806.39(2)	4.06E4	4.07E4	2.85E4
(K)DFNVGGYIQAVLDR(N)	522.93(3)	3E4	2.5E4	6.52E4
(R)LKQE[Y+45]FVVAATLQDIIR(R)	684.79(3)	5.82E4	5.22E4	4.07E4
(R)LKQEYFVVAATLQDIIR(R)	669.71(3)	4.56E4	6.18E4	8.33E4
(R)HLQII[Y+45]EINQR(F)	491.26(3)	2.51E4	2.17E4	1.74E4
(R)HLQIIYEINQR(F)	476.27(3)	3.45E4	3.84E4	7.61E4
(R)HLQIIYEINQR(F)	713.89(2)	2.15E4	2.24E4	6.86E4
(R)D[Y+45]YFALAHTVR(D)	467.56(3)	9.4E3	8.59E3	5.37E3
(R)DYYFALAHTVR(D)	452.26(3)	6.65E4	3.62E4	2.87E4
(R)DYYFALAHTVR(D)	678.31(2)	3.5E4	2.39E3	2.73E4
(R)G[Y+45]NAQE[Y+45][Y+45]DRIPELR(Q)	674.62(3)	2.87E4	not observed	not observed
(R)G[Y+45]NAQEY[Y+45]DRIPELR(Q)	659.63(3)	6.24E3	3.61E3	not observed
(R)GYNAQEY[Y+45]DRIPELR(Q)	644.63(3)	6.5E3	4.73E3	2.6E3
(R)GYNAQYYDRIPELR(Q)	629.64(3)	3.38E4	not observed	not observed
(R)GYNAQEYYDR(I)	639.77(2)	not observed	6.48E4	8.93E4

3.4 Discussion and Conclusions

Conditions for derivatization of 3NY-Ph-b with benzylamine were successfully optimized, and these conditions also performed well when this nitrated protein was diluted in a matrix of cardiac homogenate. Fluorescence spectrometry showed a showed a linear response of intensity to 3NY concentration in Ph-b, and this data enabled calculation of the limit of detection, 608nM 3NY. Parallel experiments with cardiac proteins, in the absence of 3NY-Ph-b, demonstrated that the difference in mean fluorescence intensity between non-SDT-reduced samples (3NY cannot be labeled) and SDT-reduced samples (3NY should be labeled) was not statistically significant. Thus, the amount of endogenous 3NY modifications in cardiac samples is assumed to be below the detection limit, which is consistent with nitration levels previously reported in the literature (8). For this reason, future work would benefit from nitration of cardiac proteins *in vitro*, such as by peroxynitrite, to test whether the method is capable of labeling nitrated cardiac proteins when they are present at higher concentrations. By diluting the *in-vitro*-nitrated cardiac proteins with untreated cardiac proteins, a limit of detection could also be determined for this type of sample, which would contain a variety of labeled proteins instead of a single protein analyte. discuss how low nitration levels can have significant biological impact (8).

Other model systems, such as tissues exposed to inflammatory insult, may also have higher endogenous levels of 3NY that could be more easily detected by this method. Protein oxidation products can also be concentrated in certain cellular compartments, such as mitochondria (8,15), and in certain tissues (8), such as the cataractous lens (4). It is possible to isolate some of these compartments, which could provide a more robust sample to which this technique can be applied. In addition, a similar method using 4-(aminomethyl)benzenesulfonic

acid (ABS) has been successfully applied to detect oxidative Tyr modifications in recombinant proteins exposed to oxidizing conditions (14,16).

Western blot and mass spectrometric analysis provide evidence for the removal of 3NY from 3NY-Ph-b when it is incubated with cardiac homogenate. Some of the mass spectrometry data suggest that 3NY is converted to native Tyr, but further experimentation is necessary to confirm this hypothesis. If the cardiac homogenate is capable of denitrating proteins, this may also explain the difficulties in detecting and identifying endogenous protein-bound 3NY in cardiac proteins. Under the conditions employed for preparing cardiac homogenate samples, it is not expected that enzymes would survive in their active forms. Specifically, reductive alkylation, cold ethanol precipitation, and the addition of detergent (SDS or CHAPS) create denaturing conditions. Thus, a non-enzymatic de-nitration mechanism seems more likely. Protease inhibitors are included in the initial lysis conditions, so proteolytic degradation is not expected to make a major contribution. In support of this assumption, Ponceau staining for total protein on immunoblot membranes shows the persistence of a band at the migration position of Ph-b in the presence of cardiac proteins (Fig. 3.8). In addition, mass spectrometric data shows similar sequence coverage and spectral counts for Ph-b in the absence or presence of cardiac proteins (Table 3.1).

Analysis of MS/MS data for Tyr modifications indicates that increasing amounts of cardiac protein leads to a decrease in 3NY levels, based on spectral counts (Table 3.1) and HPLC-MS peak areas (Table 3.2), and an increase in native Tyr levels for the same tryptic fragment sequences (Table 3.2). This is consistent with literature reports of conversion of 3NY to native Tyr in matrices that promote denitration (1).

3.5 References

1. Abello N, Kerstjens HAM, Postma DS, and Bischoff R. Protein tyrosine nitration: selectivity, physicochemical and biological consequences, denitration, and proteomics methods for the identification of tyrosine-nitrated proteins. *J Proteome Res* 8: 3222-3238, 2009.
2. Dairou J, Pluvinage B, Noiran J, Petit E, Vinh J, Haddad I, Mary J, Dupret J-M, and Rodrigues-Lima F. Nitration of a Critical Tyrosine Residue in the Allosteric Inhibitor Site of Muscle Glycogen Phosphorylase Impairs its Catalytic Activity. *Journal of Molecular Biology* 372: 1009-1021, 2007.
3. Dremina ES, Li X, Galeva NA, Sharov VS, Stobaugh JF, and Schöneich C. A methodology for simultaneous fluorogenic derivatization and boronate affinity enrichment of 3-nitrotyrosine-containing peptides. *Analytical Biochemistry* 418: 184-196, 2011.
4. Fu S, Dean R, Southan M, and Truscott R. The hydroxyl radical in lens nuclear cataractogenesis. *J Biol Chem* 273: 28603-28609, 1998.
5. Giese RW and Riordan JF. Nitrotyrosine internal standard for amino acid analysis. *Analytical Biochemistry* 64: 588-592, 1975.
6. Perrin DD. *Dissociation Constants of Organic Bases in Aqueous Solution: By D. D. Perrin*: Butterworths; 1965.
7. Pryor WA, Cueto R, Jin X, Koppenol WH, Ngu-Schwemlein M, Squadrito GL, Uppu PL, and Uppu RM. A practical method for preparing peroxynitrite solutions of low ionic strength and free of hydrogen peroxide. *Free Radical Biology and Medicine* 18: 75-83, 1995.

8. Radi R. Nitric oxide, oxidants, and protein tyrosine nitration. *Proc Natl Acad Sci U S A* 101: 4003-4008, 2004.

9. Schöneich C and Sharov VS. Mass spectrometry of protein modifications by reactive oxygen and nitrogen species. *Free Radical Biology and Medicine* 41: 1507-1520, 2006.

10. Sharov V, Dremina E, Galeva N, Gerstenecker G, Li X, Dobrowsky R, Stobaugh J, and Schöneich C. Fluorogenic Tagging of Peptide and Protein 3-Nitrotyrosine with 4-(Aminomethyl)benzenesulfonic Acid for Quantitative Analysis of Protein Tyrosine Nitration. *Chromatographia* 71: 37-53, 2010.

11. Sharov VS, Galeva NA, Dremina ES, Williams TD, and Schöneich C. Inactivation of rabbit muscle glycogen phosphorylase b by peroxynitrite revisited: Does the nitration of Tyr613 in the allosteric inhibition site control enzymatic function? *Archives of Biochemistry and Biophysics* 484: 155-166, 2009.

12. Sharov VS, Galeva NA, Kanski J, Williams TD, and Schöneich C. Age-associated tyrosine nitration of rat skeletal muscle glycogen phosphorylase b: characterization by HPLC–nanoelectrospray–Tandem mass spectrometry. *Exp Gerontol* 41: 407-416, 2006.

13. Skoog DA, West DM, and Holler FJ. *Fundamentals of analytical chemistry*: Saunders College Pub.; 1996.

14. Torosantucci R, Mozziconacci O, Sharov V, Schoeneich C, and Jiskoot W. Chemical Modifications in Aggregates of Recombinant Human Insulin Induced by Metal-Catalyzed Oxidation: Covalent Cross-Linking via Michael Addition to Tyrosine Oxidation Products. *Pharm. Res.* 29: 2276-2293, 2012.

15. Turko IV, Li L, Aulak KS, Stuehr DJ, Chang J-Y, and Murad F. Protein Tyrosine Nitration in the Mitochondria from Diabetic Mouse Heart: Implications to Dysfunctional Mitochondria in Diabetes. *Journal of Biological Chemistry* 278: 33972-33977, 2003.

16. Zhou S, Mozziconacci O, Kerwin BA, and Schoeneich C. Fluorogenic Tagging Methodology Applied to Characterize Oxidized Tyrosine and Phenylalanine in an Immunoglobulin Monoclonal Antibody. *Pharm. Res.* 30: 1311-1327, 2013.

Chapter 4: Effect of Amino Acid Sequence on Fluorescence Quantum Yield, Molar Absorptivity, and Reaction Yield for a Series of Model Synthetic Nitropeptides Labeled with (3R,4S)-1-(4-(aminomethyl)phenylsulfonyl)pyrrolidine-3,4-diol (APPD)

4.1 Introduction

4.1.1 Peptide Sequences and Properties

Based on a tryptic fragment of the rat muscle protein glycogen phosphorylase *b* (Ph-b) with a known nitration site when treated *in vitro* with peroxynitrite (19), the synthetic nitropeptide FSA(3NY)LER became an important model for development of this novel derivatization method. (The nitration site was identified from the rabbit homolog protein, in which the tryptic fragment sequence is FAAYLER.) Since proteomic samples contain an expansive variety of peptide sequences, each with different physical and chemical properties, we were interested to study what effects these properties may have on tagging efficiency and product characteristics. Toward this end, a series of synthetic nitropeptides was tested with the derivatization protocol optimized for FSA(3NY)LER. Replacement of leucine with glutamate to give FSA(3NY)EER or arginine to give FSA(3NY)RER alters the acidity and charge state of the peptide. The addition of a second 3NY, again in place of leucine to give FSA(3NY)(3NY)ER, enables the study of two adjacent candidates for derivatization. Some evidence for the derivatization of adjacent nitrotyrosine residues was observed in cardiac proteomic samples (see section 2.3.13). Finally, a tryptic fragment of nitrated calmodulin with the sequence VFDKDGNG(3NY)ISAAELR was previously observed (12) to give a Lys-Tyr crosslink upon derivatization by our method (see Fig. 4.1c for structure), and so this sequence was selected as the fifth model peptide in the series.

4.1.2 Derivatization Products

(3R,4S)-1-(4-(aminomethyl)phenylsulfonyl)pyrrolidine-3,4-diol (APPD) was selected for this project due to its ability to label 3NY with both an affinity moiety and a fluorophore, which makes it a promising candidate for proteomic studies of endogenous modifications with low

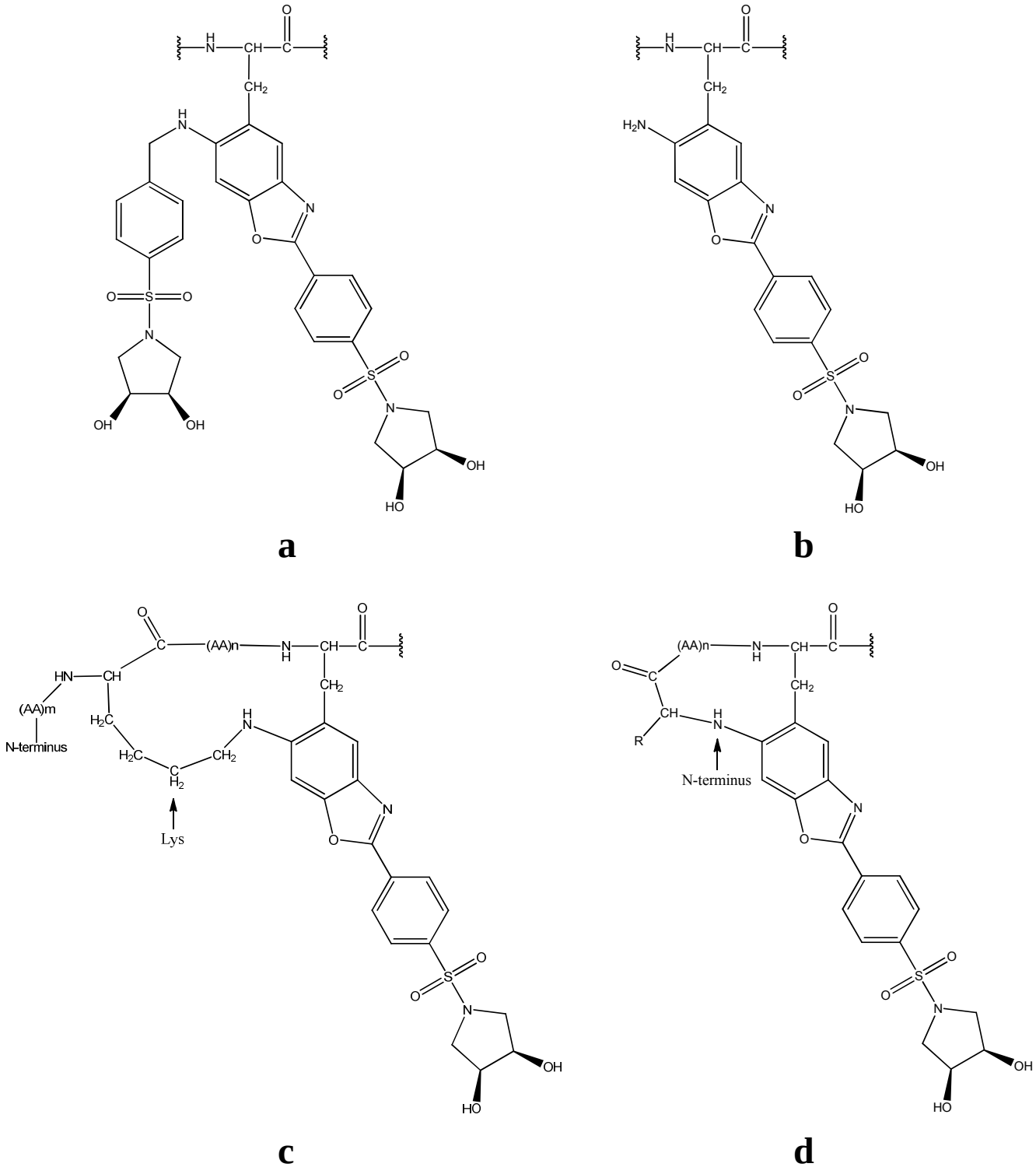

Fig. 4.1 Product structures for Tyr labeled with APPD: **(a)** $APPD_2$ **(b)** $APPD/NH_2$ **(c)** APPD/Lys cross-link **(d)** APPD/N-terminus cross-link

abundance. Previous work with model compounds, including small molecules, peptides, and proteins, indicates three possible product structures (Fig. 4.1). These include the addition of two molecules of APPD per Tyr residue (a), the addition of APPD and ammonia (b), and the addition of APPD with an intramolecular crosslink, which can involve either a Lys residue (c) or the N-terminus (d).

4.1.3 Fluorescence Quantum Yield

The fluorescence quantum yield, Φ, of a compound is defined as the number of photons emitted as fluorescence per photon absorbed, with a maximum value of 1.0 (3). Multiple processes compete with fluorescence during relaxation from the excited state back to the ground state, including internal conversion, radiationless relaxation, intersystem crossing, and phosphorescence. Thus, the fluorescence quantum yield is an important measure of the efficiency of fluorescence for a particular molecule, relative to other processes. It is also a useful indicator of the sensitivity of assays that are based on particular fluorogenic labels (20).

The relative fluorescence quantum yield of a compound can be determined by comparison to a reference compound with a known fluorescence quantum yield, according to the equation (11,14,20):

$$\Phi = \Phi_R \times \frac{F \times q_R \times A_R \times n^2}{F_R \times q \times A \times n_R^2}$$

Eq. 4.1

where the subscript *R* denotes the reference compound, Φ is the fluorescence quantum yield, *F* is the peak area of the fluorescence emission spectrum, *q* is the relative photon output of the source, *A* is the absorbance at the excitation wavelength, and *n* is the refractive index of the solvent. When the same instruments, excitation wavelengths, and solvents are used for both the reference compound and the new compound, the *q* and *n* terms cancel and can be omitted from the

calculation. If different instruments are used for measuring absorbance and fluorescence, as is often the case, care should be taken to use the same bandwidth or slit width for the incident light in both measurements, i.e. the bandwidth in the UV-visible spectrophotometer should match the excitation bandwidth in the spectroflourophotometer. Moreover, the sample should be purified to contain only the fluorescent molecule of interest in order to avoid interference, particularly in the absorbance measurement. This method was previously used by Sharov et al. (17) to determine the fluorescence quantum yield of the peptide FSA(3NY)LER labeled with 4-(aminomethyl)benzenesulfonic acid, a reagent which is very similar to APPD.

4.1.4 Absolute Peptide Quantitation

In order to determine both the chemical reaction yields and the molar absorptivities (i.e. extinction coefficients) of the various labeled peptide products, it is necessary to measure absolute quantities of these products. Amino acid analysis is particularly well-suited to this task (2,4). Using external calibration standards of amino acid mixtures, along with an internal standard, a calibration curve can be constructed using normalized peak areas for a selected amino acid, such as alanine, and then used for absolute quantitation of the alanine-containing peptide product, which has been purified from other alanine-containing substances (2,15).

Vapor-phase hydrolysis by hydrochloric acid is performed at high temperature under vacuum to release individual amino acids from the peptides (7). Complete hydrolysis of the peptide to its constituent amino acids, or at least a consistent and known extent of hydrolysis, is important for accurate quantitation. Some amino acids, such as Cys, Ser, Thr, Gln, Asn, Tyr, and Trp, are not stable under these hydrolysis conditions and thus cannot be used for accurate quantitation without specific modifications to the method.

Following hydrolysis, amino acids must be derivatized to enable detection by either UV absorption or fluorescence during high-performance liquid chromatography (HPLC), usually with a reverse-phase or ion-exchange column. A variety of methods exist, involving both pre- and post-column derivatization. In this work, *o*-phthaldialdehyde (OPA) reacts with primary amines in the presence of thiols to give fluorescent products that can be detected in low picomole amounts (5,18). Secondary amines, such as proline, are not detected by this method. Due to limited product stability, this reaction must be performed immediately prior to HPLC analysis of each sample (18).

Based on this absolute quantitation of nitropeptide, reduced peptide (i.e. aminopeptide), and labeled peptide, the yield of each reaction step can be calculated. In addition, the concentration of each solution used for spectroscopy is known. Beer's law gives the relationship

$$A = \varepsilon bc$$

Eq. 4.2

where A is absorbance, ε is molar absorptivity (i.e. extinction coefficient), b is the path length, and c is the concentration of the absorbing species. Thus, for a known analyte concentration, the measured absorbance can be used to determine the molar absorptivity of the analyte at the selected wavelength. This will allow for comparisons among different peptide sequences with regard to reaction efficiency and photochemical properties.

4.2 Experimental Methods

A flow chart of the overall methodological approach for characterizing this series of model peptides throughout the derivatization process with APPD is shown in Fig. 4.2.

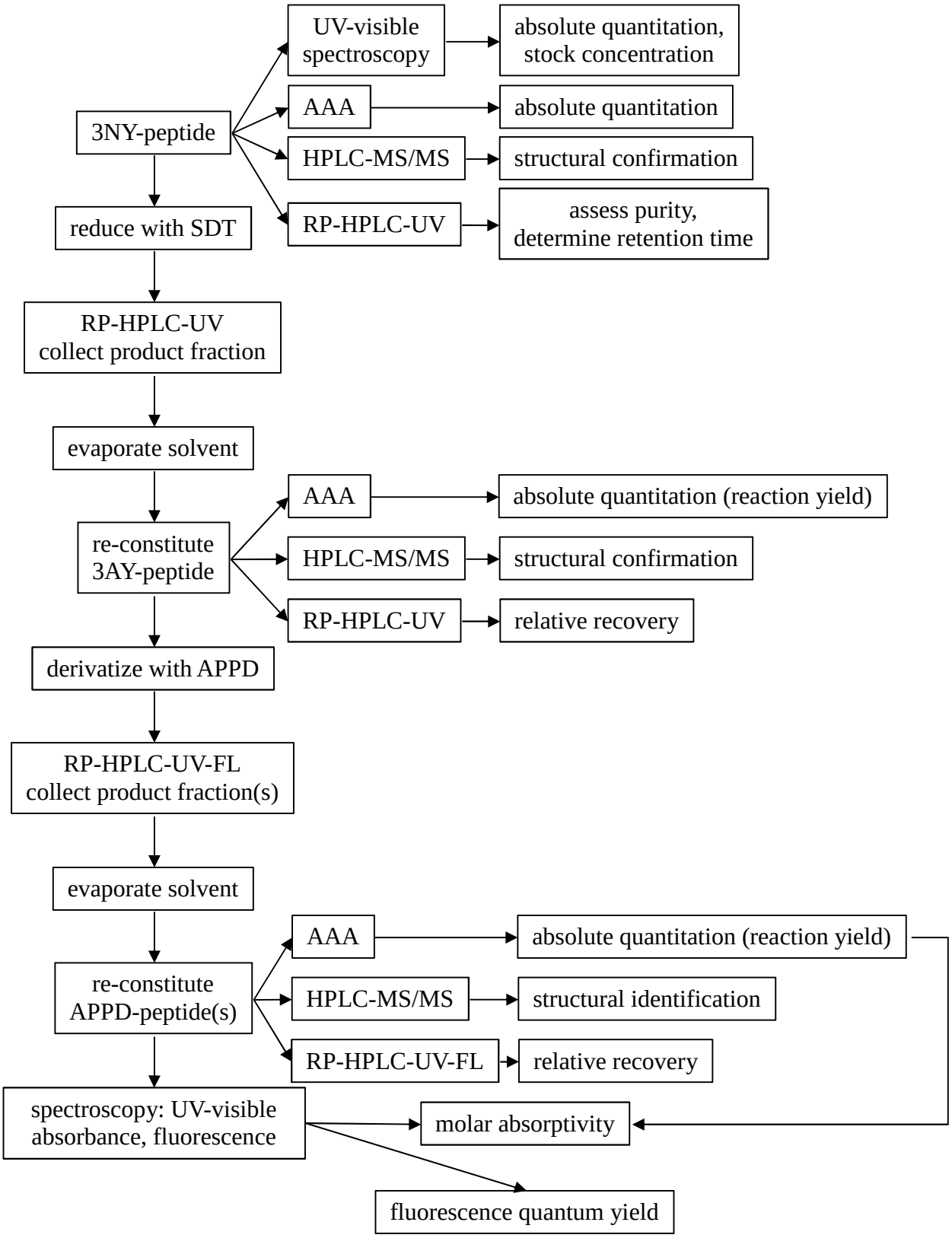

Fig. 4.2 Method flow chart for characterization of model peptides labeled with APPD. 3NY, 3-nitrotyrosine; AAA, amino acid analysis; HPLC-MS/MS, high-performance liquid chromatography with tandem mass spectrometry; RP-HPLC-UV, reverse-phase high-performance liquid chromatography with UV-visible absorbance detection; 3AY, 3-aminotyrosine; APPD, (3*R*,4*S*)-1-(4-(aminomethyl)phenylsulfonyl)pyrrolidine-3,4-diol; RP-HPLC-UV-FL, reverse-phase high-performance liquid chromatography with UV-visible absorbance and fluorescence detection.

4.2.1 Materials

Synthetic nitropeptides were prepared and purified to >95%, as determined by HPLC, by the Biochemical Research Service Laboratory at the University of Kansas using Fmoc-protected amino acids, including Fmoc-3NY (Bachem Bioscience, King of Prussia, PA, USA). Additional stock of the custom peptide FSA(3NY)LER was purchased from EZBiolab, Carmel, IN, USA.

Glutathione in its reduced form, minimum purity 98%; ammonium bicarbonate; o-phthalaldehyde (OPA); 2-mercaptoethanol; sodium acetate; L-norvaline; sodium dithionite (SDT), synonym sodium hydrosulfite, technical grade, 85%; potassium ferricyanide; trifluoroacetic acid (TFA), ≥99%, purified by redistillation, for protein sequencing; acetonitrile; methanol; and tetrahydrofuran were all purchased from Sigma-Aldrich (St. Louis, MO, USA). All mobile phase solvents were HPLC or MS grade. For reverse-phase HPLC (RP-HPLC), all mobile phases were filtered with 0.45µm Nylon-66 filters (Sigma-Aldrich, St. Louis, MO, USA).

ThioGlo®1 Fluorescent Thiol Reagent was from Calbiochem/EMD Millipore (Billerica, MA, USA) and was dissolved in acetonitrile to give a 2mM stock solution, which was stored at -20°C.

Constant-boiling, sequanal grade, 6N hydrochloric acid for vapor-phase hydrolysis of peptides was obtained from Thermo Scientific (Rockford, IL, USA), as was Amino Acid Standard H.

Monobasic potassium phosphate, enzyme grade; and 12N hydrochloric acid, Certified ACS Plus, were from Fisher Scientific (Pittsburgh, PA, USA).

Ethanol, 100% (meets USP specifications), was from Decon Laboratories, Inc., King of Prussia, PA, USA.

APPD was synthesized in-house according to a previously published method (9).

4.2.2 Peptide Derivatization and Product Isolation

Stock solutions of each peptide were prepared in 18MΩ water and concentrations determined by 3NY absorbance measurements on a Cary 50 Bio UV-Visible Spectrophotometer, using the extinction coefficient ε_{356nm} = 2,910$M^{-1}cm^{-1}$ in 0.01N hydrochloric acid (10). When not limited by solubility, the stock concentration was adjusted to 1.0mM. This method was found to be much more accurate than gravimetric analysis.

All RP-HPLC analysis was conducted with a Shimadzu 20A Series Prominence High-Performance Liquid Chromatograph (Kyoto, Japan), with all injections made by the autosampler. For the calmodulin peptide, RP-HPLC analysis of the nitropeptide solution revealed possible peptide degradation and/or impurity. For this reason, the nitropeptide was first isolated by RP-HPLC, using the gradient and method described below for post-reduction isolation. Multiple aliquots were pooled and dried to produce a stock of purified calmodulin nitropeptide, the concentration of which was determined by absorbance at 356nm, as described above, and the stock concentration was adjusted to 1.0mM.

For reduction of 3NY to 3AY, 5mM sodium dithionite (SDT) was added to 500µM peptide in 120µL total volume. SDT solutions were always prepared fresh by dissolving the solid in the appropriate amount of 18MΩ water *immediately* prior to use, in order to avoid decomposition that can occur within minutes of dissolution. After a reaction time of one minute, 100µL of the reduced peptide solution was injected onto RP-HPLC for purification, using an octadecyl stationary phase (Vydac 218TP C18, 4.6mm x 250mm, 5µm particle size, 300Å pore size; Fisher Scientific, Pittsburgh, PA, USA) and a linear gradient from 5-29% acetonitrile in water with 0.1% trifluoroacetic acid (TFA) over 24min at a flow rate of 1.0mL/min. Any remaining compounds were removed with a steep gradient from 29% to 80% acetonitrile plus

0.1% TFA over 1min and a 10min wash with this solvent, followed by 15min re-equilibration with starting conditions. Detection was performed with a photodiode array (PDA) UV-visible detector, monitored at 214nm for collection of the fraction containing the aminopeptide product (in a borosilicate glass tube), as verified by mass spectrometry (MS). This product was dried completely using a Centrivap Concentrator (Labconco, Kansas City, MO, USA) and re-constituted in 250µL 18MΩ water.

Derivatization was carried out in 50mM ammonium bicarbonate buffer at pH 9, using 500µM potassium ferricyanide and 20mM APPD to label approximately 50µM aminopeptide in a total volume of 120µL. The exact peptide concentration was dependent on the yield from the reduction step, which was determined later by amino acid analysis (see Sections 4.2.5 and 4.3.5). After 10min reaction time in the dark at room temperature, 100µL was injected onto RP-HPLC to isolate the major fluorescent product. A two-part linear gradient of acetonitrile in water with 0.1% TFA eluted the products from the octadecyl stationary phase: 5-20% over 10min, then 20-41% over 21min, with a constant flow rate of 1.0mL/min. Any remaining compounds were removed with a steep gradient from 41% to 80% acetonitrile plus 0.1% TFA over 1min and a 10min wash with this solvent, followed by 15min re-equilibration with starting conditions. Detection was primarily by fluorescence with 370nm and 510nm as the excitation and emission wavelengths, respectively. Chromatograms were also recorded with a (PDA) UV-visible detector. The fraction containing the major fluorescent product was collected in quartz tubes to avoid possible interactions between the cis-diol affinity moiety and boronate groups that may be accessible in borosilicate glass. These fractions were evaporated to dryness in a Centrivap and re-constituted in an appropriate amount of 18MΩ water for further analysis by fluorescence and UV-visible spectroscopy, MS, amino acid analysis, and HPLC. In some cases, to be noted

below, it was necessary to pool products collected from multiple reaction replicates in order to achieve concentrations high enough for subsequent analysis.

4.2.3 Preparation of Reference Compound, Glutathione-ThiGlo®1 (GSH-TG1)

The reduced form of the tripeptide glutathione (sequence γ-Glu-Cys-Gly) was labeled at a concentration of 100µM by addition of 200µM of the commercial fluorescent thiol labeling reagent ThioGlo®1, in a total of 120µL buffered at pH 7 by 20mM sodium phosphate. After two minutes, the fluorescent peptide product was purified from excess reagent by RP-HPLC, using the same conditions described above for APPD-labeled products, except the fluorescence detection excitation and emission wavelengths were 379nm and 495nm, respectively. The fluorescent fraction (with retention time ~16-18min) was collected in borosilicate glass, evaporated to dryness in a Centrivap, and re-constituted in 600µL 18MΩ water for subsequent analysis. Thiol adducts of ThioGlo®1 have fluorescence excitation and emission maxima at 379nm and 495nm, respectively, and the fluorescence quantum yield has been determined as Φ = 0.49 (6,13,21).

4.2.4 Mass Spectrometry for Product Identification

Peptides from each derivatization step were analyzed by capillary HPLC-MS. A Vydac octadecyl column (25 cm x 0.5 mm, 3.5 µm) was connected to the capillary liquid chromatography system (Waters Corporation, Milford, MA, USA). Mobile phases consisted of water/acetonitrile/formic acid at a ratio of 99%, 1%, 0.08% (v:v:v) for solvent A and a ratio of 1%, 99%, 0.06% (v:v:v) for solvent B. The following linear gradient was set: 20-80% of solvent B over 6 min, with a flow rate of 20µL min^{-1} and an injection volume of 10µL. This method was optimized for short analysis times because the peptides had previously been purified by RP-HPLC (see 4.2.2). Electrospray ionization (ESI)-MS spectra of the peptides were acquired on a

SYNAPT-G2 (Waters Corp., Milford, MA, USA). The cone voltage was 45V, and Ar was admitted to the collision cell. The spectra were acquired using a mass range of 50-2,000amu. The data were accumulated for 0.7s per cycle.

4.2.5 UV-Visible and Fluorescence Spectroscopy

UV-visible spectra were measured with a Cary 50 Bio UV-Visible Spectrophotometer, which has a fixed bandwidth of 1.5nm. Spectra were collected from 500nm to 250nm at a scan rate of 300.00nm/min. Zero and baseline measurements were taken with 18MΩ water as a blank, and the software's baseline correction function was enabled. Using the X-Y Pairs Table generated by the software, the absorbance value for wavelength 375nm (A_{375}) was used for fluorescence quantum yield calculations according to Eq. 4.1 (see 4.1.3) as the value for A or A_R for APPD-labeled peptides or GSH-TG1, respectively. This wavelength was selected as a midpoint between the maximum excitation wavelengths previously observed for APPD-labeled peptides (370nm) and GSH-TG1 (379nm), since using a single wavelength for both compounds is important for accurate quantum yield calculations.

The average A_{375} was determined for at least three replicates of each APPD-labeled peptide. One aliquot of GSH-TG1 was then diluted to match this average absorbance and used as the reference compound for the entire peptide sample set. Samples were prepared such that $0.01 < A_{375} < 0.10$ in order to avoid reabsorption and internal reflection phenomena that can interfere with accurate quantum yield calculations (1,14,20). When product yields were particularly low, this was not always possible.

Fluorescence spectra were measured with a Shimadzu RF-5301PC Spectrofluorophotometer (Kyoto, Japan) with excitation at 375nm, emission range 385-700nm, both excitation and emission slit widths set to 1.5nm, scan speed set to slow, high sensitivity, and

automatic response time. Peak areas were calculated by the software over the entire range of the spectrum and used for fluorescence quantum yield calculations according to Eq. 4.1 (see 4.1.3) as the value for F or F_R for APPD-labeled peptides or GSH-TG1, respectively.

4.2.6 Amino Acid Analysis for Peptide Quantitation

Following spectroscopic measurements, triplicates of each sample were prepared for vapor-phase hydrolysis using the Waters Pico.Tag^{TM} Workstation (Milford, MA, USA). Samples, along with 150pmol of norvaline (Nva) in 0.1N hydrochloric acid as an internal standard, were aliquotted into 6mm x 50mm borosilicate glass tubes (Pyrex Vista, Sigma-Aldrich, St. Louis, MO, USA) that had previously been washed with 8N hydrochloric acid, rinsed with 18MΩ water and 100% ethanol, and dried under vacuum. Samples were then dried under vacuum, sealed, and stored at -20°C until analysis. For APPD-labeled peptides, this was always done on the same day that the purified products were re-constituted and used for spectroscopic measurements.

For hydrolysis, 14 sample tubes were placed in the specialized reaction vessel (Eldex, Napa, CA, USA) with 200µL 6N hydrochloric acid and subjected to three cycles of evacuation and nitrogen purgation for 5s at 2psi. Hydrolysis was demonstrated to be complete for nitropeptide standards of known concentration (measured by UV-Visible spectroscopy, ε_{356} = 2910$M^{-1}cm^{-1}$) after 1.5h at 150°C under vacuum of approximately 1Torr. The hydrolyzed samples were transferred to a clean vial, which was evacuated to remove all acid fumes, and then stored -20°C until ready for HPLC analysis.

The reaction of primary amines with OPA in the presence of free thiol (2-mercaptoethanol) and Brij-35 detergent at pH 9.5 was selected for fluorescent derivatization of amino acids (5). Brij-35 stock solutions were 1% (w/v) in 190mM potassium phosphate pH 9.5

buffer, and the OPA reagent stock solution contained 15.7mM OPA, 5.3% methanol, 190mM postassium phosphate pH 9.5 buffer, and 0.2% 2-mercaptoethanol. All reagents and buffers were stored at 4°C in the dark when not in use, and the OPA reagent solution was made fresh at least every seven days. Each day, a fresh 1:1 mixture of Brij and OPA stock solutions was prepared, and hydrolyzed samples were reacted for 1min with 40µL of this mixture, followed by quenching with 80µL 0.2M monobasic potassium phosphate, pH ≤ 4.5. RP-HPLC was carried out on a SUPELCOSIL^{TM} LC-18-T octadecyl column, 15cm x 4.6mm with 3µm particle size (Sigma-Aldrich, St. Louis, MO, USA) maintained at 35°C by an Alltech 530 column heater attached to the Shimadzu system described in section 4.2.2. Derivatized amino acids were well resolved using a flow rate of 0.7mL/min and the gradient shown in Table 4.1, where mobile phase A is 95% 25mM sodium acetate, pH 5.8, with 5% THF and mobile phase B is 95% methanol with 5% THF, based on a previously published method (22).

Table 4.1 Gradient for RP-HPLC analysis of amino acids derivatized with OPA

Time (min)	%B
0.01	0
0.5	15
10	15
20	45
27	45
40	90
45	90

For absolute quantitation, five amino acid calibration standards covering the range 50-250pmol were subjected to hydrolysis conditions, derivatized, and analyzed by RP-HPLC to

construct an external calibration curve, with six replicates for each standard. Peak areas of 14 components of the Amino Acid Standard H solution were each normalized against the peak area for 150pmol Nva internal standard and plotted against the amount of amino acid in pmol. Linear relationships with $R^2 \geq 0.99$ were defined for each of these components. Ala was selected as the component of choice for peptide quantitation, due to its stability during hydrolysis, its presence in the sequence of all of the model peptides, and its good resolution from the other solution components. The Ala and Nva peaks were identified based on retention times for single-component authentic standards. The method was found to be accurate within 6% for most nitropeptide standards of known concentration, as measured using absorbance of nitrotyrosine with $\varepsilon_{356} = 2{,}910 M^{-1}cm^{-1}$ in 0.01N hydrochloric acid (10). During analysis of peptide samples, method performance was checked daily with a standard containing 150pmol AA Standard H and 150pmol Nva.

4.3 Results

4.3.1 Optimal Reaction Conditions

In order to minimize side products from the reaction of SDT with nitropeptides, it is desirable to use the lowest possible reagent concentration and a short reaction time. In order to determine the lowest amount of reagent required to completely reduce 3NY to 3AY in the FSAYLER peptide, a range of concentrations was tested and product yield compared by RP-HPLC analysis. As shown in Figure 4.3, for 500µM FSA(3NY)LER, reaction with 5mM SDT for 1min was sufficient for complete reduction and gave two products. Product 1 was identified by HPLC-MS/MS as the desired aminopeptide, FSA(3AY)LER (Fig. 4.4a). Product 2 was also characterized by LC-MS/MS (Fig. 4.4b), which suggests that it is the sulfated form of the aminopeptide. Sulfated Tyr is quite labile, readily losing SO_3 during the electrospray ionization

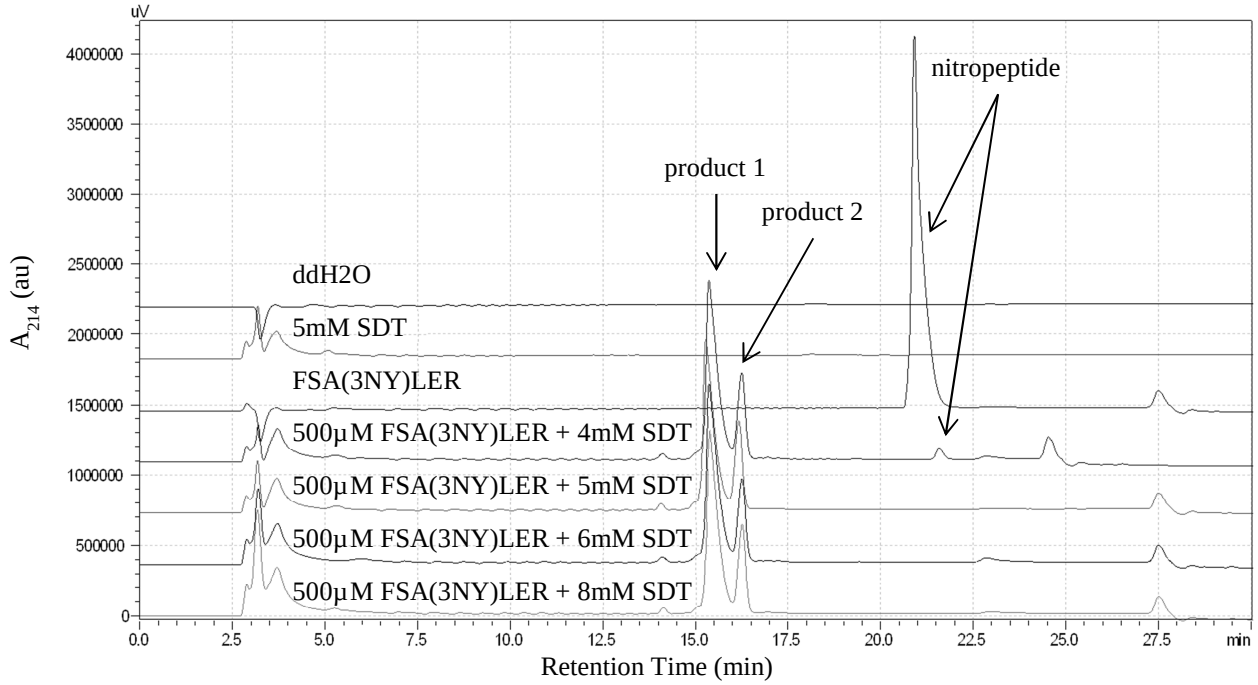

Fig. 4.3 Optimization of conditions to reduce 3NY to 3AY in FSAYLER. A range of concentrations of sodium dithionite (SDT) were added to 500µM peptide in 120µL total volume. After a reaction time of one minute, 100µL of the reduced peptide solution was injected onto RP-HPLC for purification.

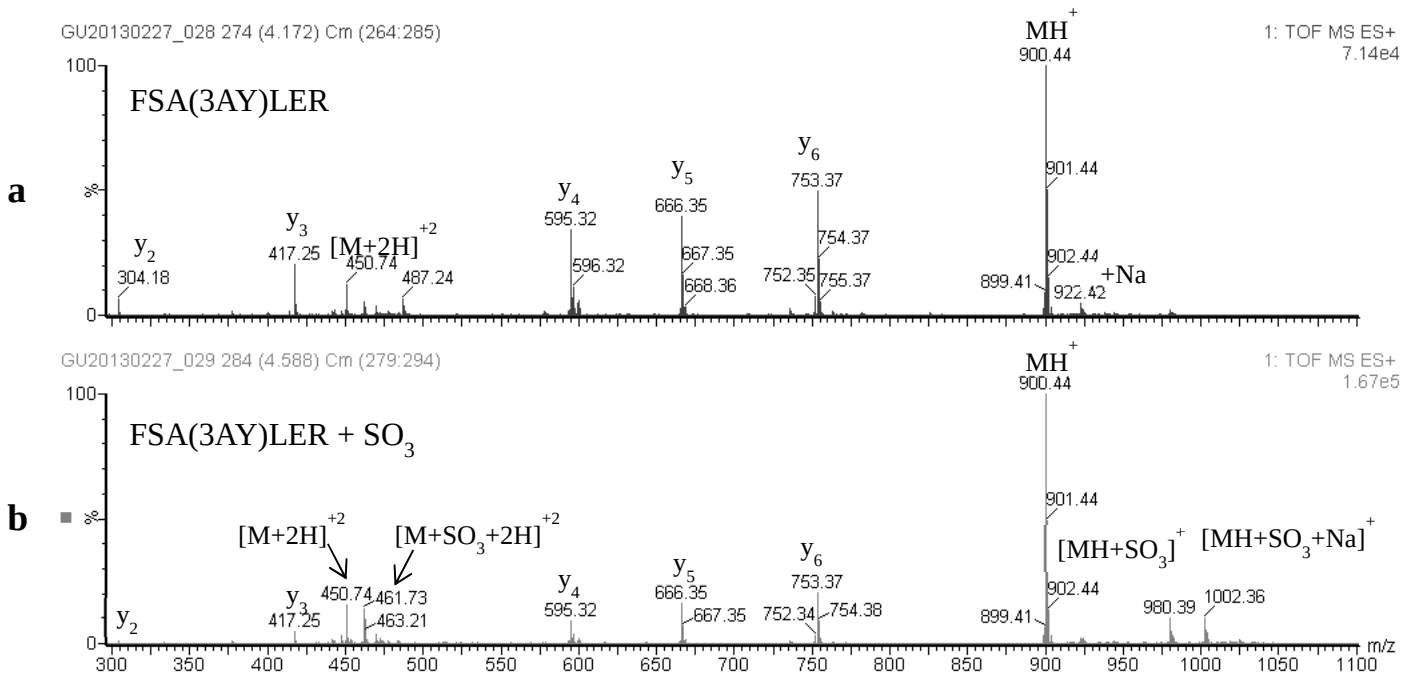

Fig. 4.4 Mass spectra for reduced FSAYLER, products 1 **(a)** and 2 **(b)**. Following reaction of 500µM FSA(3NY)LER with 5mM SDT, two products were purified by RP-HPLC, dried in a Centrivap, re-constituted in 18MΩ water, and analyzed by capillary HPLC-MS.

process (16) and thus leaving only traces of the intact product observable in the first-dimension mass spectrum, together with a significant amount of the non-sulfated aminopeptide.

To determine the optimal fluorogenic tagging conditions, a concentration matrix for the reagents potassium ferricyanide and APPD was tested with 50µM FSA(3AY)LER (estimated concentration, assuming 100% yield from reduction reaction). It has been previously demonstrated that this derivatization reaction is particularly sensitive to the potassium ferricyanide concentration (9). As shown in Fig. 4.5, based on fluorescent HPLC peak area for the desired product, potassium ferricyanide concentrations above 250µM (5-fold molar excess over peptide) and APPD concentrations above 10mM (200-fold molar excess over peptide) give the highest product yield. In order to limit the formation of side products that may occur with excess reagents, concentrations at these thresholds were selected for the rest of the study.

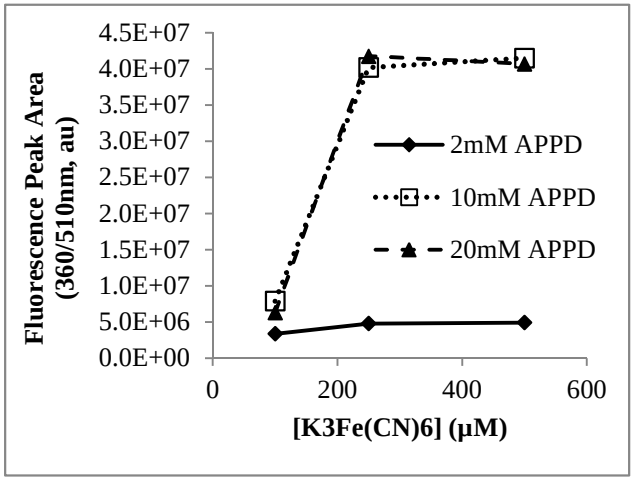

Fig. 4.5 Dependence of fluorescent HPLC peak areas on concentrations of postassium ferricyanide and APPD used to derivatize 50µM FSA(3AY)LER in 50mM ammonium bicarbonate, pH 9, for 10min at room temperature in the dark.

4.3.2 Product Isolation and Identification

These same conditions were then applied to all five model peptides, and the major products were identified by HPLC-MS/MS. MS/MS data also confirmed the structures of the nitro- and aminopeptides for each model. For the peptide FSAYYER, note that only the HPLC peak containing the peptide with both 3NY residues reduced to 3AY was collected and derivatized (peak 1, Fig. 4.6). The small amount of sulfated product observable by MS is likely

due to incomplete resolution of peaks 1 and 2 by RP-HPLC. Note that neither of these peaks absorb at 356nm, as expected in the absence of 3NY. Conversely, peaks 3 and 4 both show absorbance at 356nm (as well as 214nm), indicating that these represent 3NY-containing peptides, most likely FSA(3NY)(3AY)ER and FSA(3AY)(3NY)ER in peak 3 and FSA(3NY)(3NY)ER in peak 4. The retention time of peak 4 matches the chromatogram of the stock nitropeptide. Figures 4.7 through 4.11 show the MS/MS spectra for each APPD-labeled peptide.

All five peptides yielded the $APPD_2$-labeled peptide as a major product. For FSAYYER,

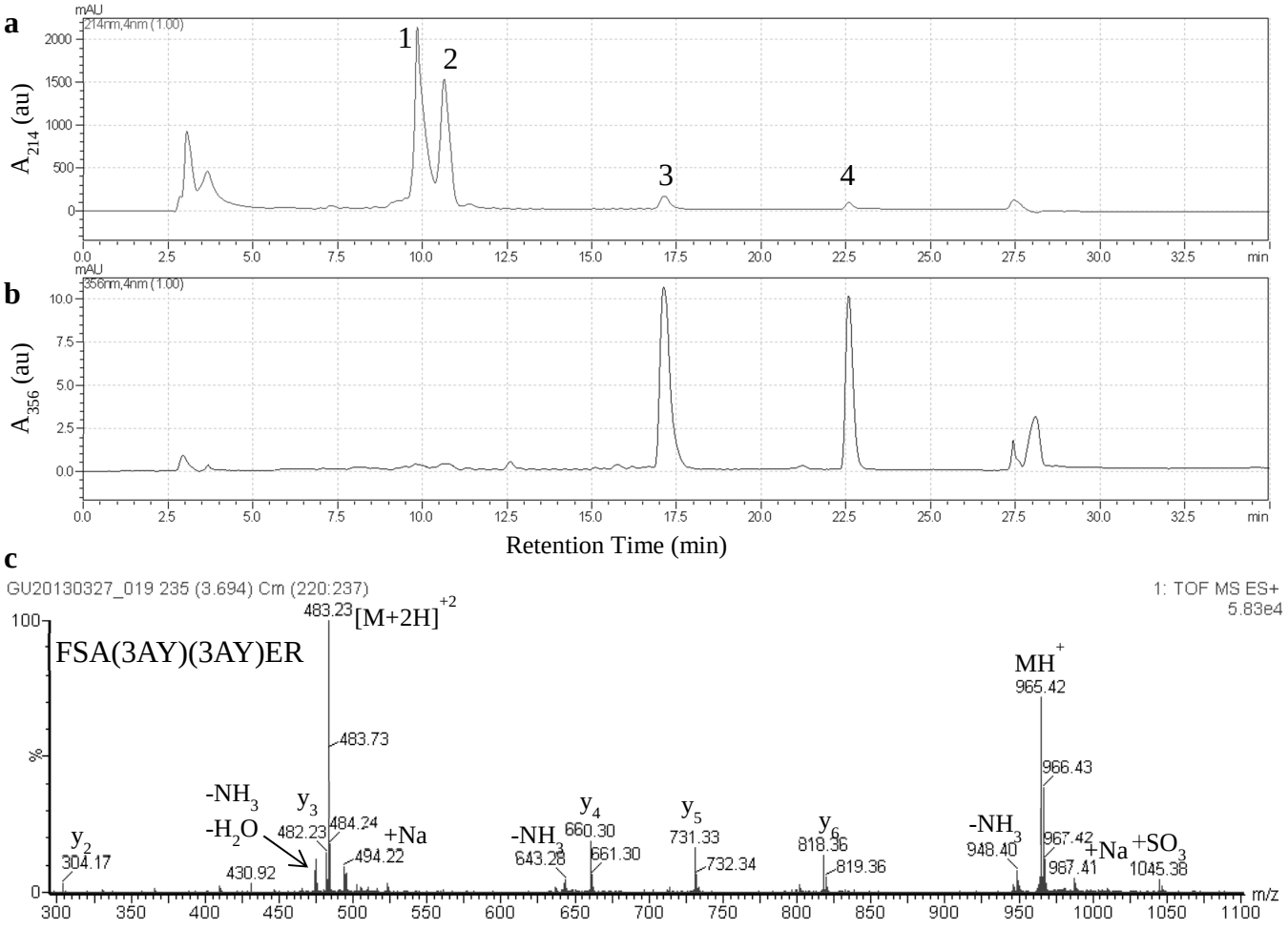

Fig. 4.6 HPLC and MS of FSAYYER reduction products: **(a)** chromatogram with UV detection at 214nm **(b)** chromatogram with UV detection at 356nm = λ_{max} for 3NY **(c)** mass spectrum for peak 1

the major product was labeled with $APPD_2$ on both Tyr residues. Due to the low product yield, purified product was collected from five samples and pooled to produce each of three replicate samples for further analysis.

For the calmodulin peptide, three products were observed in nearly equal yield: $APPD_2$ (Fig. 4.11b) and two cross-link-containing products. The MS/MS spectra suggest that one is cross-linked through the neighboring Lys residue (Fig. 4.11a) and the other is cross-linked through the N-terminus (Fig. 4.11c). As the two intramolecular cross-linked products are isobaric, the absence of y ions in particular regions of the peptide sequence is the only evidence to distinguish the two structures. The significant difference in RP-HPLC retention times is likely due to differences in peptide surface area properties, and this allows for purification of the two products for fluorescence quantum yield measurements (see section 4.3.3) and other analyses. The $APPD_2$ product was also well resolved from the other compounds for further characterization. However, since the yield of each individual product was too low for accurate analysis, each of the three products was collected from two tagging reactions, and the corresponding fractions were pooled. This process was repeated to give triplicate samples for each of the three purified products.

4.3.3 Fluorescence Quantum Yields and Other Spectroscopic Properties

Spectroscopic study of the APPD-labeled peptides revealed some important differences among different peptide sequences and especially among the different product structures resulting from the calmodulin peptide, as shown in Table 4.2. Fluorescence quantum yields were very similar for $APPD_2$-labeled FSAYLER (0.333), FSAYEER (0.355), and FSAYRER (0.376) but almost eight-fold lower for FSAYYER (0.046) labeled with the $APPD_2$-type product at both of the adjacent Tyr sites. All of these labeled peptides have absorption maxima near 372nm and

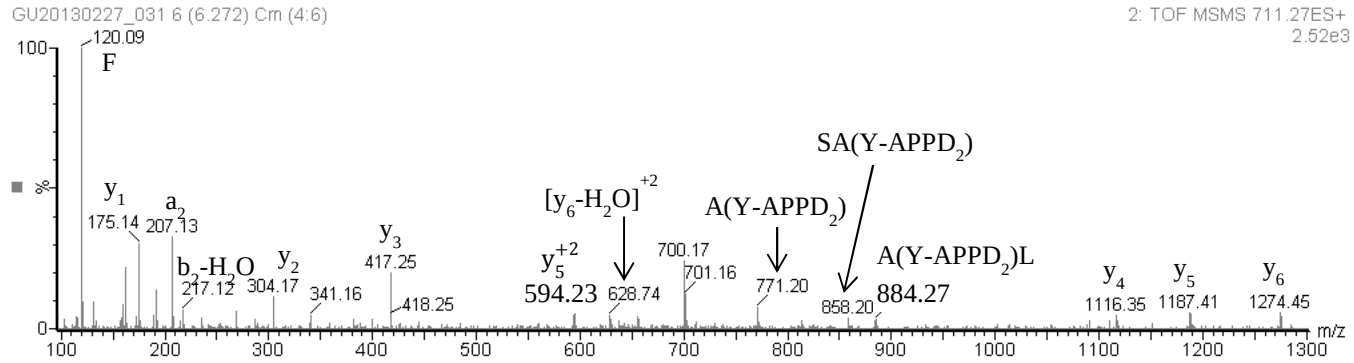

Fig. 4.7 Tandem mass spectrum for FSA(Y-APPD$_2$)LER.

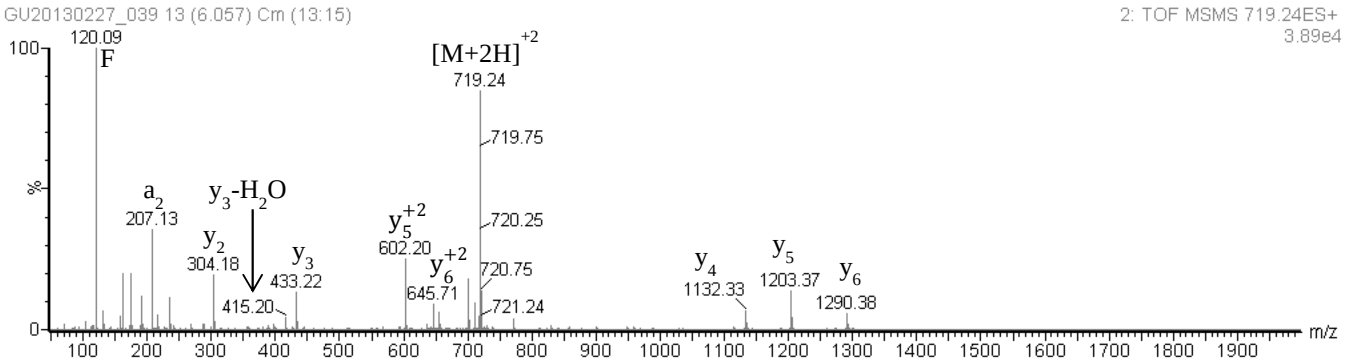

Fig. 4.8 Tandem mass spectrum for FSA(Y-APPD$_2$)EER.

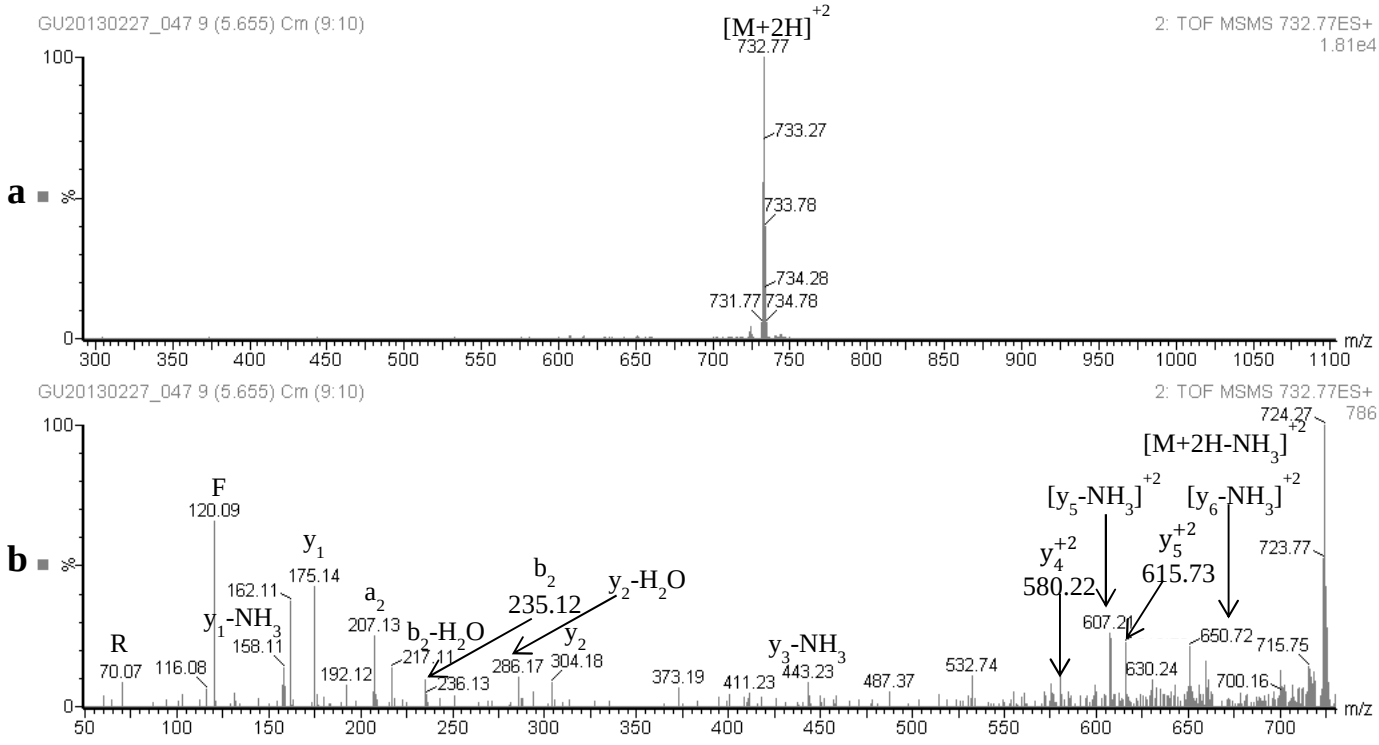

Fig. 4.9 Tandem mass spectrum for FSA(Y-APPD$_2$)RER (a) m/z 300-1100 (b) m/z 50-725.

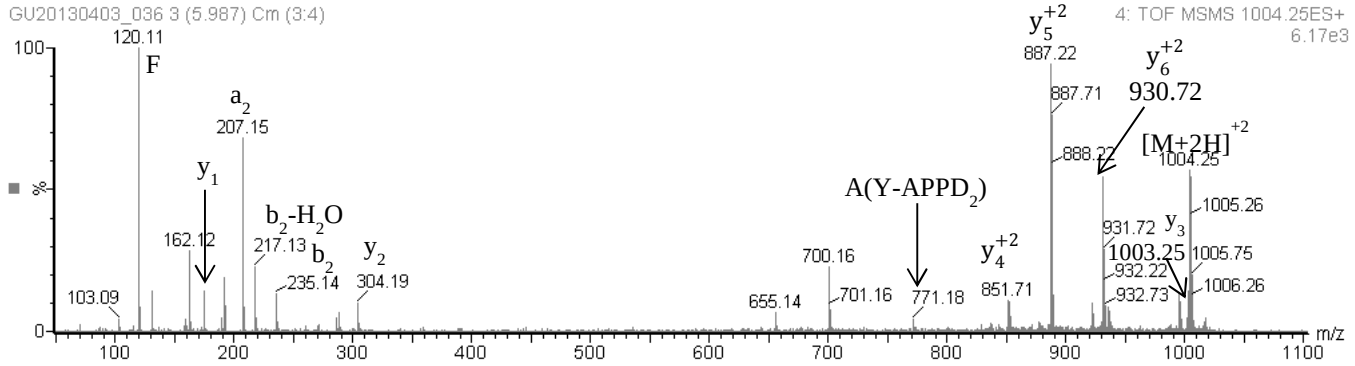

Fig. 4.10 Tandem mass spectrum for FSA(Y-APPD$_2$)(Y-APPD$_2$)ER.

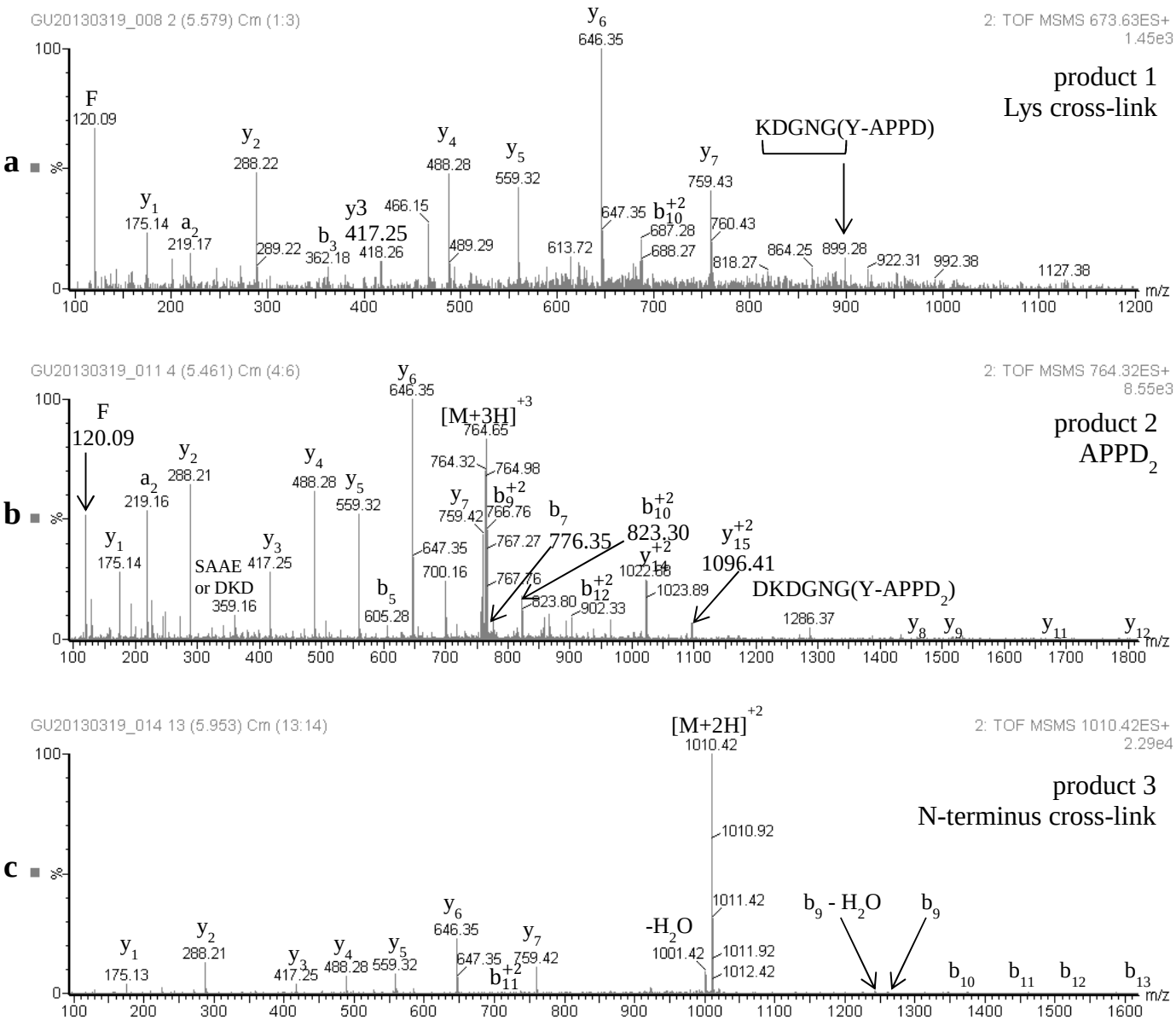

Fig. 4.11 Tandem mass spectra for APPD-calmodulin peptide products. The peptide sequence is VFDKDGNGYISAAELR. **(a)** Product 1: Y-APPD-Lys cross-link **(b)** Product 2: Y-APPD$_2$ **(c)** Product 3: Y-APPD-N-terminus cross-link

fluorescence emission maxima near 530nm. The calmodulin peptide, VFDKDGNGYISAAELR, labeled with $APPD_2$ (product 2) has similar absorption and emission maxima, although its quantum yield is lower (0.250). However, the two cross-linked calmodulin peptide-APPD products (products 1 and 3) have the quantum yields, absorption maxima, and fluorescence emission maxima that differ both from all of the $APPD_2$-type products and also from each other (see Table 4.2).

4.3.4 Reaction Yields

The yield of each reaction step was calculated based on the results of amino acid analysis. Where applicable, outliers were excluded at a confidence level of 90% or higher based on Dixon's Q test (8). The accuracy of the amino acid analysis method was also evaluated by comparison to nitropeptide quantitation by UV-visible spectrometry (Table 4.3). For all peptides except FSA(3NY)EER, for which the raw data indicate significant sample loss during vapor-phase hydrolysis, the error was less than 6%. Normalization against the internal Nva standard compensated significantly for the low sample recovery in these samples, but working near the detection limit nevertheless introduced more variability into the analysis. Largely due to this source of experimental error, the reaction yields for the reduction of 3NY to 3AY by SDT is reported based on both the AAA and the UV-visible data for quantitation of the starting material, the nitropeptide (Table 4.4). These yields are similar for all peptide sequences, in the range 48-63% (using UV-visible data for starting material). It is likely that the remainder of the starting material is converted to the sulfated form of the aminopeptide, as suggested by the HPLC-MS data (see Fig 4.4). In addition, the RP-HPLC chromatograms (see Fig. 4.3 as an example) show loss of the nitropeptide peak and nearly equal peak areas for the desired aminopeptide product and the putative sulfated aminopeptide side product.

Table 4.2 Spectoscopic data for APPD-labeled peptides

Peptide	Absorbance λ_{max}	Fluorescence $(\lambda_{em})_{max}$	A_{375}	Fluorescence Area	Reference A_{375}	Reference Fluorescence Area	Fluorescence Quantum Yield
FSAYLER	372.0	536.0	0.0330	2408.591	0.0331	3582.682	0.330
	373.0	533.0	0.0330	2479.055			0.340
	370.5	530.4	0.0374	2747.076			0.333
	374.0	535.0	0.0377	2749.175			0.330
mean	**372.4**	**533.6**	**0.0353**	**2595.974**			**0.333**
standard deviation	1.5	2.5	0.0026	178.031			0.005
FSAYEER	373.0	529.0	0.0552	4359.021	0.0512	5454.080	0.363
	373.0	530.6	0.0537	4121.700			0.353
	372.5	531.8	0.0545	4148.742			0.350
mean	**372.8**	**530.5**	**0.0545**	**4209.821**			**0.355**
standard deviation	0.3	1.4	0.0008	129.917			0.007
FSAYRER	371.0	531.4	0.0716	5609.145	0.0620	6153.151	0.387
	372.0	528.4	0.0568	4198.811			0.365
	371.0	524.0	0.0660	5030.395			0.376
mean	**371.3**	**527.9**	**0.0648**	**4946.117**			**0.376**
standard deviation	0.6	3.7	0.0075	708.934			0.011
FSAYYER	371.0	530.0	0.0177	194.320	0.0161	1946.963	0.044
	369.0	527.2	0.0172	204.999			0.048
	371.0	529.8	0.0203	230.787			0.046
mean	**370.3**	**529.0**	**0.0184**	**210.035**			**0.046**
standard deviation	1.2	1.6	0.0017	18.748			0.002
VFDKDGNGYISAAELR							
product 1	373.1	528.2	0.0027	55.171	0.0055	658.162	0.084
	367.0	541.4	0.0066	307.429			0.191
	373.1	542.4	0.0095	383.109			0.165
mean	**371.1**	**537.3**	**0.0063**	**248.570**			**0.147**
standard deviation	3.5	7.9	0.0034	171.709			0.056
product 2	373.1	529.4	0.0098	637.347	0.0104	1247.178	0.266
	364.5	527.8	0.0158	868.161			0.225
	373.1	530.8	0.0105	664.966			0.259
mean	**370.2**	**529.3**	**0.0120**	**723.491**			**0.250**
standard deviation	5.0	1.5	0.0033	126.046			0.022
product 3	363.5	517.2	0.0283	2989.571	0.0257	3073.507	0.433
	363.5	514.2	0.0362	3747.316			0.424
	363.0	511.4	0.0278	2838.774			0.418
mean	**363.3**	**514.3**	**0.0308**	**3191.887**			**0.425**
standard deviation	0.3	2.9	0.0047	486.889			0.007

Table 4.3 Accuracy of AAA for nitropeptides (relative to UV-Vis determination)

Peptide	Error
FSA(3NY)LER	6%
FSA(3NY)EER	23%
FSA(3NY)RER	3%
FSA(3NY)(3NY)ER	4%
VFDKDGNG(3NY)ISAAELR	6%

Table 4.4 Reduction reaction yields by AAA

Peptide	AAA Yield	UV Yield
FSA(3AY)LER	53% ± 3%	57% ± 3%
FSA(3AY)EER	82% ± 4%	63% ± 3%
FSA(3AY)RER	60% ± 4%	62% ± 4%
FSA(3AY)(3AY)ER	48% ± 10%	48% ± 10%
VFDKDGNG(3AY)ISAAELR	52% ± 2%	49% ± 2%

Three of the peptides showed APPD tagging reaction yields of 35% or better: FSAYLER, FSAYEER, and FSAYRER, in order of increasing yield (Table 4.5). However, FSAYYER and all of the calmodulin peptide products showed very low yields, 3-7%. Some attempts to improve the yield of labeled FSAYYER by altering reagent concentrations were unsuccessful (data not shown). These yields reflect not only efficiency of the labeling reaction, but also recovery from the purification and re-constitution processes.

4.3.5 Molar Absorptivities

The molar absorptivities, ε, of the tagged peptides range from approximately 6,600-29,000$M^{-1}cm^{-1}$, as shown in Table 4.5. Each value was calculated at the wavelength of maximum absorption (see Table 4.2). For the labeled FSAYYER peptide, ε represents the molar absorptivity of each individual Y-$APPD_2$ residue. Peptide sequence and product structure do lead to significant differences in ε. Despite triplicate sample sets for both the tagging reactions and the amino acid analysis, some of the ε values have large standard deviations. This is

particularly the case when product yields are low, specifically for FSAYYER and the calmodulin peptide, and thus may be the result of experimental error inherent in measuring samples with very low analyte concentration.

Table 4.5 Tagging yields and molar absorptivities. *value omitted based on Q-test

Peptide	Yield	Concentration (μM)	A_{max}	ε ($M^{-1}cm^{-1}$)
FSA(Y-$APPD_2$)LER	35% ± 23%			
		4.0 ± 0.9	0.0331	8200
		1.5 ± 0.3	0.0375	24632*
		4.2 ± 3.2	0.0379	8922
			mean:	**8561**
			st dev:	**511**
FSA(Y-$APPD_2$)EER	43% ± 3%			
		4.3 ± 0.05	0.0554	12878
		4.1 ± 0.3	0.0538	13197
		4.2 ± 0.5	0.0546	12863
			mean:	**12979**
			st dev:	**188**
FSA(Y-$APPD_2$)RER	70% ± 5%			
		6.6 ± 0.2	0.0719	10851
		7.6 ± 0.4	0.0572	7480
		7.6 ± 0.3	0.0663	8721
			mean:	**9017**
			st dev:	**1705**
FSA(Y-$APPD_2$)(Y-$APPD_2$)ER	3% ± 1%			
		0.39 ± 0.01	0.0180	23339
		0.67 ± 0.28	0.0175	13053
		0.91 ± 0.43	0.0207	11335
			mean:	**15909**
			st dev:	**6492**
VFD(K-)DGNG(-Y-APPD)ISAAELR	6% ± 3%			
		0.56 ± 0.05	0.0028	5028
		1.00 ± 0.44	0.0068	6783
		1.22 ± 0.56	0.0097	7941
			mean:	**6584**
			st dev:	**1467**
VFDKDGNG(Y-$APPD_2$)ISAAELR	5% ± 2%			
		0.61 ± 0.09	0.0101	16502
		1.06 ± 0.28	0.0166	15697
		0.79 ± 0.39	0.0107	13466
			mean:	**15222**
			st dev:	**1573**
(-NH)VFDKDGNG(-Y-APPD)ISAAELR	7% ± 1%			
		1.08 ± 0.08	0.0307	28345
		1.32 ± 0.02	0.0397	30152
		1.06 ± 0.04	0.0300	28306
			mean:	**28934**
			st dev:	**1055**

4.4 Discussion and Conclusions

A major challenge of proteomic analysis is the wide diversity of targets in every sample, with the goal being the identification (and, ultimately, quantitation) of each one without bias. Moreover, analysis of low-abundance post-translational modifications like 3NY and DOPA makes full labeling and sequence coverage especially crucial. Therefore, it is important to understand how derivatization reactions and their products behave with peptide targets possessing a range of physicochemical properties.

In the present study, the reduction of 3NY to 3AY by SDT showed little dependence on peptide sequence. On the other hand, the efficiency of the tagging reaction and the spectroscopic properties of the products showed significant variation. Peptides with the sequence FSAYXER displayed similar behavior, except when a second 3NY residue was introduced adjacent to the original one. The FSAYYER peptide showed very low product yield, which may result not only from poor chemical yield but also from solubility limitations. The APPD moieties add significant hydrophobic character to any labeled peptide, as evidenced by long RP-HPLC retention times, and introducing $APPD_2$ labels at two adjacent amino acid residues would be expected to greatly reduce the solubility of labeled peptide in water. Indeed, fluorescent residue was observed by eye in the quartz collection tubes upon examination under a UV lamp after reconstituting the labeled peptide and transferring it to a clean container. The fluorescence quantum yield for APPD-labeled FSAYYER was also extremely low. This may be the result of fluorescence quenching or some other physicochemical and/or electronic interaction between the adjacent fluorophores.

The calmodulin peptide is an interesting case because it provides an opportunity to compare three different product structures. While chemical yields were similar for each of the

three products, they differed in RP-HPLC retention times, absorption and emission maxima, fluorescence quantum yields, and molar absorptivities. Notably, even the isobaric amine-Tyr cross-linked products (products 1 and 3) were significantly different from each other in all of these areas. The only difference between these structures is the location of the amine, whether on the nearby Lys (product 1) or the N-terminus (product 3). While chemically very similar, it is reasonable to expect that properties of stereochemistry and dynamics could be significantly different and consequently produce differences in the quantum physical and electronic properties of the compounds.

4.5 References

1. Allen MW. Technical Note 52019: Measurement of Fluorescence Quantum Yields. Madison, WI, USA: Thermo Fisher Scientific; 2010.
2. Anders JC. Advances in amino acid analysis. *Biopharm* 15: 32-39+, 2002.
3. Anslyn EV and Dougherty DA. *Modern Physical Organic Chemistry* Sausalito, California, USA: University Science Books; 2006.
4. Bartolomeo MP and Maisano F. Validation of a reversed-phase HPLC method for quantitative amino acid analysis. *J Biomol Tech* 17: 131-137, 2006.
5. Benson JR and Hare PE. o-Phthalaldehyde: Fluorogenic Detection of Primary Amines in the Picomole Range. Comparison with Fluorescamine and Ninhydrin. *Proceedings of the National Academy of Sciences of the United States of America* 72: 619-622, 1975.
6. Calbiochem. Data Sheet 595501 Rev. 19. 2011.
7. Davidson I. Hydrolysis of Samples for Amino Acid Analysis. 2002, pp. 111-122.
8. Dean RB and Dixon WJ. Simplified Statistics for Small Numbers of Observations. *Analytical Chemistry* 23: 636-638, 1951.

9. Dremina ES, Li X, Galeva NA, Sharov VS, Stobaugh JF, and Schöneich C. A methodology for simultaneous fluorogenic derivatization and boronate affinity enrichment of 3-nitrotyrosine-containing peptides. *Analytical Biochemistry* 418: 184-196, 2011.

10. Giese RW and Riordan JF. Nitrotyrosine internal standard for amino acid analysis. *Analytical Biochemistry* 64: 588-592, 1975.

11. Girgis AS, Kalmouch A, and Hosni HM. Synthesis of novel 3-pyridinecarbonitriles with amino acid function and their fluorescence properties. *Amino Acids* 26: 139-146, 2004.

12. Hong SJ. A proteomic study of protein tyrosine nitration [Ph.D.]. United States -- Kansas: University of Kansas; 2008. 147 p.

13. ME L, J-R Y, KA L, and RE D. New thiol active fluorophores for intracellular thiols and glutathione measurement. In: *Fluorescence Microscopy and Fluorescent Probes*, edited by J S. Springer, 1996, pp. 229-234.

14. Morris JV, Mahaney MA, and Huber JR. Fluorescence quantum yield determinations. 9,10-Diphenylanthracene as a reference standard in different solvents. *The Journal of Physical Chemistry* 80: 969-974, 1976.

15. Rutherfurd SM and Gilani GS. Amino Acid Analysis. In: *Current Protocols in Protein Science*. John Wiley & Sons, Inc., 2001.

16. Salek M, Costagliola S, and Lehmann WD. Protein Tyrosine-O-Sulfation Analysis by Exhaustive Product Ion Scanning with Minimum Collision Offset in a NanoESI Q-TOF Tandem Mass Spectrometer. *Analytical Chemistry* 76: 5136-5142, 2004.

17. Sharov V, Dremina E, Galeva N, Gerstenecker G, Li X, Dobrowsky R, Stobaugh J, and Schöneich C. Fluorogenic Tagging of Peptide and Protein 3-Nitrotyrosine with 4-

(Aminomethyl)benzenesulfonic Acid for Quantitative Analysis of Protein Tyrosine Nitration. *Chromatographia* 71: 37-53, 2010.

18. Sharov VS, Ferrington DA, Squier TC, and Schöneich C. Diastereoselective reduction of protein-bound methionine sulfoxide by methionine sulfoxide reductase. *FEBS Letters* 455: 247-250, 1999.

19. Sharov VS, Galeva NA, Dremina ES, Williams TD, and Schöneich C. Inactivation of rabbit muscle glycogen phosphorylase b by peroxynitrite revisited: Does the nitration of Tyr613 in the allosteric inhibition site control enzymatic function? *Archives of Biochemistry and Biophysics* 484: 155-166, 2009.

20. Williams ATR, Winfield SA, and Miller JN. Relative fluorescence quantum yields using a computer-controlled luminescence spectrometer. *Analyst* 108: 1067-1071, 1983.

21. Yang J-R and Langmuir ME. Synthesis and properties of a maleimide fluorescent thiol reagent derived from a naphthopyranone. *Journal of Heterocyclic Chemistry* 28: 1177-1180, 1991.

22. Zaidi A, Barŕon L, Sharov VS, Schöneich C, Michaelis EK, and Michaelis ML. Oxidative Inactivation of Purified Plasma Membrane Ca2+-ATPase by Hydrogen Peroxide and Protection by Calmodulin†. *Biochemistry* 42: 12001-12010, 2003.

Chapter 5: Conclusions and Future Directions

5.1 Summary and Conclusions

The goal of this dissertation project was to develop and apply a novel derivatization method for labeling 3-nitrotyrosine (3NY) and 3,4-dihydroxyphenylalanine (DOPA) in order to facilitate proteomic studies of these oxidative post-translational modifications in cardiac tissue from a rat model of aging. Benzylamine (BA) reacts with DOPA and 3AY (formed from 3NY by reduction with sodium dithionite, SDT) in the presence of the oxidant potassium ferricyanide to give fluorescent 2-phenylbenzoxazole products. Two substituted benzylamine reagents have also been synthesized and applied in this method: 4-(aminomethyl)benzenesulfonic acid (ABS) and (3*R*,4*S*)-1-(4-(aminomethyl)phenylsulfonyl)pyrrolidine-3,4-diol (APPD).

This method had previously been developed with model compounds, ranging from small molecules to peptides to purified proteins (1,2), and the task of translating it to a complex biological sample, like cardiac homogenate, is not trivial. By nature, proteomic studies aim to detect, identify, and quantify not a single analyte, but hundreds (or more). Each of these analytes may respond differently to sample preparation steps and particularly to the derivatization chemistry, as demonstrated with a series of model peptides (Chapter 4). Moreover, the biological matrix often contains reactive or otherwise interfering species, and the use of protein-stabilizing solution additives, like detergents and reducing agents, can further complicate analysis. One manifestation of this problem is the loss of 3NY from the model protein glycogen phosphorylase *b* (Ph-b) upon mixing with cardiac homogenate (Chapter 3). Cleaning steps to remove interfering species, excess reagents, and side products after each step in the method are necessary but open the door for significant sample losses and experimental bias, as explored in Chapters 2 and 3. Finally, bottom-up proteomic identifications rely upon matching tandem mass spectrometry (MS/MS) spectra from complex samples of tryptic peptides to database information

on theoretical fragmentation patterns for known protein sequences in the proteome of the species under study. Given the likelihood of false identification, stringent criteria must be applied for confident identifications. Moreover, assignment of an identified modification (e.g., +45amu for nitration) to a particular residue in the peptide (e.g., Tyr) is best evidenced when peptide bond cleavage occurs on both sides of the modified residue during collision-induced dissociation in the mass spectrometer. Meeting all of these criteria requires sufficient signal-to-noise ratio in mass spectrometric experiments, which is particularly difficult to achieve for low-abundance species like 3NY and DOPA in the presence of an overwhelming matrix of other, non-modified cardiac peptides.

In response to these challenges, many aspects of the sample preparation and derivatization procedures were optimized, using both cardiac homogenates and model systems. By size-exclusion high-performance liquid chromatography (SE-HPLC), calibrated with protein molecular-weight standards, it was demonstrated that the fluorescent products in cardiac samples were indeed labeled proteins. In several experiments, a significant difference in fluorescence intensity was observed for samples that were reduced with SDT compared to those that were not. Since 3NY, but not DOPA, requires this reduction step for labeling, this difference can be attributed to the presence of 3NY. Indeed, for the model protein Ph-b nitrated *in vitro* with peroxynitrite and mixed with cardiac proteins, the fluorescence intensity showed a linear dependence on the amount of 3NY (as determined by UV-visible absorbance measurements of the pure, nitrated protein). For cardiac proteins, the comparison of reduced and non-reduced samples did not always give consistent results. Similarly, comparisons of cardiac homogenates from old and young rats did not give consistent results regarding age-dependency of 3NY or

DOPA levels. This variability may be due to 3NY levels below the limit of detection, changes in experimental conditions that can affect labeling, and/or animal-to-animal variations.

For systematic study of labeling properties for different analytes, the method was applied to a series of model nitro-peptides with varying sequences. While changing the acid-base properties of a single residue adjacent to 3NY did not significantly affect labeling efficiency, fluorescence quantum yield, wavelengths of fluorescence maxima, or molar absorptivity, other sequence changes had dramatic effects. The placement of a second 3NY residue adjacent to the first resulted in very low product yield and very small fluorescence quantum yield. A longer peptide with a completely unrelated amino acid sequence formed three distinct fluorescent products upon labeling, each with their own chemical yields and spectroscopic properties. Importantly, intramolecular cross-links formed in this peptide between the labeled Tyr and either the nearby Lys ε-amino group or the N-terminal amino group.

5.2 Future Directions

Nitration of cardiac proteins *in vitro* should provide a more robust system to finalize optimal reaction conditions and investigate the inconsistencies observed for comparisons of reduced and non-reduced samples and of old and young rat tissues. The role of protein precipitation protocols can also be more thoroughly evaluated with these samples. By mixing nitrated cardiac proteins with untreated ones at varying ratios, a calibration curve could be constructed for cardiac proteins, similar to that based on nitrated Ph-b. Using the information gained with this model system, the next step is to subject samples containing only endogenous DOPA and 3NY to the optimized labeling protocol, followed by mass spectrometry analysis in order to identify sites carrying the benzoxazole label. Other tools to improve the chances for success in this goal include APPD labeling followed by boronate-affinity HPLC for enrichment

of labeled analytes and ultra-high-performance liquid chromatography with mass spectrometry for improvement of column capacity and resolution. Both of these strategies should mitigate ion suppression and other interferences from the large number non-modified peptides in the cardiac samples.

Further information can also be gained from model systems. For instance, another calibration curve for labeled 3NY-Ph-b in a mixture of cardiac proteins could be constructed based on SE-HPLC fluorescent peak area of the Ph-b peak. This separation, though crude, could improve the assay's limit of detection. Model peptides labeled with each of the three benzylamine-type reagents can provide insights into characteristic fragments that may form by gas-phase reactions in the mass spectrometer. As long as these fragmentations remain unknown, if they exist, the proteomic search algorithms will be unable to find labeled peptides. The same is true for any side products that may form during derivatization, which may or may not be fluorescent.

As an extension of the model peptide series, more peptide sequences could be tested, particularly to focus on the effect of secondary structure on labeling efficiency and spectroscopic properties. The accessibility of Tyr residues can be an important parameter for derivatization yield, and the interactions that contribute to secondary structure could alter the fluorescent and absorption properties of labeled Tyr. For further investigation of primary structure effects, variations in the distance between 3NY and Lys or the N-terminus could identify the preferred conditions for generating intramolecular cross-links during fluorogenic derivatization.

5.3 References

1. Pennington J, Schöneich C, Stobaugh J. Selective Fluorogenic Derivatization with Isotopic Coding of Catechols and 2-Amino Phenols with Benzylamine: A Chemical Basis

for the Relative Determination of 3-Hydroxy-tyrosine and 3-Nitro-tyrosine Peptides. *Chromatographia* 66: 649-659, 2007.

2. Sharov VS, Dremina ES, Pennington J, Killmer J, Asmus C, Thorson M, Hong SJ, Li X, Stobaugh JF, Schöneich C. Selective Fluorogenic Derivatization of 3-Nitrotyrosine and 3,4-Dihydroxyphenylalanine in Peptides: A Method Designed for Quantitative Proteomic Analysis. *Methods in Enzymology* Volume 441: 19-32, 2008.